Óbuda University

PhD thesis

Controller-managed automated therapy and tumor growth model identification in the case of antiangiogenic therapy for most effective, individualized treatment

by

Johanna Sájevicsné Sápi

Supervisor:

Levente Adalbert Kovács PhD, habil.

Doctoral School of Applied Informatics and
Applied Mathematics

Budapest, 2015

Contents

Acknowledgments

First and foremost, I would like to express my special appreciation to my supervisor, *Dr. Levente Kovács*. Without his assistance and useful advice in every step throughout my studies, this dissertation would have never been accomplished. He is a great leader, researcher – and let me say – friend.

I would like to thank my teachers, from whom I learnt a lot. During my Bachelor's studies at Semmelweis University *Dr. András Jávor*, *Dr. Péter Csépe* and *Zoltán Sára* launched me on my way to medical and informatics sciences. I have to thank *Prof. Zoltán Benyó* who is one of the founders of biomedical engineering in Hungary; his persistent work provided me the possibility of my Master's studies at Budapest University of Technology and Economics. *Dr. Katalin Friedl* and *Prof. Béla Lantos* were exemplary to me during my PhD studies at Budapest University of Technology and Economics with their knowledge and modesty.

I would also like to thank Rector *Prof. Imre J. Rudas* and the leaders of the Doctoral School of Applied Informatics and Applied Mathematics at Óbuda University, *Prof. Aurél Galántai* and *Prof. László Horváth* for their support.

I have to thank my colleagues with whom I have worked together in the current research topic, *Dániel András Drexler*, *Dr. István Harmati* and *Annamária Szeles*.

I express my warm thanks to *my parents*, who supported me during my studies; especially to my father, who have lead me throughout my academic journey.

I would like to say special thanks to *my husband*, who encouraged me throughout my research. Without his heartening and sincere love, none of this work would have happened.

I would like to say special thanks to *my twin sister*. She taught me in the bathroom of the primary school when we were approximately 9 years-old how to write big numbers correctly. In addition she has always helped and supported me during my whole life. Also, I want to say thanks to all my family members: *my grandmothers*, *my grandfather*, *my sisters* and *my brothers-in-law*. I am very grateful having such a big and lovely family.

This thesis stands as a testament to God's unconditional love. *Soli Deo Gloria!*

List of Figures

List of Tables

Abstract

Examination of tumor growth and optimal administration of anticancer drugs belongs not only to basic medical research, but to the fields of biomedical engineering and applied informatics as well. The aim of physiological modeling and control is to study, understand and model biological processes, then to apply identification and control strategies upon it. By designing closed-loop control systems, the empirically determined and constant drug dosage prescribing medical protocols could become model-based. Model-based design enables the automated treatment of cancer diseases by the personalized administration of antiangiogenic (new blood vessel creation inhibitor) drugs. In this way, more effective remedial solutions can be found and individualized treatment for the patient.

This approach is a completely novel one and may lead to a breakthrough in cancer therapies. Optimizing cancer treatments would improve efficiency, decrease treatment cost and minimize the side effects of cancer therapy (i.e. improves the patient's quality of life); thus analysis and synthesis of cancer therapies from an engineering point of view is needed.

The dissertation contains two main thesis groups. The first thesis group provides linear control synthesis for antiangiogenic therapy over the simplified tumor growth model of Hahnfeldt et al. 1999. Two different control methods were applied to design linear controllers. Linear state-feedback control was carried out with pole placement and LQ optimal control as well. Since not every state variables of the system can be measured, a linear observer was designed for both state-feedback methods. I investigated several parameter changes to observe the effect of the different control parameters: four operating points, three pole acceleration values (in the case of pole placement) and three saturation limits were analyzed; in addition, R weighting matrix (in the case of LQ optimal control) was examined over a wide range of values. Every simulation result was evaluated based on three criteria which are relevant from the medical and engineering points of view.

The other applied method is robust (H_∞) control. Taking into account the fact that every model contains uncertainties and measurement noises, there is a need for systems which satisfy the requirements not only for its nominal values but also in the presence of perturbations. I designed a stabilizing robust controller, where ideal system and weighting functions were chosen in the light of physiological aspects. The results of Robust control were compared to the results based on LQ optimal control and the Hungarian OEP (National Health Insurance Fund of Hungary) protocol.

The second thesis group provides tumor growth model identification. Specific animal experiments were performed to investigate tumor growth dynamics and create new tumor growth models. Tumor growth was investigated without therapy and under angiogenic inhibition. Linear model identification of tumor growth dynamics without therapy using parametric identification was carried out on two tumor types (C38 colon adenocarcinoma and B16 melanoma). Linear model identification of C38 colon adenocarcinoma growth dynamics under bevacizumab inhibition was performed using parametric identification as well. The resulting models are clinically valid and sufficiently simple to be manageable for both real-life applicability and controller design.

The relationship between the measured tumor attributes during the experiments (tumor mass, tumor volume and vascularization) was examined using linear regression analysis. Tumor volumes were calculated using caliper-measured data and small animal MRI measurement results. A two-dimensional mathematical model was created for tumor volume evaluation from caliper-measured data; it resulting in more precise tumor volume evaluation than the Xenograft Tumor Model Protocol. Effective dosage of angiogenic inhibitor for optimal cancer therapy was also investigated, and quasi-continuous therapy was found to be more effective than protocol-based therapy.

Absztrakt

A tumornövekedés és az optimális daganatellenes szerek adagolásának vizsgálata nem csupán az orvostudomány kutatási területéhez tartozik, hanem az orvosbiológiai/egészségügyi mérnöki és az alkalmazott informatikai kutatási területekhez is. Az élettani folyamatok modellezésének és szabályozásának célja, hogy tanulmányozza, megértse és modellezze az egyes biológiai folyamatokat, majd identifikációs és szabályozótervezési módszertant alkalmazzon a felállított modellre. Zárt hurkú szabályozások tervezésével az empirikusan meghatározott és konstans gyógyszeradagolást előíró orvosi protokollok modell-alapúvá válhatnak. A modell-alapú tervezés lehetővé teszi a daganatos betegségek automatizált kezelését az antiangiogén (új ér képződését gátló) gyógyszerek egyéni adagolásával. Ezáltal még hatékonyabb megoldások találhatók a gyógyításban és a beteg személyre szabott kezelésben részesíthető.

Ez a megközelítés teljesen új és áttöréshez vezethet a daganatterápiában. Az optimalizált daganatellenes kezelések növelhetik a hatékonyságot, csökkenthetik a terápiás költségeket, emellett a mellékhatásokat minimalizálhatják, így javítva a páciens életminőségét. Ezek alapján világos, hogy a daganatellenes kezelések mérnöki szempontból történő analízise és szintézise szükséges.

A disszertáció két fő téziscsoportot tartalmaz. Az első téziscsoport lineáris szabályozási szintézist ír le az angiogenikus gátlás alatt lévő tumornövekedési modell (Hahnfeldt et al. 1999) egyszerűsített változatára. Két különböző szabályozási metódus került alkalmazásra lineáris szabályozó tervezése céljából. Lineáris állapotvisszacsatolással megvalósított szabályozás lett kidolgozva állapotvisszacsatolás és LQ optimális szabályozás használatával. Tekintve, hogy a rendszer nem minden állapotváltozója mérhető, lineáris állapotmegfigyelő is lett tervezve mindkét állapotvisszacsatolási módszerhez. Számos paraméter változtatásának hatását vizsgáltam a rendszerre: négy munkapont, három pólusgyorsítási érték (pólusáthelyezéses állapotvisszacsatolás esetén) és három szaturációs limit lett vizsgálva; emellett az R súlyozó mátrix értéke tág tartományban került vizsgálatra (LQ optimális szabályozás esetén). Valamennyi szimulációs eredmény három kritérium alapján lett értékelve, melyek orvosi és mérnöki szempontból is releváns követelmények.

A másik alkalmazott szabályozási metódus a robusztus (H_∞) szabályozás. Figyelembe véve a tényt, hogy minden modell tartalmaz bizonytalanságokat és mérési zajokat, szükséges olyan rendszereket tervezni, amelyek nem csak a nominális értékek fennállása

esetén teljesítik a követelményeket, hanem perturbációk fennállása esetén is. Olyan stabilizáló robusztus szabályozót terveztem, ahol az ideális rendszer és a súlyozó függvények az élettani szempontok figyelembevételével lettek megválasztva. A robusztus szabályozás eredményei az LQ optimális szabályozás és az OEP (Országos Egészségbiztosítási Pénztár) protokoll alapú kezelés eredményeivel összehasonlításra kerültek.

A második téziscsoport tumornövekedési modell identifikációját írja le. Speciális állatkísérleteket kerültek kivitelezésre a tumornövekedési dinamika vizsgálatának és új tumornövekedési modellek felállításának érdekében. A tumornövekedési dinamika terápia alkalmazása nélkül, valamint angiogén gátlás alatt is vizsgálva lett. A terápia nélküli tumornövekedés lineáris modell-identifikációja két tumor esetén (C38 colon adenocarcinoma és B16 melanoma) lett megalkotva parametrikus identifikáció használatával. Szintén parametrikus identifikáció használatával lett megalkotva a bevacizumab gátlás alatt lévő C38 colon adenocarcinoma növekedési dinamikájának identifikációja. A létrehozott modellek klinikailag validak, és kellően egyszerűek ahhoz, hogy kezelhetőek legyenek mind a valós alkalmazhatóság, mind a szabályozótervezés szempontjából.

A kísérletek során mért tumor jellemzők (tumor tömeg, térfogat és vascularizáltság) közötti kapcsolat lineáris regresszió analízis segítségével lett vizsgálva. A tumor térfogat értéke a tolómérővel és a kisállat MRI-vel mért értékek alapján is lett számítva. A tumor térfogat becslése céljából egy kétdimenziós matematikai modell került megalkotásra, mely a tolómérővel mért értékeket használja. Ez a becslés sokkal pontosabb eredményeket szolgáltat, mint a Xenograft tumor modell protokoll. Az optimális daganatterápia megvalósításához szükséges antiangiogenikus szer hatékony adagolása szintén vizsgálva lett, és a kvázi-folytonos terápia hatékonyabbnak bizonyult, mint a protokoll alapú kezelés.

1 Introduction

The key of scientific success in every field nowadays depends on interdisciplinary design. Medical treatment is not an exception either; engineers and doctors have to work together to find more effective solutions in healing. Cancer is the leading cause of death all over the world. In the EU, the total estimated number of cancer casualties for 2014 is 1.323 million (Malvezzi et al. 2014). In the clinical practice, there are general protocols for cancer therapies (such as chemotherapy, radiotherapy). However, these treatments have many side effects and tumor cells can become resistant to chemotherapy drugs which on the one hand makes the usage of new drugs necessary (Perry 2008), and on the other hand it increases the treatment cost. That is the reason why a new dynamically-developing therapeutic group called Targeted Molecular Therapies (TMTs) (Gerber 2008) has appeared. These therapies gain more and more importance as they specifically fight against different cancer mechanisms, being more effective and having limited side effects compared to conventional cancer therapies (Kreipe and Wasielewski 2007). Nevertheless, protocols for cancer treatments (also for TMTs) are determined empirically and are comprised of constant drug dosage.

The aim of physiological modeling and control is to study, understand and model biological processes, then to apply identification and control strategies on it. By designing closed-loop control systems, the protocols could become model-based. Model-based design enables the automated treatment of cancer diseases by the personalized administration of TMT drugs. In this way, more effective solutions can be found in healing and offering individualized treatment for the patient. This approach is completely novel and may lead to a breakthrough in cancer therapies. Optimizing cancer treatments would improve efficiency, decrease treatment cost and minimize the side effects of cancer therapy (i.e. improves the patient's quality of life); thus analysis and synthesis of cancer therapies from an engineering point of view is needed.

In the outlined research field the basis of every therapy and further research is physiological and pathophysiological knowledge. This knowledge has to be applied paired with engineering knowledge to create a model which describes tumor growth.

Tumor growth dynamics can be modeled without therapy and under a certain cancer

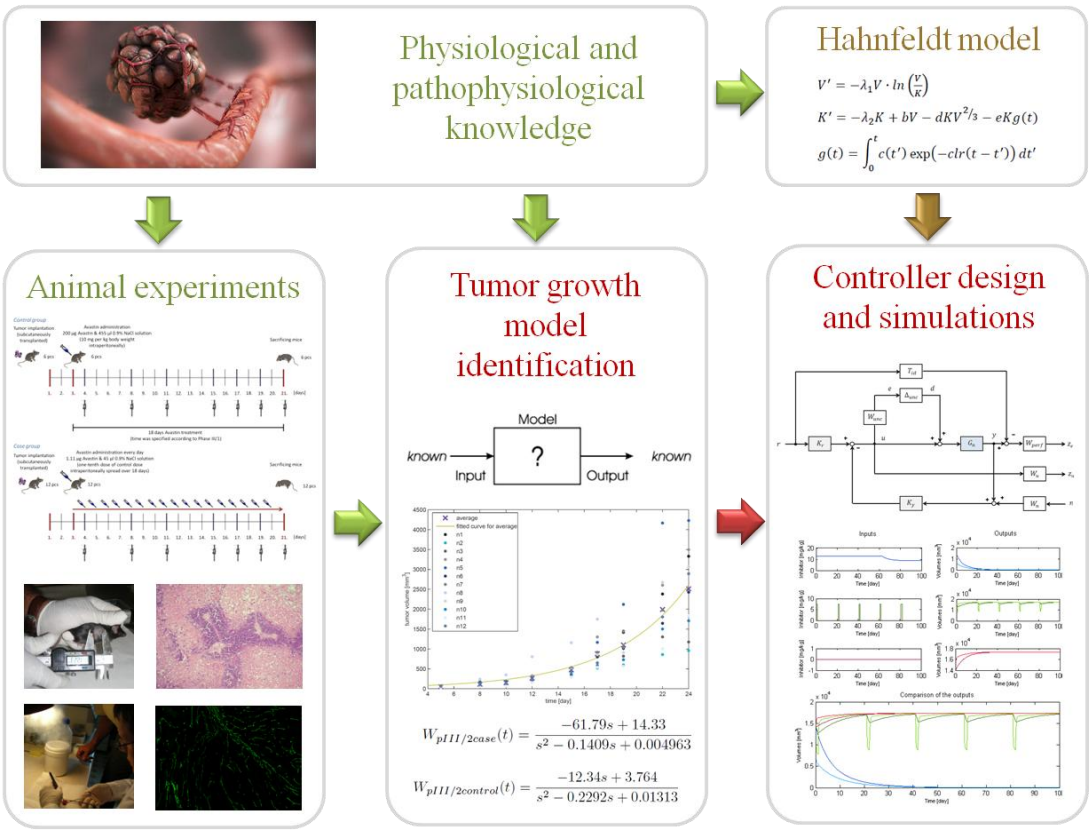

Figure 1.1: Concept of my research. Tumor growth dynamics under angiogenic inhibition is described by Hahnfeldt model. I have investigated the model, designed controllers and made simulations. In the light of new medical researches, it has become clear that there is a strong need to revise this tumor growth model. Animal experiments were done to create a new model.

treatment as well. A promising targeted molecular therapy that arose in the last decade is antiangiogenic therapy (Pluda 1997; Kelloff et al. 1994) which aims to stop tumor angiogenesis (i.e. forming new blood vessels) as, without a blood supply, tumors cannot grow (Bergers and Benjamin 2003). A clinically validated tumor growth model under angiogenic inhibition was developed at Harvard University by Hahnfeldt et al. 1999. The model describes the reduction of tumor volume based on endothelial reduction. The Hahnfeldt model and its simplified form has been used by most researchers working in the field of antiangiogenic control to design controllers and perform simulations.

Nevertheless, the Hahnfeldt model has some limitations according to the newest medical research in the field of angiogenic tumor growth (Döme et al. 2007; Femke

and Griffioen 2007). The original theoretical concept of angiogenesis was endothelial sprouting; accordingly, new blood vessels sprout from existing ones (O'Reilly et al. 1997). Endothelial cells undergo disorganized sprouting, proliferation and regression, and become dependent on the vascular endothelial growth factor (VEGF) (McDonald 2008), one of the most important proangiogenic factors in tumor growth. Hence, in inhibiting VEGF in tumors, one can stop sprouting angiogenesis (Chang et al. 2012). Most of the angiogenic inhibitors act in that way and this is the key point in angiogenic inhibition studies.

However, later on, it has became clear that VEGF inhibition leads to apoptosis (process of programmed cell death) only in newly-built vessels in tumors, but does not have an effect on vessels which have already existed (Petersen 2007). That means that there is a strong need to revise the existing tumor growth model, since, according to the Hahnfeldt model, every blood vessel can be eliminated by the drug. Specific animal experiments were performed to investigate tumor growth under angiogenic inhibition, and taking into account the newest results of vascularization in tumor cells, new tumor growth models were created. (Figure 1.1).

According to the above mentioned problems, the dissertation seeks to provide solution for two main issues – and therefore contains two main thesis groups:

Thesis group 1. Protocols for medical treatment comprise constant drug dosage, which can be effective in terms of reducing the progression of the diseases; however, nowadays the problem seems more complex. From multidisciplinary point of view the aim is to design a controller which is on the one hand able to minimize the input signal as far as possible (in order to have less side effects and greater cost-effectiveness) and on the other hand results in appropriately low tumor volume.

Thesis group 2. In the literature there are models for tumor growth under angiogenic inhibition, however these models are mechanistic or semi-mechanistic models built up from physical equations, and they have not been validated with in vivo data in most of the cases; in addition the existing validated models are overly difficult. Consequently, there is a strong need to create a mathematical model which describes the tumor growth dynamics under angiogenic inhibition. This model has to take into account the previously mentioned models and their results, but it also has to be sufficiently simple to be manageable for both real-life applicability and controller design.

2 Physiological and Pathophysiological Background

In this chapter, the physiological and pathophysiological background of the interdisciplinary research topic is presented. In Section 2.1, the most commonly used, conventional cancer treatments (surgical oncology, radiation therapy and chemotherapy) are summarized. In the next section (Section 2.2), new types of cancer fighting therapies, called Targeted Molecular Therapies (TMTs) are discussed. These therapies are based on specific pathway in the growth and development of tumor cells, thus TMTs specifically fight against different cancer mechanisms. Finally, in the last section (Section 2.3) the antiangiogenic therapy and its usability are presented.

2.1 Conventional Cancer Treatments

The oldest form of cancer treatment is curative treatment, when the tumor is completely or partially removed. In **surgical oncology** the cancer and an area of healthy tissue surrounding is removed (Pollock 2008). Surgical intervention is most effective in the treatment of localized primary tumor disease (Feig, Berger, and Fuhrman 2006). The most common organs, where surgical oncology is used are: esophagus, stomach, duodenum, colon, liver, pancreas (Holzheimer and Mannick 2001).

In the nineteenth century, when scientific oncology was born with use of the modern microscope (ACS 2011), scientists have got the instruments to observe the basics of cancer mechanisms and processes. They have found that tumor cells are dividing rapidly, so the first modern therapies were based on this very typical property of tumor cells. The earliest use of **radiation therapy** was alternative to surgical intervention for unresectable lesions. Radiotherapy can be used as monotherapy (specifically for cancers at early stages), but more often used in combinated treatment (with surgical oncology or chemotherapy) to "stop metastases at their source" (Connell and Hellman 2009). In radiation therapy high-energy photons (gamma rays and x-rays) and charged particles (electrons) are used (Gazda and Lawrence 2001). Unfortunately ionizing radiation also has an undesirable

effect: toxicity to normal surrounding tissues through DNA damage. This effect is called *organs at risk* (Samson et al. 2010).

The other therapy based on the fact that tumor cells are rapidly dividing is **chemotherapy**. In this case, different chemical agents are used to destroy cancer cells by interfering with the ability of cells to grow or multiply. Tumor cells' response to chemotherapy can be different (Page and Takimoto 2001). *Complete response* is the disappearance of disease (tumor is undetectable) and for a specified interval there is no cancer recrudesce. *Partial response* is at least 50% size reduction with no appearance of new disease. *Minimal response (stable disease)* is less than a partial response. When existing disease growths or a new disease appears during the chemical treatment, it's called *progression*. Besides that chemotherapy can be effective, there are also side effects: (1) chemical agents has effects on certain healthy cells of the patient as well, (2) tumor cells can become resistant towards the used drug, which makes the usage of higher dose or totally new drugs necessary (Perry 2008).

Summarizing conventional cancer therapies (Holland and Frei 2003): with surgical oncology the tumor cells can be totally removed (*zero-order kinetics*), in contrast to chemotherapy or radiation therapy, where only a fraction of tumor cells are killed (*first-order kinetics*). When a cancer has been removed by surgery, chemotherapy or radiotherapy may be used to keep the cancer from coming back (*adjuvant therapy*).

2.2 Targeted Molecular Therapies (TMTs)

Targeted Molecular Therapies represent a new and modern trend of fighting cancer. We can group cancer treatments by specificity. Classical therapies, like radiation therapy and chemotherapy are based on rapidly dividing cells, but not only cancer cells are dividing rapidly, there are also highly proliferative normal tissues (for example bone marrow, hair, gastrointestinal epithelium). Because of that, classical therapies have significant side effects (anemia, alopecia, nausea and vomiting, nerve problems, skin problems (Samson et al. 2010)) and these treatments are toxic to all cells. Developing new radiation methods (like *proton therapy* (Goitein and Jermann 2003) or *intensity modulated radiation therapy* (Goffman and Glatstein 2002)), and new chemotherapy agents can be a solution to reduce this problem. Nevertheless a totally new approach is not to alter conventional cancer therapies, but search for methods which are specific against certain cancer mechanisms. Treatments which are based on specific molecules which target a signaling pathway in the growth and development of a tumor cell is called *Targeted Molecular Therapies (TMTs)*. Some of these specific molecules may be present in normal tissues, but in tumor cells

they are often mutated or overexpressed (Gerber 2008).

At an early stage of developing TMTs there were antibodies which affect overall immune function, thus there was requisite to develop such target molecules, which only have effect on tumor cells (Kelloff et al. 1994). The most often targeted signaling pathways in TMTs are EGFR/HER1 (epidermal growth factor receptor, human epidermal growth factor receptor), VEGF (vascular endothelial growth factor) and HER2. The pathways of inhibition can be (Gerber 2008): (p1) binding and neutralizing ligands, (p2) occupying receptor-binding sites, (p3) blocking receptor signaling within the cancer cell, (p4) interfering with downstream intra-cellular molecules.

There are two main types of targeted molecular therapies. *Monoclonal antibodies* (O'Mahony and Bishop 2006) are usually large molecules and target (p1) and (p2) pathways (extracellular components inhibition). (For a receptor inhibition therapy study see for example Nishimoto et al. 2009). Monoclonal antibodies have protein structure, which is denatured in the gastrointestinal tract; therefore these drugs are administered intravenously. They do not have significant drug interactions, because they do not undergo hepatic metabolism. FDA (U.S. Food and Drug Administration) have approved 11 monoclonal antibodies for cancer therapy until 2011 (see Figure 2.1). The other main type of targeted molecular therapy is *small molecule inhibitors*. These inhibitors are smaller than antibodies, thus because of their size, they can enter cells and target (p3) and (p4) pathways (Frank 2012), typically tyrosine kinase signaling (intracellular components inhibition). Small molecule inhibitors are usually administered orally rather than intravenously. Contrast to monoclonal antibodies, they undergo hepatic metabolism, so there may be drug interactions.

Targeted molecular therapies have several different types, based on specific properties of tumor development and growth.

- There are special cancer types, where tumor cells need hormones to grow. These cancers can be treated by *hormone therapy*. There are several ways to switch off the hormonal effects (Dinda 2012): (1) prevent the body from producing and secreting the hormone, (2) block or eliminate the hormone receptors, (3) block hormone signaling pathway. The most important hormone therapies are anti-androgen therapy (e.g. against prostate cancers (Ohlmann, Kamradt, and M. 2012)), anti-estrogen therapy (e.g. against breast cancer (Verma et al. 2011)), aromatase inhibitor therapy (e.g. against breast cancer for menopausal women (Tao et al. 2011)).

- Using one's own immune system to fight cancer is called *immunotherapy* (Waldmann

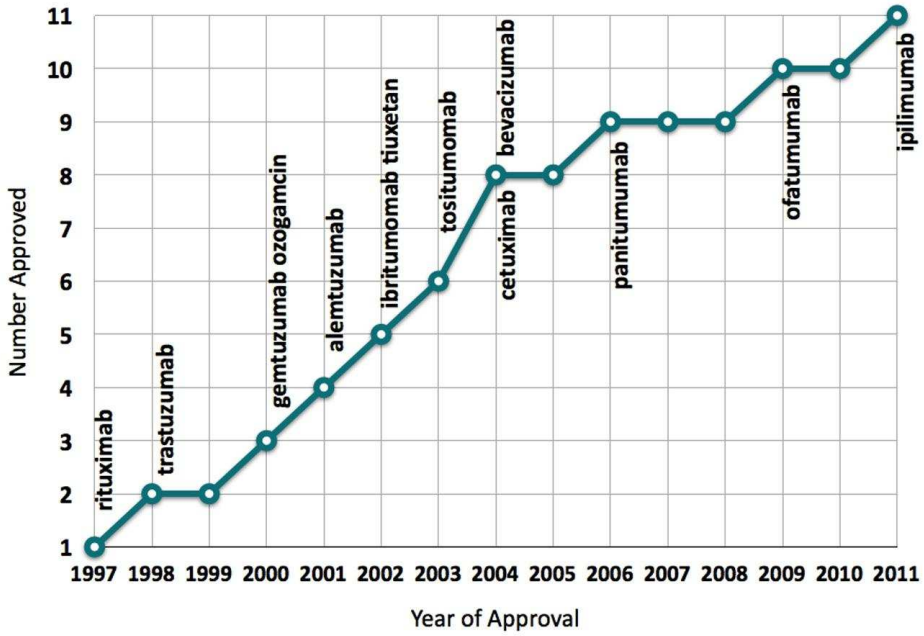

Figure 2.1: FDA approved monoclonal antibodies (mAbs) for cancer therapy (Becker 2011)

2003). If the immune system has already recognized cancer cells, the immune system can be stimulated to fight more effectively against cancer (active immunotherapy). Other solution is not to wait for immune system to recognize cancer cells, but give adequate immune system components for the patient (passive immunotherapy).

- There are already effective biological processes, where it is possible to interfere in the level of genes. *Gene therapy* (Kaur, Long, and Dufour 2012) can be used in somatic genes (results phenotypic changes) or germ line genes (results genotypic changes).

- *Revertant therapy* is a potential "natural gene therapy", based on a newly discovered process called revertant mosaicism (spontaneous reversal of an affected somatic cell to a wild-type phenotype) (Lai-Cheong, McGrath, and Uitto 2011).

- Another therapy is *checkpoint-dependent inhibition of DNA replication* (Kastan and Bartek 2004), which means a cell-cycle-dependent regulation of DNA replication in tumors (Tachibana, Gonzalez, and Coleman 2005).

- Apoptosis (process of programmed cell death) have key effect on tumor growth and survival, so there are *cancer therapies based on apoptosis* (Lowe and Lin 2000,

Kasibhatla and Tseng 2003).

- *Antiangiogenic therapy* acts against new blood vessel formation of tumor cells (see Section 2.3).

The main differences between conventional cancer therapies and targeted molecular therapies are not only the acting ways, but also the goals. Using conventional treatments, there is no need to know how cancer cells are developing and which mechanisms are used to circumvent the immune system. In surgical oncology the cancer is simply removed; radiation therapy and chemotherapy affect against rapidly dividing cells, thus these treatments are toxic to all cells. Conventional cancer therapies' goal is to eliminate the tumor mass, but with time the tumor can recrudesce and give metastasis. Targeted molecular therapies represent a new approach: these treatments act in specific molecular ways, and the goal is to prevent tumor cells from grow and develop; hence, prevent toxicity. This is more important than eliminate the tumor mass – for the patients there is a better chance of survival if they have inactive tumor mass, than if they do not have tumor for a while, but there is the risk of recurrence. To develop targeted therapies, it is required to analyze tumor growth and explore causal factors, but with this knowledge these therapies have led to truly tailored therapy (Gerber 2008) with reduced side effects (Kreipe and Wasielewski 2007).

2.3 Antiangiogenic Therapy

2.3.1 Angiogenesis

Angiogenesis is the process of forming new blood vessels, which occurs normally in the human body at specific times. During embryogenesis, blood vessels form from angioblasts (this process is called vasculogenesis). Angiogenesis also takes place in adults, although it is a relatively infrequent event (in normal circumstances occurs only in case of high altitude (low oxygen concentration), regeneration of tissue during wound healing and in women during certain phases of the menstrual cycle) (Hoeben et al. 2004). The process of angiogenesis is precisely controlled by proangiogenic and antiangiogenic factors thus as a result there is angiogenic balance in the body.

All cells need oxygen and nutrients, which can be picked up from nearby capillaries. Tumor cells are dividing rapidly, so there is an extra need for oxygen. When proliferation begins, small sized tumor can pick up enough oxygen – in this phase tumor is an avascular nodule (dormant), in a steady-state level of proliferating and apoptosing cells (Bergers and Benjamin 2003). After a certain size ($1 - 2$ mm diameter) tumor development stops,

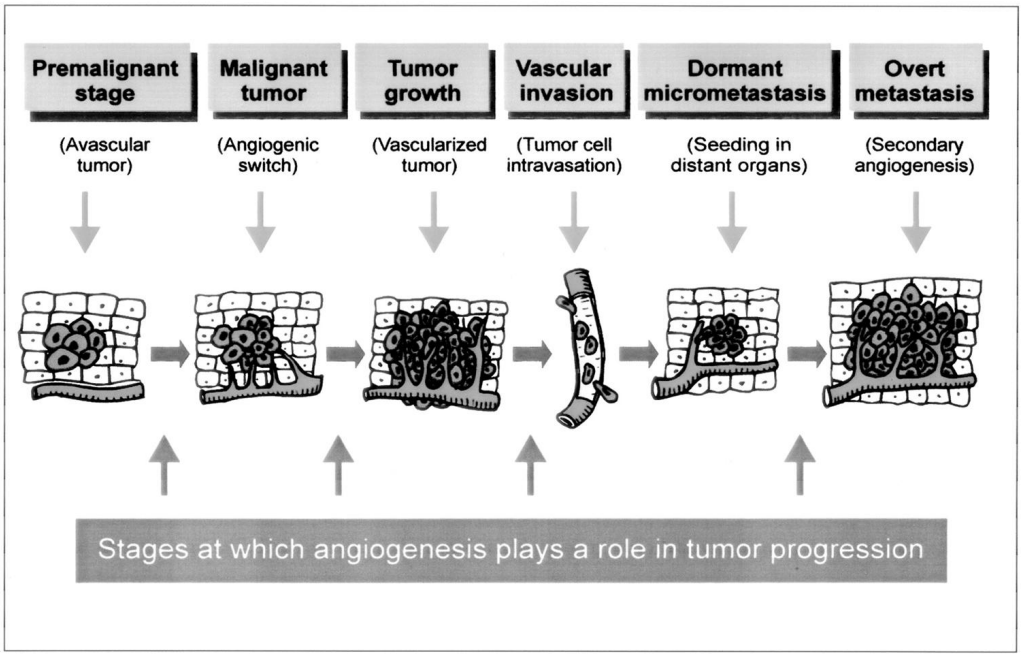

Figure 2.2: Angiogenesis in cancer development, growth, and metastasis (Hoeben et al. 2004)

because the diffusion of oxygen through tissues is limited to 100 to 200 μm. Tumor needs own blood vessels to grow, however forming new vessels is inhibited by the body's antiangiogenic factors. Tumor have to break through this strict control – the process when tumor become able to form own blood vessels is called angiogenic switch. This switch ensures exponential tumor growth. The next phase is intravasation: the invasion of tumor cells into the blood stream. By this process, cancer cells can be spread to distant organs to form dormant micrometastases, which can induce secondary angiogenesis (Hoeben et al. 2004). Figure 2.2 presents a summary of angiogenesis in cancer development, growth and metastasis.

2.3.2 Antiangiogenic Therapy

Tumor-induced neoangiogenesis is the process of forming new blood vessels by sprouting from existing vessels. After the process of forming, new blood vessels undergo changes in phenotype (this process is called vascular remodeling). These processes and thus newly formed blood vessels are disease-specific. In tumors endothelial cells undergo disorganized

sprouting, proliferation and regression, and become dependent on VEGF (McDonald 2008). Vascular endothelial growth factor is one of the most important proangiogenic factors in tumor growth. Because of that inhibiting VEGF signaling in tumors stops sprouting angiogenesis. However, it is important to note that VEGF inhibition leads to apoptosis only in newly built vessels in tumors, but don't have effect on vessels which have been already existing (Petersen 2007).

Blood-vessel formation will continue as long as the tumor grows, therefore tumors produce VEGF constitutively. (This is why there is an expression that "tumors are wounds that do not heal" (Hoeben et al. 2004)). VEGF circulates in the serum, thus the level of circulating VEGF is a useful marker of tumor status and prognosis in most types of human cancer (Karayiannakis et al. 2002). High serum level of VEGF indicates unfavorable clinical parameters like disease progression, lack of response to chemotherapy, and poor survival (Hoeben et al. 2004). A difficulty in developing antiangiogenic therapy is the monitoring of response to therapy, because decrease of tumor size is a slow process. Nevertheless changes in hemodynamic parameters occur soon after the start of the therapy. There are several ways in medical imaging to detect these parameters' changes (e.g. perfusion CT, perfusion MRI, contrast-enhanced ultrasound) (Kalva, Namasivayam, and Sahani 2008).

There are several angiogenesis inhibitors used in clinical application (Dredge, Dalgleish, and J. B. Marriott 2003). Research of new antiangiogenic drugs are based on the collaboration of scientists and clinicians (Kerbel and Folkman 2002). Widely used inhibitors in cancer therapies are endostatin (O'Reilly et al. 1997) and bevacizumab (Ellis and Haller 2008).

As it was discussed previously, targeted molecular therapies' and thus antiangiogenic therapy's aim is to prevent tumor cells from grow and develop, not to eliminate the whole tumor mass. If the tumor can be kept in a dormant state and the cellular proliferation rate is balanced by the apoptotic rate, the tumor will be unable to grow in size beyond a few millimeters (Pluda 1997). In contrast to chemotherapy, it will not result in toxicity in the body. This characteristic is very important in cancer therapies, because a large number of cancer patients die of therapy-related toxicities, and chemotherapy can impair intellect too (this cognitive impairment is called chemobrain) (Srinivas 2010). Resistance to chemotherapy is based on the genetic instability, heterogeneity and high mutational rate of tumor cells. Since endothelial cells are genetically stable, homogeneous and have a low mutational rate, antiangiogenic therapy (effecting directly to endothelial cells) induce little or no drug resistance (Kerbel 1997; Boehm et al. 1997) and antiangiogenic drugs pose no risk of a chemobrain. Moreover, researches prove that antiangiogenic agents can

improve survival by increasing tolerance to chemotherapy-induced toxicity (Zhang et al. 2011).

3 Tumor Growth Model under Angiogenic Inhibition – Hahnfeldt Model

The current chapter discusses the tumor growth model under angiogenic inhibition. In Section 3.1, the nonlinear model is presented – first the original model published by Hahnfeldt et al. 1999 (Subsection 3.1.1), and later the simplified model with which I have worked (Subsection 3.1.2). Positivity (Sub-subsection 3.1.3), equilibrium points (Sub-subsection 3.1.4) and controllability of the model (Sub-subsection 3.1.5) are investigated. In Section 3.2, the linearized model is presented which was created using operating point linearization (Subsection 3.2.1). Non-zero steady states and stability (Section 3.2.2), and finally observability and controllability of the linearized model (Section 3.2.3) are examined.

3.1 Nonlinear Model

3.1.1 The Original Model

Hahnfeldt et al. elaborated a dynamic model for tumor growth under antiangiogenic therapy (Hahnfeldt et al. 1999). In their experiments mice were injected with Lewis lung carcinoma cells. After about $3-10$ days, mice were randomized into four groups. Three groups received different angiogenic inhibitors (angiostatin, endostatin and TNP-470), the fourth group was the control group (received injections of the vehicle alone).

The nonlinear model is defined by the equations:

$$V' = -\lambda_1 V \log\left(\frac{V}{K}\right) \tag{3.1}$$

$$K' = -\lambda_2 K + bV - dKV^{2/3} - eKg(t) \tag{3.2}$$

$$g(t) = \int_0^t c(t')exp(-clr(t-t'))dt'). \tag{3.3}$$

The tumor growth dynamics is described by (3.1) that is a Gompertzian growth, in order to describe precisely the physiological knowledge of tumor growth slowdown.

Consequently, the state variable V is the tumor volume in mm^3. The vascular support dynamics is described by (3.2), and incorporates the stimulatory effect of the tumor on vasculature support growth (with rate b), the inhibitory effect of the tumor and the vasculature (with rate d), and the effect of the angiogenic inhibitor (with rate e). The state variable K is the supporting vasculature volume in mm^3, and the input variable g is the concentration of the administered inhibitor in mg/kg. The third equation (3.3) incorporates the clearance of the inhibitor through a first-order system, and considers the administered inhibitor as input. Exact values of the parameters can be found in Table 3.1.

Table 3.1: Parameters of the original model of Hahnfeldt et al. 1999

Par.	**Exact value of the parameter**	**Meaning of the parameter**
λ_1	0.192 1/day	tumor growth rate
λ_2	0.0 1/day	spontaneous loss of functional vasculature[a]
d	0.00873 1/day·mm^2	endogenous inhibition of previously generated vasculature
b	5.85 1/day	stimulatory capacity of the tumor to the vasculature
e		inhibition of tumor vasculature due to administered inhibitor
	$e_E = 0.66$ kg/day·mg	administered inhibitor is endostatin
	$e_A = 0.15$ kg/day·mg	administered inhibitor is angiostatin
	$e_T = 1.3$ kg/day·mg	administered inhibitor is TNP-470
clr		clearance rate
	$clr_E = 1.7$ 1/day	administered inhibitor is endostatin
	$clr_A = 0.38$ 1/day	administered inhibitor is angiostatin
	$clr_T = 10.1$ 1/day	administered inhibitor is TNP-470

[a] Experiments show that this parameter is always zero.

3.1.2 The Simplified Model

The original model was analyzed and transformed in several studies (d'Onofrio and Cerrai 2009; d'Onofrio, A. Gandolfi, and Rocca 2009). One of the most important modifications is continuous infusion therapy (Ledzewicz and Schättler 2005), where the input (the inhibitor administration rate) is equal to the concentration of administered inhibitor

(serum level of inhibitor), therefore (3.3) is removed from the model. Note that in the works of D. A. Drexler, L. Kovács, et al. 2011; D. A. Drexler, J. Sápi, et al. 2012, the clearance of the inhibitor is also considered.

The simplified model of tumor growth can be described by a second-order nonlinear system of differential equations (A. D'Onofrio and A. Gandolfi 2004):

$$\dot{x}_1(t) = -\lambda_1 x_1(t) \log\left(\frac{x_1(t)}{x_2(t)}\right) \tag{3.4}$$

$$\dot{x}_2(t) = b x_1(t) - d x_1(t)^{2/3} x_2(t) - e x_2(t) u(t) \tag{3.5}$$

$$y = x_1. \tag{3.6}$$

In this description x_1 is the tumor volume, x_2 is the endothelial volume and u is the concentration of the administered inhibitor.

This tumor growth model has some limitations. The tumor can not be totally eliminated by the angiogenic therapy in reality, the smallest achievable tumor volume is the avascular state of the tumor; however this model does not grab this phenomenon. Thus, I incorporated a lower limit of 1 mm^3 into the state variables when I used the model for simulation.

Hereinafter the thesis discusses the simplified model (referred as model).

3.1.3 Positivity of the Model

Considering the real physiological system, the positivity of the model is a desirable property. Positivity means, that if the system variables are positive at an initial time t_0, then they remain positive (or nonnegative) for the whole time $t \geq t_0$. The positivity of the system may be verified by examining the rate of change of the state variables if they are (close to) 0. If the rate of change near 0 is positive or 0, then the positivity of the state variable is guaranteed. This requires that the solution of the differential equation exists and it is continuous. These conditions are true for this model with positive initial conditions; however the proof is omitted here.

Suppose, that $x_1(t_0), x_2(t_0) > 0$ for some initial time t_0, and examine the derivatives of the state variables at some time $t \geq t_0$. The rate of change of the tumor volume if it is close to zero is:

$$\lim_{x_1(t)\to 0} \dot{x}_1(t) = \lim_{x_1(t)\to 0} -\lambda_1 x_1(t) \log\left(\frac{x_1(t)}{x_2(t)}\right), \; t \geq t_0 \tag{3.7}$$

that is

$$\lim_{x_1(t)\to 0} \dot{x}_1(t) = 0,\ t \geq t_0 \tag{3.8}$$

even if $x_2(t) \to 0$ at the same time. Thus $x_1(t) \geq 0$ for $t \geq t_0$.

The rate of change of the vasculature support near zero is

$$\lim_{x_2(t)\to 0} \dot{x}_2(t) = \lim_{x_2(t)\to 0} bx_1(t) - dx_1(t)^{2/3}x_2(t) - ex_2(t)u,\ t \geq t_0 \tag{3.9}$$

that equals to

$$\lim_{x_2(t)\to 0} \dot{x}_2(t) = bx_1(t) \geq 0,\ t \geq t_0. \tag{3.10}$$

Thus $x_2(t) \geq 0$, for $t \geq t_0$. The positivity of the system is thus verified. Note that the positivity does not depend on the sign of the input u.

3.1.4 The Equilibrium Points of the Model

The equilibrium points of the model are the x_1, x_2 pairs at which the rate of change of the variables are zero. Thus the set of equilibrium points can be found by finding the solutions of

$$0 = -\lambda_1 x_1 \log\left(\frac{x_1}{x_2}\right) \tag{3.11}$$

$$0 = bx_1 - dx_1^{2/3}x_2 - ex_2u. \tag{3.12}$$

The trivial solution is $x_1 = x_2 = 0$ mm^3, however, since it is supposed that the initial tumor volume is not zero, and the therapy can not eliminate the whole tumor, I ignore this solution here and later. The nontrivial solution of (3.11) is $x_1 = x_2$. Let $y = x_1 = x_2$ be the volume satisfying (3.11). Then (3.12) reduces to

$$0 = by - dy^{5/3} - eyu. \tag{3.13}$$

Since $y \neq 0$ mm^3, this equation can be further simplified into

$$0 = b - dy^{2/3} - eu. \tag{3.14}$$

Suppose, that the input u is a constant positive value, denote this by u_∞. Then the

solution y_∞ of (3.14) is

$$y_\infty = \left(\frac{b - eu_\infty}{d} \right)^{3/2}, \tag{3.15}$$

which expresses that given a constant serum level u_∞, the resulting equilibrium tumor volue is y_∞. Given the desired y_∞ tumor volume, one can calculate the required constant inhibitor serum level as

$$u_\infty = \frac{b - dy_\infty^{2/3}}{e}. \tag{3.16}$$

This equlibrum point is asymptotically stable, since $b - eu_\infty$ is constant, and $y^{2/3}$ is strictly monotonously increasing for positive y, so the right-hand side of (3.14) is negative if $y > y_\infty$, and positive if $y < y_\infty$.

If there are no inhibitors present ($u = 0$), tumor and endothelial cells grow with no control input, and the steady state volume is a very high value. In this case steady state volume depends only on the type of the tumor and the patient:

$$y_\infty = \left(\frac{b}{d} \right)^{3/2}. \tag{3.17}$$

Tumor growth without antiangiogenic therapy leads to high steady state tumor volume ($y_\infty = 1.734 \cdot 10^4$ mm^3) and it represents the lethal steady state case (upper part of Figure 3.1). Using angiogenic inhibition, tumor size can be reduced from a high tumor volume to a low value. In the lower part of Figure 3.1 the effect of constant 5 mg/kg endostatin inhibition was simulated.

3.1.5 The Controllability of the Model

In the previous subsection the static behaviour of the system was analyzed. Using (3.16), one can calculate for example the amount of inhibitor needed to maintain the tumor in avascular state. However, equations (3.15) and (3.16) does not take the dynamics of the system into consideration. By applying the results of control engineering, we can affect the dynamics of the system that is the speed and characteristics of the tumor volume decreasing to the avascular state.

In order to apply control techniques, the controllability of the model needs to be checked. In this subsection the analyzis of controllability using the Lie Algebra Rank Condition (LARC) is performed (Isidori 1995).

The tumor model is a nonlinear, input affine, single input single output (SISO) system

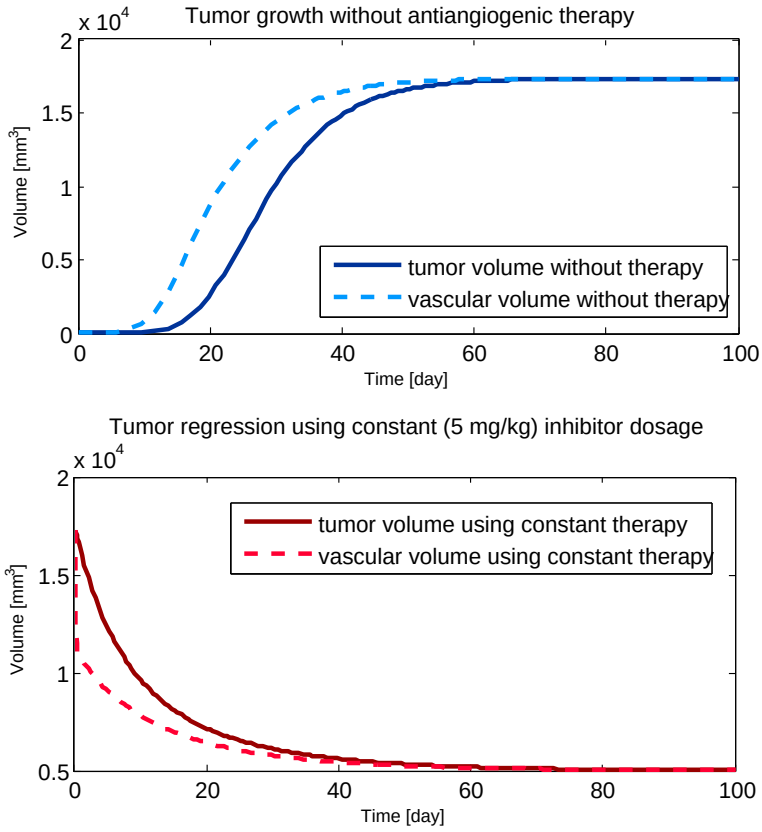

Figure 3.1: Tumor growth without angiogenic therapy (upper figure) and under constant angiogenic inhibition (lower figure)

that can be written in a general form as

$$\dot{x}(t) = f\left(x(t)\right) + g\left(x(t)\right) u(t) \tag{3.18}$$

$$y(t) = h\left(x(t)\right). \tag{3.19}$$

In the current application, the drift vector field at x is

$$f\left(x\right) = \begin{pmatrix} -\lambda_1 x_1 \log\left(\dfrac{x_1}{x_2}\right) \\ b x_1 - d x_1^{2/3} x_2 \end{pmatrix}, \tag{3.20}$$

the control vector field at the point x is

$$g(x) = \begin{pmatrix} 0 \\ -ex_2 \end{pmatrix}, \tag{3.21}$$

and the output vector field at x is

$$h(x) = x_1. \tag{3.22}$$

The nonlinear system is controllable, if the Lie algebra generated by the control and drift vector fields span the whole state space. Thus it is needed to check whether g and the Lie bracket of f and g are linearly independent. The Lie bracket of two vector fields at the point x is

$$[f, g](x) = (\partial_x f)(x) g(x) - (\partial_x g)(x) f(x). \tag{3.23}$$

The Lie bracket of the vector fields f and g at the point at is thus

$$[f, g](x) = \begin{pmatrix} -\lambda_1 e x_1 \\ b e x_1 \end{pmatrix}. \tag{3.24}$$

The linear independence of g and $[f, g]$ can be checked by examining the rank of the matrix valued function Δ with columns g and $[f, g]$:

$$\Delta(x) = \begin{bmatrix} 0 & -\lambda_1 e x_1 \\ -ex_2 & b e x_1 \end{bmatrix}, \tag{3.25}$$

that has the determinant

$$\det(\Delta(x)) = -\lambda_1 e^2 x_1 x_2. \tag{3.26}$$

The matrix $\Delta(x)$ is full rank, whenever its determinant is not zero. From (3.26) the determinant is zero if a) $x_1 = 0$ mm^3, however this case was already excluded; or b) $x_2 = 0$ mm^3. In these situations the model is not controllable. Note that if $x_2 = 0$ mm^3, then the tumor is in the avascular state, and the input required to maintain the tumor in that state can be calculated using the static equation (3.16). Note that $\Delta(x)$ has the same image space as the linear subspace spanned by controllability Lie algebra (Isidori 1995), thus the system is controllable in every point x where (3.26) is not zero. We can now conclude that the nonlinear model of tumor growth is controllable whenever $x_1 \neq 0$ mm^3 and $x_2 \neq 0$ mm^3.

3.2 Linear Model

3.2.1 Operating Point Linearization

The tumor model is nonlinear, but the control techniques I apply later are linear, thus a linear approximation of the tumor growth model is needed for design purposes. A linear dynamic model is usually written in the form

$$\dot{x}(t) = Ax(t) + Bu(t) \tag{3.27}$$
$$y(t) = Cx(t) + Du(t), \tag{3.28}$$

where (3.27) defines the dynamics of the system, and (3.28) defines the output of the system. The linear approximation of the tumor growth model is acquired by first-order approximation at specific operating point x and $u = 0$ mg/kg, i.e.

$$A(x,u) = \left(\partial_x(f+gu)\right)(x,u), \tag{3.29}$$
$$B(x,u) = \left(\partial_u(f+gu)\right)(x,u), \tag{3.30}$$
$$C(x,u) = \left(\partial_x(h)\right)(x,u), \tag{3.31}$$
$$D(x,u) = \left(\partial_u(h)\right)(x,u), \tag{3.32}$$

which yields in this special case

$$A(x) = \left(\partial_x f\right)(x), \tag{3.33}$$
$$B(x) = g(x), \tag{3.34}$$
$$C(x) = \left(\partial_x h\right)(x), \tag{3.35}$$
$$D(x) = 0. \tag{3.36}$$

The matrices of the linear model acquired at the operation point x are

$$A = \begin{bmatrix} -\lambda_1 \cdot \log\left(\frac{x_1}{x_2}\right) - \lambda_1 & \lambda_1 \frac{x_1}{x_2} \\ b - \frac{2}{3} d \cdot x_1^{-\frac{1}{3}} \cdot x_2 & -d \cdot x_1^{\frac{2}{3}} \end{bmatrix} \tag{3.37}$$

$$B = \begin{bmatrix} 0 \\ -ex_2 \end{bmatrix} \tag{3.38}$$

$$C = \begin{bmatrix} 1 & 0 \end{bmatrix} \tag{3.39}$$

$$D = \begin{bmatrix} 0 \end{bmatrix} \tag{3.40}$$

The vector x is chosen such that both of its components are equal. Let x_{12} be the value of the tumor volume at the operating point x, then the vector x is $x = [x_{12}, x_{12}]^\top$.

3.2.2 Non-Zero Steady States and Stability of the Linearized Model

As it was discussed in Subsection 3.1.4, if the system is in steady state (the system is in an equilibrium point), tumor volume and vascular volume are equal ($x_1 = x_2$). Let this steady state volume be $x_1 = x_2 = x_{10}$. Then the system matrix A (3.37) reduces to

$$A_\infty = \begin{bmatrix} -\lambda_1 & \lambda_1 \\ b - \frac{2}{3} d \cdot x_{10}^{\frac{2}{3}} & -d \cdot x_{10}^{\frac{2}{3}} \end{bmatrix}. \tag{3.41}$$

The characteristic equation of the system matrix A in general form:

$$\text{If } A = \begin{bmatrix} a_{11} & a_{12} \\ a_{21} & a_{22} \end{bmatrix}, \text{then}$$

$$\det(\lambda I - A) = (\lambda - a_{11})(\lambda - a_{22}) - a_{12}a_{21}. \tag{3.42}$$

The characteristic equation of A_∞ is

$$\begin{aligned}\Delta(s) &= (s-(-\lambda_1))\cdot\left(s-\left(-d\cdot\sqrt[3]{x_{10}{}^2}\right)\right)-\lambda_1\cdot\left(b-\frac{2}{3}d\cdot\sqrt[3]{x_{10}{}^2}\right)\\ &= s^2+\left(d\cdot\sqrt[3]{x_{10}{}^2}+\lambda_1\right)\cdot s+\frac{5}{3}d\lambda_1\sqrt[3]{x_{10}{}^2}-\lambda_1 b. \end{aligned} \tag{3.43}$$

The roots of the characteristic equation, i.e. the eigenvalues of the system matrix are

$$s_{1,2}=\frac{-\left(d\cdot\sqrt[3]{x_{10}{}^2}+\lambda_1\right)\pm\sqrt{\left(d\cdot\sqrt[3]{x_{10}{}^2}+\lambda_1\right)^2-4\cdot\left(\frac{5}{3}d\lambda_1\sqrt[3]{x_{10}{}^2}-\lambda_1 b\right)}}{2}. \tag{3.44}$$

If $x_{10}=0$ mm^3, there is a stable and an unstable pole in the system. Increasing the x_{10} operating point, the stable pole accelerates and the unstable pole becomes stable. If $x_{10}=8062$ mm^3, the system is on the boundary of stability. For high x_{10} values the poles will form stable complex conjugate pairs.

3.2.3 Observability and Controllability of the Linearized Model

Controllability and observability matrices are the following in general form:

$$M_c=\begin{bmatrix} B & AB & A^2B & \dots & A^{n-1}B \end{bmatrix} \tag{3.45}$$

$$M_o=\begin{bmatrix} C \\ CA \\ CA^2 \\ \dots \\ CA^{n-1} \end{bmatrix}, \tag{3.46}$$

where n is the order of the system. The model is controllable if M_c has full rank n, and observable if M_c has full rank n.

The linearized model in non-zero steady state has the following controllability and observability matrices:

$$M_c = \begin{bmatrix} 0 & -e\lambda_1 x_{10} \\ -ex_{10} & edx_{10}^{\frac{5}{3}} \end{bmatrix} \tag{3.47}$$

$$M_o = \begin{bmatrix} 1 & 0 \\ -\lambda_1 & \lambda_1 \end{bmatrix}. \tag{3.48}$$

The matrices in (3.47) and (3.47) are full rank for every $x_{10} \neq 0$, thus the linearized system is controllable and observable in every operating point.

4 Controller Design for the Tumor Growth Model

Most of the researchers applied the Hahnfeldt model to design controller and perform simulations in the field of antiangiogenic control.

The most relevant modifications of the original model were done by A. D'Onofrio and A. Gandolfi 2004; and Ergun, Camphausen, and Wein 2003. Ledzewicz and Schättler 2007; Ledzewicz and Schättler 2008 discussed the optimal scheduling problem of a given amount of inhibitors in order to minimize the primary tumor volume, and in Ledzewicz and Schättler 2009 they investigated the extension of the model. D'Onofrio and Gandolfi designed bang-bang control (A. D'Onofrio and A. Gandolfi 2004), while in Ergun, Camphausen, and Wein 2003; Ledzewicz and Schättler 2007, singular controls were designed. Ledzewicz, J. Marriott, et al. 2010 investigated suboptimal strategies, piecewise constant protocols. Kassara and Moustafid 2011 applied a set-valued control method.

A. D'Onofrio, Ledzewicz, et al. 2009 examined a multi-control problem, where angiogenic inhibitors were scheduled in combination with a chemotherapeutic agent. They solved this problem by bang-bang control; the optimal control contains a segment where the control signal is singular and follows a time-varying feedback. In Ledzewicz and Schättler 2007; Ledzewicz, J. Marriott, et al. 2010, the control strategy is based on the tumor volume and the carrying capacity. However, in clinical practice; only tumor volume can be measured.

Nonetheless, all these studies were only theoretical, the applied control strategies are nonlinear, and their practical feasibility was not discussed.

The current chapter is organized as follows: in Section 4.1, the linear state-feedback control, which was applied to the Hahnfeldt model is presented. First, the state-feedback design is discussed (Subsection 4.1.1) using pole placement (Sub-subsection 4.1.1) and LQ optimal control (Sub-subsection 4.1.1), after linear observer design is presented (Subsection 4.1.2). The simulation results of the four designed controllers (state feedback with pole placement, LQ control method, state feedback with pole placement and observer,

LQ control method with observer) can be found in Subsection 4.1.3. The section ends with the conclusions in Subsection 4.1.4.

In the second section (Section 4.2), the robust (H_∞) control, which was applied to the Hahnfeldt model is presented. The control design is discussed in Subsection 4.2.1. In this subsection desing structure (Sub-subsection 4.2.1), H_∞ suboptimal solutions (Sub-subsection 4.2.1) and the choosing of the ideal system and the weighting functions in light of physiological aspects (Sub-subsection 4.2.1) are discussed in detail. Subsection 4.2.2 contains the simulation results and Subsection 4.2.3 discusses the conclusions. In Subsection 4.2.4, one can find the investigation of robust control with sensitivity analysis (sensitivity analysis can be found in Sub-subsection 4.2.4, while the effect of parametric perturbation on the closed-loop system can be found in Subsubsection 4.2.4).

The chapter ends with Thesis Group 1 in Section 4.3.

4.1 Linear State-Feedback Control

In this section I apply a linear control technique, state-feedback to the nonlinear tumor growth model. I use two different design methodologies: Pole Placement and Linear Quadratic (LQ) optimal control. Since these control strategies require the knowledge of the state-variables, but in practice, usually only the tumor volume is measured, I design a linear state observer, that gives an estimation of the state variables based on input and output measurements. The stability and the equilibrium points of the closed-loop system are analyzed.

4.1.1 State-Feedback Design

In the case of a state-feedback, the input of the system is calculated as a linear combination of the state variables:

$$u = -Kx, \tag{4.1}$$

where K is a matrix in general. In this case, the model is a second-order SISO system, thus K is a vector with two components, i.e. $K = [k_1, k_2]$.

Since the real control input is the inhibitor serum level that can not be negative, nonnegativity of the input signal is required. The input signal is

$$u = -k_1 x_1 - k_2 x_2, \tag{4.2}$$

which is nonnegative for all $x_1, x_2 \geq 0$ mm^3 if

$$k_1 \leq 0 \tag{4.3}$$

$$k_2 \leq 0. \tag{4.4}$$

Thus (4.3) and (4.4) give conditions on the choice of the vector K, in order to satisfy the nonnegativity of the input.

Using state-feedback on the nonlinear model, the dynamics of the closed-loop system becomes

$$\dot{x}_1(t) = -\lambda_1 x_1(t) \log\left(\frac{x_1(t)}{x_2(t)}\right) \tag{4.5}$$

$$\dot{x}_2(t) = bx_1(t) - dx_1^{2/3}(t)x_2(t) - ex_2(t)\left(-k_1 x_1(t) - k_2 x_2(t)\right). \tag{4.6}$$

The nontrivial equilibrium points can be calculated as checking when (4.5) and (4.6) are zero. The first equation is zero whenever the state-variables are equal, i.e. $x_1 = x_2$. Using the notation $y := x_1 = x_2$, the second equation equals becomes

$$0 = by - dy^{5/3} + ey^2\left(k_1 + k_2\right). \tag{4.7}$$

Since the $y = 0$ mm^3 solution is excluded for physiological reasons (the tumor regression stops when the tumor reaches its avascular state), the equation can be simplified into

$$0 = -\frac{d}{e}y^{2/3} + \left(k_1 + k_2\right)y + \frac{b}{e}. \tag{4.8}$$

This equation can be rearranged into

$$\frac{d}{e}y^{2/3} = \left(k_1 + k_2\right)y + \frac{b}{e} \tag{4.9}$$

that can be visualized as the intersection of the curve $d/e\, y^{2/3}$, and the line $(k_1 + k_2)\, y + b/e$ as in Figure 4.1. Since the tumor model is positive, and $y = 0$ mm^3 is excluded, $y > 0$ mm^3 holds, and from the (4.3)-(4.4) positivity conditions of the input signal the slope of the line is negative, and because of the positivity of the parameters b and e, the offset of the line is positive.

Denote the intersection point of the line and the curve with y^*. Then the $[y^*, y^*]^\top$ point is the equilibrium point of the system. This equilibrium point is asymptotically stable, since if $y > y^*$, the right-hand side of (4.8) is negative, because $y^{2/3}$ is strictly

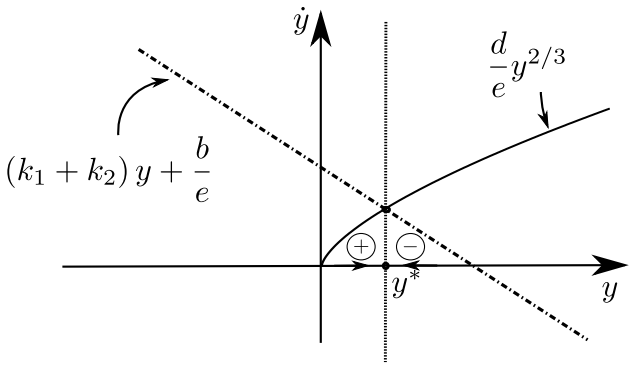

Figure 4.1: The equilibrium point of the closed-loop system. The equilibrium y^* is the intersection of the curve $d/e\,y^{2/3}$ (solid) and the line $(k_1+k_2)\,y+b/e$ (dashdot). The rate of change of the vasculature volume is the difference of the line and the curve.

increasing, while $(k_1+k_2)\,y$ is strictly decreasing, thus the vasculature volume decreases. If $y<y^*$, then the right-hand side of (4.8) is positive, thus the vasculature volume is increasing. Graphically this can be viewed as the right-hand side of (4.8) is positive, if the curve $d/ey^{2/3}$ is smaller than the line, while it is negative, if the curve is greater than the line (Figure 4.1). The figure also shows, that the equilibrium point tends to zero as k_1+k_2 tends to minus infinity. From these results we can conclude, that if we apply a state-feedback K with negative elements, then the closed loop system is stable with a positive equilibrium point and the input signal is always positive, and if the norm of K becomes larger, the positive equilibrium point becomes smaller.

The exact value of the equilibrium y^* can be acquired by solving the fractional order polynomial equation (4.8). Write the equation in a general form with coefficients $c_1=-d/e<0$, $c_2=k_1+k_2<0$, $c_3=b/e>0$ as

$$c_1y^{2/3}+c_2y+c_3=0. \tag{4.10}$$

This equation can be rearranged into

$$-c_1y^{2/3}=c_2y+c_3. \tag{4.11}$$

After cubing this equation, we get

$$-c_1^3y^2=(c_2y+c_3)^3. \tag{4.12}$$

After rearranging the terms, we get a simple third-order polynomial equation

$$c_2^3 y^3 + \left(3c_2^2 c_3 + c_1^3\right) y^2 + 3c_2 c_3^2 y + c_3^3 = 0, \tag{4.13}$$

that can be solved either numerically or symbolically. The intersection point y^* in Figure 4.1 is the only real solution of (4.13).

Pole Placement

In control engineering literature, there are several ways of designing the feedback matrix K. One strategy is to describe the desired dynamics of the closed-loop system. If the system to be controlled is linear, with dynamics $\dot{x}(t) = Ax(t) + Bu(t)$, then the closed-loop system with the state-feedback $u = -Kx$ admits the differential equation

$$\dot{x}(t) = (A - BK)\, x(t) = A_c x(t). \tag{4.14}$$

In the course of pole placement, we define the desired poles of the closed-loop system, i.e. the eigenvalues of A_c, and choose K such that the poles of A_c will be the ones we have specified. This can be achieved using the Ackermann's formula

$$K = e_n^\top M_c^{-1}\,(A, B)\, \varphi_c\,(A)\,, \tag{4.15}$$

where e_n is the nth unit vector, M_c is the controllability matrix, and $\varphi_c\,(A)$ is the characteristic polynomial of A_c evaluated at A.

The controllability matrix is defined as

$$M_c\,(A, B) = \begin{bmatrix} B & AB \end{bmatrix} \tag{4.16}$$

that is full rank if the linear model parameters A, B were calculated at a nonzero operating point, since we have already showed that the system is controllable if $x_1 \neq 0$ mm^3 and $x_2 \neq 0$ mm^3.

LQ Optimal Control

The aim of the LQ optimal control design strategy is not to describe the poles of the closed-loop system, but to find the input u that minimizes the control transients defined

as the linear functional

$$F(x,u) = \int_{-\infty}^{\infty} \left(x^{\top}(t) Q x(t) + u^{\top}(t) R u(t) \right) dt \tag{4.17}$$

with the linear constraints

$$\dot{x}(t) = Ax(t) + Bu(t), \tag{4.18}$$

where R and Q are positive definite design matrices. A typical choice for the matrix Q is $Q = C^T C$, in this case the first term in the linear functional in the case of a SISO system is $x^{\top} Q x = x^{\top} C^{\top} C x = (Cx)^{\top} Cx = y^{\top} y = y^2$, and the functional reduces to the form

$$F(x,u) = \int_{-\infty}^{\infty} \left(y^2(t) + R u^2(t) \right) dt, \tag{4.19}$$

that has to be minimized with the constraint (4.18). The value of R in (4.19) affects the total input during the control transient. Large R attempts to minimize the input, while small R allows high inputs (L. Kovács, Ferenci, et al. 2012). The solution of the minimization problem is in the form of a statefeedback $u = -Kx$, with the state-feedback matrix

$$K = R^{-1} B^{\top} P, \tag{4.20}$$

where P is the positive definite solution of the Control Algebraic Ricatti Equation (CARE)

$$PA + A^{\top} P - P B R^{-1} B^{\top} P + Q = 0. \tag{4.21}$$

One can see the design structure of linear state-feedback control in Figure 4.2.

4.1.2 Linear Observer Design

Application of state-feedback requires the knowledge of the state variables. However, in the case of the tumor model, the state variable x_2 (vascular volume) can not be measured, thus it is necessary to use an estimation for this variable (J. Sápi, D. A. Drexler, I. Harmati, et al. 2012; L. Kovács, Szalay, Ferenci, D. A. Drexler, et al. 2011; L. Kovács, Szalay, Ferenci, J. Sápi, et al. 2012). In the case of linear systems, the application of state observers solve this problem. A state-observer is a dynamic system with the differential equation

$$\dot{z}(t) = Fz(t) + Gy(t) + Hu(t), \tag{4.22}$$

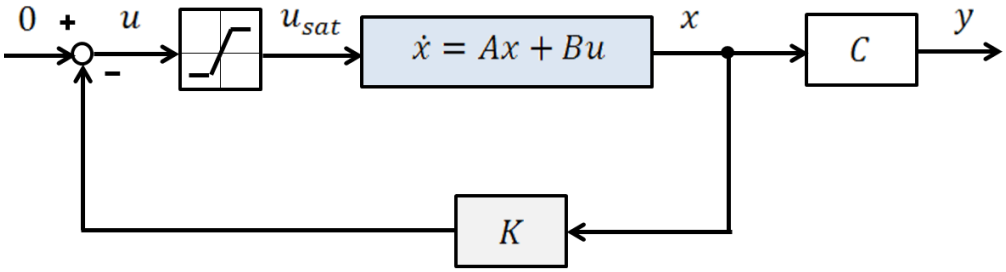

Figure 4.2: Design structure for linear state-feedback control. In the case of pole placement, the feedback matrix K is calculated by using the Ackermann's formula; in the case of LQ optimal control, K is calculated from the solution of the CARE equation. Since linear controller strategies may result in high valued control signal, saturation was applied for the control signal in light of physiological aspects.

where z is the internal state of the observer, y is the output of the observed system, while u is the input of the observed system. The internal state z serves as an estimation to the x state of the original system. The design matrices G, F and H are acquired using the design equations

$$G = \left(e_n^\top M_c^{-1} \left(A^\top, C^\top\right) \varphi_o(A^\top)\right)^\top \tag{4.23}$$

$$F = A - GC \tag{4.24}$$

$$H = B. \tag{4.25}$$

The expression $\varphi_o\left(A^\top\right)$ in (4.23) is the characteristic polynomial of the matrix A_o describing the dynamics $\dot{z}_e(t) = A_o z_e(t)$ of the estimation error in the case of a linear system, evaluated at the matrix $A^\top$. The eigenvalues of the matrix A_o have to be defined during the design process. Note that the error dynamics is defined by A_o only if the observed system is linear, however it is not the case in this situation. The error dynamics in the case of a nonlinear observed system will be analyzed later.

The equations of the closed-loop system with the application of state-feedback and the

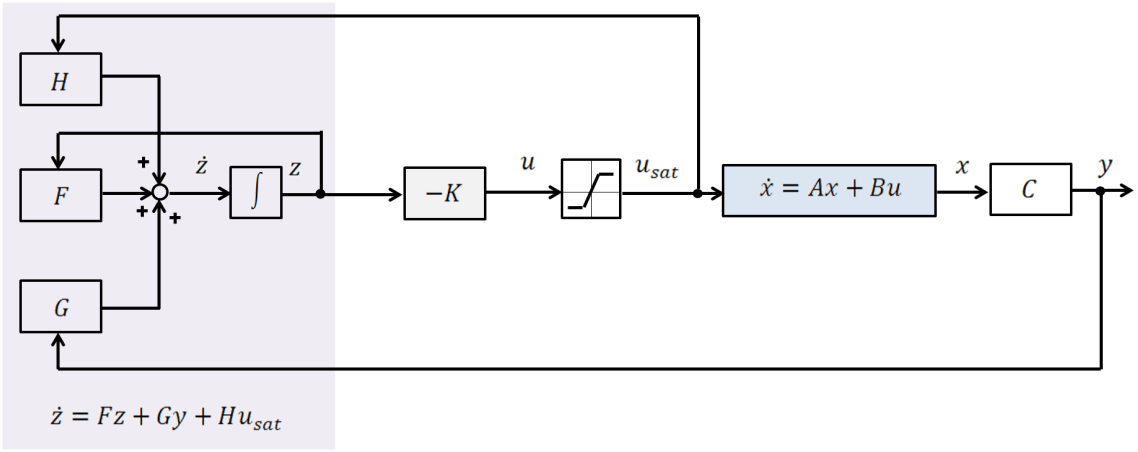

Figure 4.3: Design stucture for linear state-feedback with observer. Since linear controller strategies may result in high valued control signal, saturation was applied for the control signal in light of physiological aspects.

linear observer is

$$\dot{x}_1(t) = -\lambda_1 x_1(t) \log\left(\frac{x_1(t)}{x_2(t)}\right) \tag{4.26}$$

$$\dot{x}_2(t) = b x_1(t) - d x_1^{2/3}(t) x_2(t) - e x_2(t) u(t) \tag{4.27}$$

$$\dot{z}(t) = F z(t) + G y(t) + H u(t) \tag{4.28}$$

$$u(t) = -K z(t). \tag{4.29}$$

The last equation expresses the fact that the state-feedback is based on the z estimated state variables instead of the original x variables. However, this affects the equilibrium of the closed-loop system. In the equilibrium point, let $y := x_1 = x_2$, and $u = \dfrac{b - dy^{2/3}}{e}$ the equilibra for equations (4.26) and (4.27). The equilibrium for the observer dynamics (4.28) is

$$0 = Fz + Gy + H\frac{b - dy^{2/3}}{e}, \tag{4.30}$$

from which we have

$$z = F^{-1}\left(-Gy - H\frac{b - dy^{2/3}}{e}\right). \tag{4.31}$$

Substituting this result and the equilibrium for u into (4.29) results in

$$\frac{b - dy^{2/3}}{e} + KF^{-1}\left(-Gy - H\frac{b - dy^{2/3}}{e}\right) = 0, \tag{4.32}$$

that can be rearranged into the form

$$-\frac{d}{e}\left(1 - KF^{-1}H\right)y^{2/3} - KF^{-1}Gy + \left(1 - KF^{-1}H\right)\frac{b}{e} = 0. \tag{4.33}$$

This equation for the equilibrium tumor volume has the same form as (4.10), with coefficients

$$c_1 = -\frac{d}{e}\left(1 - KF^{-1}H\right) \tag{4.34}$$

$$c_2 = -KF^{-1}G \tag{4.35}$$

$$c_3 = \left(1 - KF^{-1}H\right)\frac{b}{e}. \tag{4.36}$$

The steady state tumor volume is the solution of (4.33), and is asymptotically stable, if the coefficients of the polynomial satisfy $c_1 < 0$, $c_2 < 0$ and $c_3 > 0$, as it has already be shown in the previous subsections. These conditions are satisfied if

$$1 - KF^{-1}H > 0 \tag{4.37}$$

$$KF^{-1}G > 0. \tag{4.38}$$

If the observed system was linear, the steady state estimation error of a well-designed observer was zero. However, in this case the observed system is nonlinear, thus there is estimation error even in an equilibrium point. Define the estimation error of the observer as

$$z_e = x - z, \tag{4.39}$$

then the differential equation for the estimation error is

$$\dot{z_e}(t) = \dot{x}(t) - \dot{z}(t). \tag{4.40}$$

Using the expressions (3.18) and (4.28) for the derivatives, we get

$$\dot{z_e}(t) = f\left(x(t)\right) + g\left(x(t)\right)u(t) - Fz(t) - Gy(t) - Hu(t). \tag{4.41}$$

Substituting the state-feedback equation (4.29) and using $y(t) = Cx(t)$, in addition

adding $Fx - Fx$ results in

$$\dot{z_e}(t) = f\left(x(t)\right) - g\left(x(t)\right) Kz(t) - Fz(t) - GCx(t) + HKz(t) + Fx(t) - Fx(t). \quad (4.42)$$

After some manipulation we get

$$\dot{z_e}(t) = Fz_e(t) + \Big(f\left(x(t)\right) - Fx(t) - GCx(t)\Big) + \Big(H - g\left(x(t)\right)\Big) Kz(t). \quad (4.43)$$

At the equilibrium point, $\dot{z_e}(t) = 0$, thus we can express z_e as

$$z_e = -F^{-1}\left(\left(f\left(x\right) - Fx - GCx\right) + \left(H - g\left(x\right)\right) Kz\right). \quad (4.44)$$

At the equilibrium point, $f\left(x\right) - g\left(x\right) Kz = 0$ also holds, thus

$$z_e = -F^{-1}\left(-Fx - GCx + HKz\right). \quad (4.45)$$

Substituting $z = x - z_e$, after some manipulation we get the result for the estimation error at the steady-state

$$z_e = \left(I + \left(I - F^{-1}HK^{-1}\right)^{-1} F^{-1}GC\right) x. \quad (4.46)$$

If the equilibrium point of the tumor volume calculated as the solution of (4.33) is y^*, then the estimation error in the equilibrium is

$$z_e = \left(I + \left(I - F^{-1}HK\right)^{-1} F^{-1}GC\right) \begin{bmatrix} y^* \\ \\ y^* \end{bmatrix}. \quad (4.47)$$

One can see the design stucture of linear state-feedback with observer in Figure 4.3.

4.1.3 Simulation Results

The model parameters used at the simulations are the ones described in Hahnfeldt et al. 1999: $\lambda_1 = 0.192$ 1/day, $b = 5.85$ 1/day, $d = 0.00873$ 1/day·mm^2, $e = 0.66$ 1/day·mg (using endostatin as angiogenic inhibitor). The tumor volume was saturated from below at 1 mm^3 to imitate that the tumor volume can not fall below the avascular state.

The model was linearized in different operation points for controller design purposes as described by (3.37)-(3.40). Three operating points were analyzed (low operating

point: $x_{10} = 100$ mm^3, medium operating point: $x_{10} = 5000$ mm^3, high operating point: $x_{10} = 10000$ mm^3).

Four different control strategies were realized under *MATLAB 7.9.0 (R2009b)* environment: (C1) state feedback with pole placement, (C2) LQ control method, (C3) state feedback with pole placement and observer, (C4) LQ control method with observer. The controller design was carried out according to the linearized model; however the simulations were carried out with the nonlinear model. The simulations were run from the 0th day until the 100th day of the therapy. The initial value of the tumor volume and the endothelial volume was the uncontrolled equilibrium in every case, i.e. both volumes were 17340 mm^3 (see Subsection 3.1.4 and Figure 3.1).

The desired poles in the case of pole placement were defined as a times the fastest stable pole of the linearized system, where a is an acceleration parameter. I have chosen this strategy, since in this case the amount of acceleration depends on the pole of the linearized system, so undesired oscillations can be avoided that occur if the specified pole is much faster than the system. The disadvantage of this strategy is that the closed-loop system will be slow, if the poles of the system are slow. Three different values of the parameter a were analyzed: $a = 3$, $a = 5$ and $a = 8$.

The poles of the observer were chosen as five times the fastest stable pole of the linearized system.

The positive definite matrices in the case of LQ design were chosen as follows: $Q = C^\top C$, thus the linear functional to be minimized is (4.19), and the value of R, being a scalar in this case, was varied in the interval $[10^3, 10^6]$.

Since linear controller strategies may result in high or negative valued control signal, saturation was applied for each controller. Negative valued control signal is physically not feasible, however the control signal does not have to be saturated from below in our case, since it was proved in Subsection 4.1.1 that if one apply a state-feedback K with negative elements, then the closed loop system is stable with a positive equilibrium point and the input signal is always positive. High valued control signal is physiologically dangerous, thus the control signal is saturated from above. The limits of the saturation were chosen such that the control signal is physiologically feasible, the analyzed limits are $u_{max} = 25$ mg/kg, $u_{max} = 15$ mg/kg and $u_{max} = 13$ mg/kg.

The controller strategies were evaluated by three criteria: (i) the total concentration of the administered inhibitor during the treatment (mg/kg), (ii) the steady state inhibitor concentration at the end of the treatment (mg/kg), (iii) the steady state tumor volume at the end of the treatment (mm^3).

Simulation results (shown in Table 4.1) are divided into five groups.

Evaluated criterion: total concentration of the administered inhibitor during the treatment (mg/kg)		State feedback with pole placement (C1)			LQ control method (C2)		State feedback with pole placement and observer (C3)			LQ control method with observer (C4)	
		accel.: 3	accel.: 5	accel.: 8	R: 10^3	R: 10^6	accel.: 3	accel.: 5	accel.: 8	R: 10^3	R: 10^6
operating point: 100 mm^3	saturation: 25 mg/kg	1424	1502	1580	1292	1289	1388	1463	1531	1271	1269
	saturation: 15 mg/kg	1272	1328	1383	1169	1167	1241	1298	1353	1151	1152
	saturation: 13 mg/kg	1224	1277	1300	1132	1130	1196	1248	1286	1118	1116
operating point: 5000 mm^3	saturation: 25 mg/kg	866	1014	1126	1131	657	633	767	900	1022	618
	saturation: 15 mg/kg	834	954	1041	1044	649	625	745	859	1022	616
	saturation: 13 mg/kg	823	935	1015	1017	645	620	737	846	997	612
operating point: 10000 mm^3	saturation: 25 mg/kg	546	777	954	1129	523	0	98	324	1101	480
	saturation: 15 mg/kg	546	768	909	1042	523	0	98	324	1021	480
	saturation: 13 mg/kg	546	761	894	1016	522	0	98	324	996	480

Evaluated criterion: steady state inhibitor concentration at the end of the treatment (mg/kg)		State feedback with pole placement (C1)			LQ control method (C2)		State feedback with pole placement and observer (C3)			LQ control method with observer (C4)	
		accel.: 3	accel.: 5	accel.: 8	R: 10^3	R: 10^6	accel.: 3	accel.: 5	accel.: 8	R: 10^3	R: 10^6
operating point: 100 mm^3	saturation: 25 mg/kg	8.8	8.8	8.9	8.7	8.7	8.8	8.8	8.8	8.7	8.7
	saturation: 15 mg/kg	8.8	8.8	8.9	8.7	8.7	8.8	8.8	8.9	8.7	8.7
	saturation: 13 mg/kg	8.8	9.6	13.0	8.7	8.7	8.8	9.0	10.0	8.7	8.7
operating point: 5000 mm^3	saturation: 25 mg/kg	7.2	7.9	8.3	8.3	5.8	5.6	6.5	7.3	8.2	5.5
	saturation: 15 mg/kg	7.2	7.9	8.3	8.3	5.8	5.6	6.5	7.3	8.2	5.5
	saturation: 13 mg/kg	7.1	7.9	8.3	8.3	5.8	5.6	6.5	7.3	8.2	5.5
operating point: 10000 mm^3	saturation: 25 mg/kg	5.2	6.7	7.6	8.3	4.8	0.0	0.9	3.1	8.2	4.4
	saturation: 15 mg/kg	5.2	6.7	7.6	8.3	4.8	0.0	0.9	3.1	8.2	4.4
	saturation: 13 mg/kg	5.2	6.7	7.6	8.3	4.8	0.0	0.9	3.1	8.2	4.4

Evaluated criterion: steady state tumor volume at the end of the treatment (mm^3)		State feedback with pole placement (C1)			LQ control method (C2)		State feedback with pole placement and observer (C3)			LQ control method with observer (C4)	
		accel.: 3	accel.: 5	accel.: 8	R: 10^3	R: 10^6	accel.: 3	accel.: 5	accel.: 8	R: 10^3	R: 10^6
operating point: 100 mm^3	saturation: 25 mg/kg	10	4	2	50	52	18	7	3	63	65
	saturation: 15 mg/kg	10	4	2	50	52	18	7	3	64	65
	saturation: 13 mg/kg	11	4	3	50	52	18	7	3	64	65
operating point: 5000 mm^3	saturation: 25 mg/kg	1458	628	265	259	3608	3966	2425	1289	334	4105
	saturation: 15 mg/kg	1478	628	265	259	3608	3966	2425	1289	334	4105
	saturation: 13 mg/kg	1478	628	265	259	3608	3966	2425	1289	334	4105
operating point: 10000 mm^3	saturation: 25 mg/kg	4703	2049	886	264	5459	17350	14650	9224	338	6150
	saturation: 15 mg/kg	4703	2049	886	264	5459	17350	14650	9224	338	6150
	saturation: 13 mg/kg	4703	2049	886	264	5459	17350	14650	9224	339	6150

Notation: Group 1 | Group 2 | Group 3 | Group 4 | Group 5

Table 4.1: Simulation results for all of the investigated controller types. Notation: *Group 1*: tumor volume was not reduced; *Group 2*: high steady state tumor volume; *Group 3*: medium steady state tumor volume; *Group 4*: low steady state tumor volume; *Group 5*: nearly avascular steady state tumor volume, successful control. Simulation period was 100 days.

Group 1: controller (C3) in high operating point with $a = 3$ acceleration. These controls were inefficient, because the *tumor volume did not decrease at all*. The reason is that the desired poles of the closed-loop system are too slow, which results in too low control signal.

Group 2: controller (C1) in high operating point with $a = 3$ acceleration, controller (C2) in medium and high operating point with weighting matrix $R = 10^6$, controller (C3) in medium operating point with $a = 3$ acceleration, controller (C3) in high operating point with $a = 5$ and $a = 8$ acceleration, controller (C4) in medium and high operating point with weighting matrix $R = 10^6$. These controls resulted in *high steady state tumor volume*. In the case of pole placement – (C1) and (C3) controllers – it can be explained by the same reason as it was in Group 1: the desired poles of the closed-loop system are too slow. In the case of LQ control method – (C2) and (C4) controllers – the weighting matrix R was chosen to a high value in order to minimize the input (according to cost-effectiveness and side effect reasons). However, the cost-effectiveness point of view should not totally overwrite the therapeutic aspect. As a general rule, it can be said, that increasing the operating point, the control signals become too low to sufficiently reduce the tumor volume (because of the nonlinearity of the system).

Group 3: controller (C1) in medium operating point with $a = 3$ and $a = 5$ acceleration, controller (C1) in high operating point with $a = 5$ and $a = 8$ acceleration, controller (C3) in medium operating point with $a = 5$ and $a = 8$ acceleration. These controls resulted in *medium steady state tumor volume*. Also in this group it can be observed that small acceleration and high operating point eventuate in great values of tumor volume; and it is especially true for the additive effect of these two parameters. In addition, in this group one can also notice the fact that controllers with observer always have worse effect than controllers without observer. It can be explained by the state variable estimation of the observer, since if the system is nonlinear, the estimation error is never zero as it is expressed by (4.47).

Group 4: controller (C1) in medium operating point with $a = 8$ acceleration, controller (C2) in medium and high operating point with weighting matrix $R = 10^3$, controller (C4) in medium and high operating point with weighting matrix $R = 10^3$. These controls eventuated in *low steady state tumor volume*. Analyzing this group, two important results become clear. On the one hand, we can state that the only effective solution for high operating points is LQ control method with weighting matrix $R = 10^3$. On the other hand, we can ascertain that LQ control method with weighting matrix $R = 10^3$ results in better solution according to two criteria than LQ control method with weighting matrix $R = 10^6$. Applying weighting matrix $R = 10^6$, approximately half amount of

total dosage of the administered inhibitor have to be used than in the case of weighting matrix $R = 10^3$; however the steady state tumor volume is not two times bigger, but more than ten times bigger in the case of weighting matrix $R = 10^6$ than in the case of weighting matrix $R = 10^3$. Since our aim is to find an optimal solution according to multiple criteria, we have to investigate lower values of weighting matrix R.

Group 5: all controllers in low operating point resulted in *nearly avascular steady state tumor volume*, i.e. these *controls are successful*. From successful controllers, suboptimal controllers can be chosen which have the best result for a certain criterion. The best result for total concentration of the administered inhibitor during the treatment (1116 mg/kg) was achieved by controller (C4) with 13 mg/kg saturation and weighting matrix $R = 10^6$. The best result for the steady state inhibitor concentration at the end of the treatment (8.7 mg/kg) was achieved by (C2) and (C4) controllers (the same result with every parameters). Finally, the best result for the steady state tumor volume at the end of the treatment (2 mm^3) was achieved by controller (C1) with 25 mg/kg and 15 mg/kg saturation values and $a = 8$ acceleration. One can see that controllers which are the best for one criterion have near-optimal values for the other criteria.

Summarizing, simulation results showed that the nonlinear model have to be linearized in a low operating point to achieve successful control. The lowest steady state tumor volume at the end of the treatment can be reached by using state feedback with pole placement. However according to various aspects, the most effective control is LQ control method: (a) for two criteria (total concentration of the administered inhibitor during the treatment and steady state inhibitor concentration at the end of the treatment) this controller had the best results; (b) the minimal value of the third criterion can be well approximated with LQ control method; (c) this is the only controller, which ensures successful control for high operating points.

According to the above mentioned results – viz. low operating point and small value of R weighting matrix seemed beneficial – I have improved the analyzed range of R from $R = [10^3, 10^6]$ to $R = [10^{-1}, 10^6]$; in addition I have examined one more operating point, $x_{10} = 10$ mm^3 (J Sápi, D A Drexler, I Harmati, Z. Sápi, et al. 2015). The whole range of R was investigated by dividing each order of magnitude into ten equal parts. I have run simulations for all of these investigation points (R values) at each operating point with each saturation value. I repeated it for each criterion. Consequently it resulted in 36 curves (4 operating points $\cdot$ 3 saturation values $\cdot$ 3 criteria) with discrete R investigation points, and the minima for all curves was found. Results in the newly investigated $R = [10^{-1}, 10^3]$ range with the new operating point are shown in Table 4.2.

One can see from Table 4.2, that similarly to the previous results, low operating points

Evaluated criterion: total concentration of the administered inhibitor during the treatment (mg/kg)		R = 0.1	R = 1	R = 10	R = 100	R = 1000
operating point: 10 mm^3	saturation: 25 mg/kg	1556	1500	1486	1483	1483
	saturation: 15 mg/kg	1367	1329	1318	1316	1316
	saturation: 13 mg/kg	1300	1277	1268	1266	1266
operating point: 100 mm^3	saturation: 25 mg/kg	1369	1430	1365	1308	1292
	saturation: 15 mg/kg	1353	1288	1227	1184	1169
	saturation: 13 mg/kg	1293	1243	1184	1144	1132
operating point: 5000 mm^3	saturation: 25 mg/kg	1380	1439	1345	1245	1131
	saturation: 15 mg/kg	1351	1283	1210	1131	1044
	saturation: 13 mg/kg	1293	1238	1168	1096	1017
operating point: 10000 mm^3	saturation: 25 mg/kg	1405	1439	1345	1244	1129
	saturation: 15 mg/kg	1351	1283	1209	1130	1042
	saturation: 13 mg/kg	1293	1238	1168	1096	1016

Evaluated criterion: steady state inhibitor concentration at the end of the treatment (mg/kg)		R = 0.1	R = 1	R = 10	R = 100	R = 1000
operating point: 10 mm^3	saturation: 25 mg/kg	8.8	8.8	8.8	8.8	8.8
	saturation: 15 mg/kg	8.9	8.8	8.8	8.8	8.8
	saturation: 13 mg/kg	12.3	9.6	9.3	9.3	9.3
operating point: 100 mm^3	saturation: 25 mg/kg	8.8	8.7	8.7	8.7	8.7
	saturation: 15 mg/kg	8.8	8.8	8.7	8.7	8.7
	saturation: 13 mg/kg	10.7	8.9	8.7	8.7	8.7
operating point: 5000 mm^3	saturation: 25 mg/kg	8.7	8.8	8.7	8.6	8.3
	saturation: 15 mg/kg	8.9	8.8	8.7	8.6	8.3
	saturation: 13 mg/kg	10.6	8.9	8.7	8.6	8.3
operating point: 10000 mm^3	saturation: 25 mg/kg	8.8	8.8	8.7	8.6	8.3
	saturation: 15 mg/kg	8.9	8.8	8.7	8.6	8.3
	saturation: 13 mg/kg	10.6	8.9	8.7	8.6	8.3

Evaluated criterion: steady state tumor volume at the end of the treatment (mm^3)		R = 0.1	R = 1	R = 10	R = 100	R = 1000
operating point: 10 mm^3	saturation: 25 mg/kg	2	4	5	5	5
	saturation: 15 mg/kg	2	4	5	5	5
	saturation: 13 mg/kg	3	4	5	5	5
operating point: 100 mm^3	saturation: 25 mg/kg	3	8	21	41	50
	saturation: 15 mg/kg	3	8	21	41	50
	saturation: 13 mg/kg	3	8	21	41	50
operating point: 5000 mm^3	saturation: 25 mg/kg	3	9	28	86	259
	saturation: 15 mg/kg	3	9	28	86	259
	saturation: 13 mg/kg	3	9	28	86	259
operating point: 10000 mm^3	saturation: 25 mg/kg	3	9	28	86	264
	saturation: 15 mg/kg	3	9	28	86	264
	saturation: 13 mg/kg	3	9	28	86	264

Table 4.2: Simulation results for LQ control method in the extended range of R, with a new operating point. Suboptimal controls for both criteria are marked. Simulation period was 100 days.

resulted in the lowest steady state tumor volume values. If the nonlinear model was linearized at the new, lowest operating point ($x_{10} = 10$ mm^3), the steady state tumor volume is nearly independent from the value of weighting matrix R and also from the saturation value. However, in higher operating points, the saturation has important

effect on the total concentration of the administered inhibitor. Investigating the results in a given operating point with a given value of R, one can see that the saturation value does not influence the steady state inhibitor concentration and the steady state tumor volume, nevertheless it affects the total concentration of the administered inhibitor. It was symbolically proved in Section 4.1. Decreasing the saturation limit, the total concentration of the administered inhibitor is also decreasing, whilst the steady state inhibitor concentration and the steady state tumor volume remain the same value. It means that lower saturation value is not only appropriate due to physiologycal aspects (less side effects) and economic considerations (better cost-effectiveness), but also because of engineering point of view. Note that in a given operating point with a given value of R, using different saturation limits, if the resulting "steady state" inhibitor concentration values are not exactly the same, it means the simulation period (100 days) was not long enough to achieve the steady state (e.g. in the case of $x_{10} = 10$ mm^3 and $R = 0.1$).

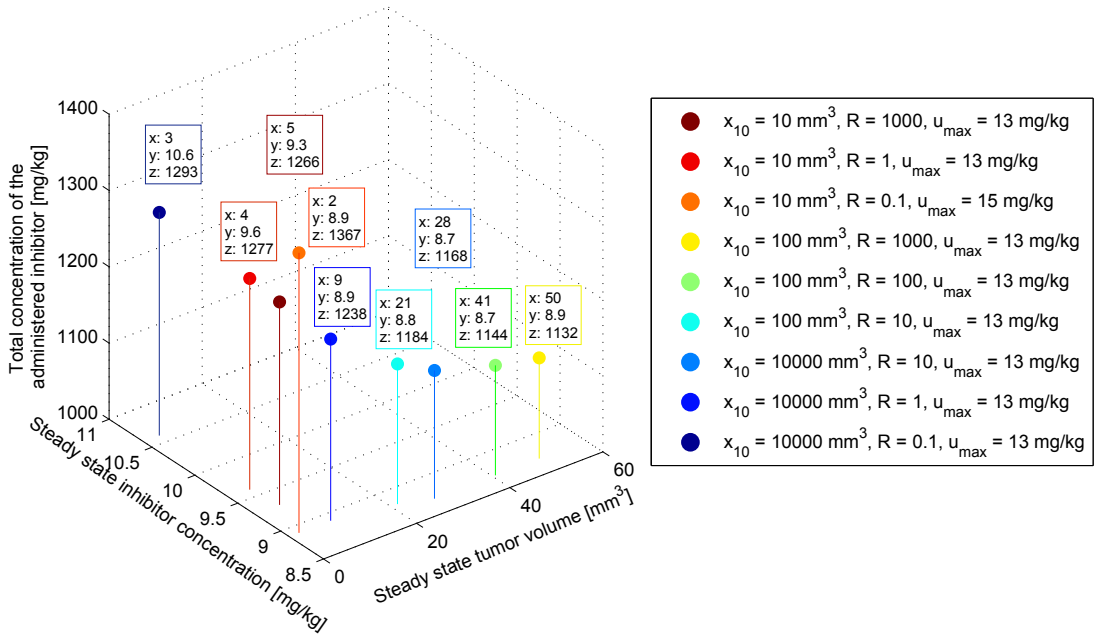

Figure 4.4: Visualization of suboptimal controls which have near-optimal values for both criteria. Axes are the evaluated three criteria.

As it was found that using the $x_{10} = 10$ mm^3 operating point, the steady state tumor volume is nearly independent from R and saturation value; one can see that choosing $R = 0.1$ weighting matrix value has the same effect. In that case the steady state

tumor volume is nearly independent from the operating point and the saturation limit. Necessarily the combined usage of these two parameters ($x_{10} = 10$ mm^3 operating point and $R = 0.1$ weighting matrix) results in the lowest steady state tumor volume (2 mm^3).

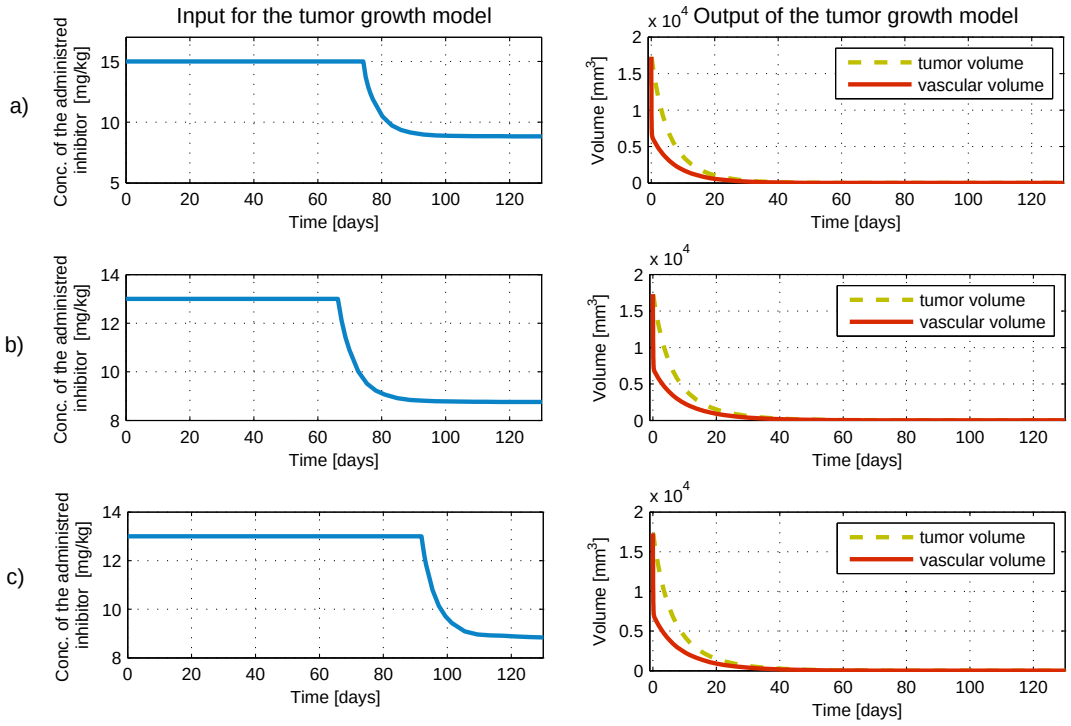

Figure 4.5: Input and output signals of the tumor growth model in the case of suboptimal contol parameters. a) Controller: LQ control method, $x_{10} = 10$ mm^3, $R = 0.1$, $u_{max} = 15$ mg/kg. Period of maximum inhibitor dosage is 74 days, achieving the steady state inhibitor dosage in 101 days, achieving the steady state tumor volume in 73 days. b) Controller: LQ control method, $x_{10} = 100$ mm^3, $R = 10$, $u_{max} = 13$ mg/kg. Period of maximum inhibitor dosage is 66 days, achieving the steady state inhibitor dosage in 97 days, achieving the steady state tumor volume in 67 days. c) Controller: LQ control method, $x_{10} = 10000$ mm^3, $R = 0.1$, $u_{max} = 13$ mg/kg. Period of maximum inhibitor dosage is 92 days, achieving the steady state inhibitor dosage in 121 days, achieving the steady state tumor volume in 89 days.

It is not trivial to determine the goal of this tumor control. On the one hand, necessarily every therapy which fights against cancer aims to reduce the tumor volume as far as possible. However on the other hand the price of low tumor volume has to be paid twice: as financial cost and also as side effect cost. That is the reason why I have created two

more criteria beside the steady state tumor volume to evaluate the result of the control. Total concentration of the administered inhibitor can be calculated in the first, intense period of the treatment to approximate both cost types of the tumor reduction. Steady state inhibitor concentration is an important indicator, since long-term targeted molecular therapies are promising field of cancer treatment (Tang et al. 2011). Considering all of these criteria, choosing the control which will be the base of the therapy is a trade-off issue, which has to be answered by medical professionals. From engineering point of view there are controls, which have near-optimal values for both criteria; we can call them suboptimal controls. I marked these suboptimal controls in Table 4.2 and visualized in 3D, where the axes are the evaluated three criteria (Figure 4.4). Marker colors are the same in Table 4.2 and Figure 4.4.

Three controls, which have suboptimal parameters, are shown in Figure 4.5. In every case the input signal has two phases. In the first phase the value of the input signal is equal to the saturation limit. This period of maximum inhibitor dosage depends on the saturation limit and the value of R weighting matrix. From therapeutic point of view, short period of maximum inhibitor dosage is desirable for less strain on the human body. However, the period of maximum inhibitor dosage has an inverse relationship with the steady state tumor volume. The smaller period of maximum inhibitor, the higher tumor volume is at steady state. This constant phase is followed by the decreasing of the input value, until the steady state inhibitor dosage will be reached.

The output of the tumor growth model contains the tumor volume and the vascular volume. Vascular volume means tumor's own blood vessels, which support the oxygen and nutrient uptake for the tumor cells. Since tumor growth and survival depends on the capacity of these blood vessels, change of the vascular volume is the engine of tumor growth and reduction. This mechanism can be seen in the output plots of Figure 4.5; the first process is always the decrease of the vascular volume, after that occurs the decrease of the tumor growth.

4.1.4 Conclusion

I presented a linear control synthesis for antiangiogenic therapy over the simplified tumor growth model of Hahnfeldt et al. 1999. First, the model's control properties were analyzed, and then state feedback controllers and observer were designed and investigated.

The first simulation results showed that the nonlinear model have to be linearized in low operating point to achieve successful control; increasing the operating point, the control signals become too low to sufficiently reduce the tumor volume (because of the nonlinearity). Small acceleration and high operating point eventuate in great values of

tumor volume; and it is especially true for the additive effect of these two parameters. In the case of LQ control method the $R = [10^3, 10^6]$ range was investigated and I have found that the only effective solution for high operating points is LQ control method with weighting matrix $R = 10^3$. Moreover, controls with weighting matrix $R = 10^3$ results in better solution according to all the three criteria than controls with weighting matrix $R = 10^6$. Since the aim was to find an optimal solution according to multiple criteria, I have investigated lower values of weighting matrix R as well.

According to the above mentioned results, I have improved the analyzed range of R from $R = [10^3, 10^6]$ to $R = [10^{-1}, 10^6]$; in addition I have examined one more operating point, $x_{10} = 10$ mm^3. Low operating points resulted in the lowest steady state tumor volume values. If the nonlinear model was linearized at the new, lowest operating point, the steady state tumor volume was nearly independent from the value of weighting matrix R and also from the saturation value. However, in higher operating points, the saturation had important effect according to the total concentration of the administered inhibitor. In a given operating point with a given value of R, decreasing the saturation limit, the total concentration of the administered inhibitor was also decreasing, whilst the steady state inhibitor concentration and the steady state tumor volume remained the same value. Using the $R = 0.1$ weighting matrix, the steady state tumor volume is nearly independent from the operating point and the saturation limit. Necessarily the combined usage of these two parameters ($x_{10} = 10$ mm^3 operating point and $R = 0.1$ weighting matrix) resulted in the lowest steady state tumor volume.

In every investigated case the input signal had two phases. In the first phase the value of the input signal was equal to the saturation limit; this constant phase was followed by the decrease of the input value, until the steady state inhibitor dosage could be reached. Considering all of the criteria, choosing the control which will be the base of the therapy is a trade-off issue, which has to be answered by medical professionals. From engineering point of view there are controls, which have near-optimal values for both criteria – these are the suboptimal controls.

4.2 Robust (H_∞) Control

Protocols for medical treatment comprise constant drug dosage, which can be effective in terms of reducing the progression of the diseases; however, nowadays the problem seems more complex. From multidisciplinary point of view the aim is to design a controller which is on the one hand able to minimize the input signal as far as possible (in order to have less side effects and greater cost-effectiveness) and on the other hand results

in appropriately low tumor volume (A Szeles, D A Drexler, J Sápi, I Harmati, et al. 2014; A Szeles, D A Drexler, J Sápi, Z. Sápi, et al. 2013; D A Drexler et al. 2012). In biomedical applications experts always faced with two major problems: understanding the physiological behavior of a system and transform it into a model; and finding sufficiently sensitive methods and sensors to detect the required states and values. However, there always will be model uncertainties and measurement noises; thus, there is a need for systems which satisfy the requirements not only for its nominal values but also in the presence of perturbations. These aspects can be taken into account using H_∞ control methodology that represents the goal of the current section as well.

4.2.1 H_∞ Control Design

Design Structure

The tumor growth model described by (3.4-3.6) was linearized in the $x_{10} = 100$ mm^3 operation point for controller design purposes. The system is unstable in that point (see Subsection 3.2.2), but controllable and observable (see Subsection 3.2.3).

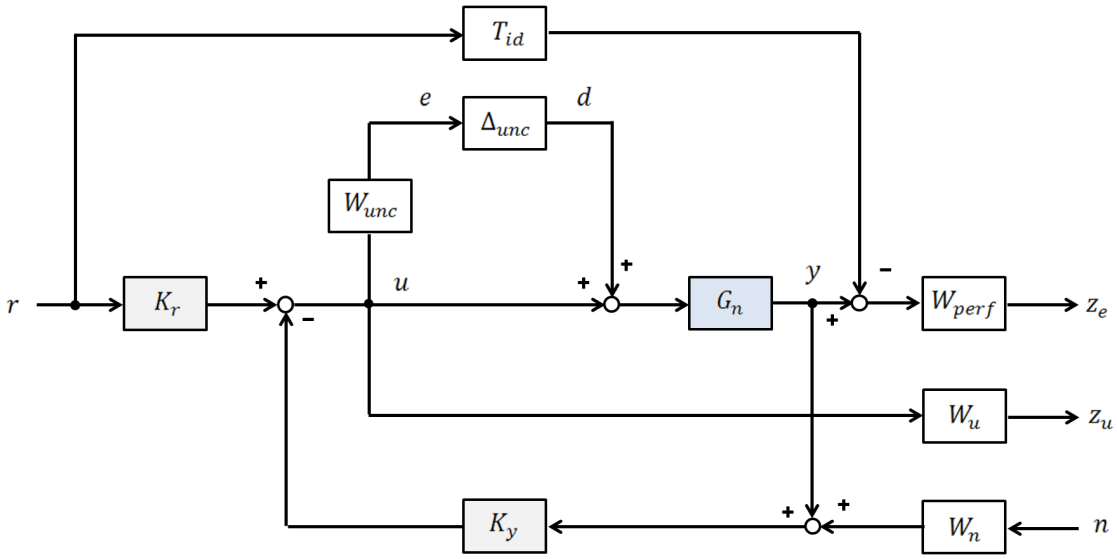

Figure 4.6: The closed-loop interconnection structure for H_∞ controller design

For controller design, first the closed-loop interconnection structure was created (Figure 4.6). The closed-loop system includes the feedback structure of the nominal model G_n. K

is the two-degrees of freedom controller, which consists of two parts: K_r is the feedforward branch and K_y is the feedback branch. Differences between the nominal model and the real system are taken into account using input multiplicative uncertainty, G_{unc} (Bokor, Gáspár, and Szabó 2012):

$$G_{unc}(s) = W_{unc}(s) \cdot (I + \Delta_{unc}(s)) . \tag{4.48}$$

Weighting function W_n seeks to minimize the influence of sensor noise. Limitation of the control input is achieved by the weighting function W_u, which penalizes larger deflections. Ideal system is described by T_{id} transfer function. Weighting function W_{perf} seeks to penalize differences between the output of the nominal model and the ideal plant.

Signals of the system are the following: r is the reference signal, u is the control input, y is the output of the nominal model, n is the measurement noise, e is the modeling error, d is the disturbance caused by the uncertainty of the model, z_u is the penalized control input and z_e is the penalized difference between the output of the nominal model and the ideal model.

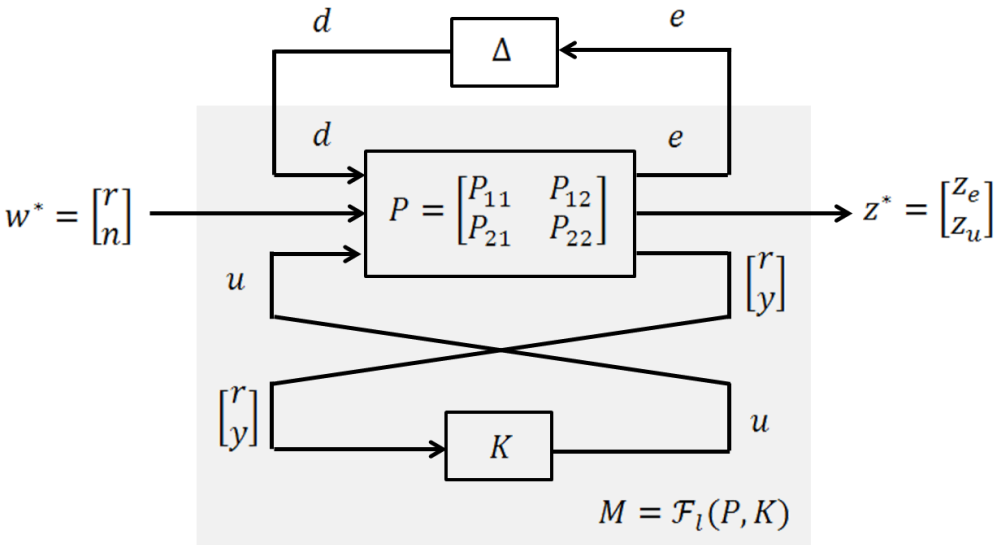

Figure 4.7: The generalized $\Delta - P - K$ structure

The generalized structure of H_∞ control design is formulated in $\Delta - P - K$ (Figure 4.7). The detailed $\Delta - P - K$ structure is described as follows:

$$\begin{bmatrix} e \\ z_e \\ z_u \\ \hline r \\ y \end{bmatrix} = \left[\begin{array}{ccc|c} 0 & 0 & 0 & W_{unc} \\ W_{perf}G_n & -W_{perf}T_{id} & 0 & W_{perf}G_n \\ 0 & 0 & 0 & W_u \\ \hline 0 & 1 & 0 & 0 \\ G_n & 0 & W_n & G_n \end{array}\right] \cdot \begin{bmatrix} d \\ r \\ n \\ u \end{bmatrix} \tag{4.49}$$

P is called the generalized plant and partitioned as

$$P = \left[\begin{array}{c|c} P_{11} & P_{12} \\ \hline P_{21} & P_{22} \end{array}\right] \tag{4.50}$$

Input of the generalized plant is:

$$w = \begin{bmatrix} d \\ w^* \\ u \end{bmatrix}, \tag{4.51}$$

where $w^* = [r\ n]^\top$ is the external input and $w_{min} = [d\ w^*]^\top$.
Output of the generalized plant is:

$$z = \begin{bmatrix} e \\ z^* \\ r \\ y \end{bmatrix}, \tag{4.52}$$

where $z^* = [z_e \; z_u]^\top$ is the external output to be penalized and $z_{min} = [e \; z^*]^\top$.

The closed-loop function M can be derived as the lower linear fractional transformation of the pair (P, K)

$$z_{min} = \left[P_{11} + P_{12}K\left(I - P_{22}K\right)^{-1}P_{21}\right] w_{min} = \mathcal{F}_l(P,K)w_{min} \tag{4.53}$$

$$M = \mathcal{F}_l(P,K). \tag{4.54}$$

H_∞ Suboptimal Solution

The objective is to find a stabilizing controller K to minimize the output z_{min}, in the sense of $||w||_\infty \leq 1$. It is equivalent to minimizing the H_∞-norm of M from w_{min} to z_{min}:

$$\min_{K_s} ||\mathcal{F}_l(P,K)||_\infty, \tag{4.55}$$

where K_s is an element of the set of stabilizing K controllers; this is called the H_∞ optimization problem (Zhou 1996). Since the solution of the optimization problem is not obvious, in practice, it is usually satisfactory to find a stabilizing controller K such the H_∞-norm of the closed-loop function is less than a given positive number:

$$||M||_\infty = ||\mathcal{F}_l(P,K)||_\infty < \gamma, \tag{4.56}$$

where

$$\gamma > \gamma_0 = \min_{K_s} ||\mathcal{F}_l(P,K)||_\infty. \tag{4.57}$$

It is called as the H_∞ suboptimal problem.

System-performance specifications can usually be interpreted as a reduction of z^* with respect to w^*. Robustness and performance can be investigated by the partition blocks of M

$$\left[\begin{array}{c} e \\ \hline z^* \end{array}\right] = \left[\begin{array}{c|c} M_{11} & M_{12} \\ \hline M_{21} & M_{22} \end{array}\right] \cdot \left[\begin{array}{c} d \\ \hline w^* \end{array}\right] \tag{4.58}$$

The scope of the H_∞ controller design is to guarantee robust performance of the system. This can be realized by fulfilling the conditions of Robust Stability and Nominal Performance. To guarantee Nominal Stability, the system must be internally stable, which means that the created transfer function is stable from all inputs to all outputs.

Robust Stability is achieved by fulfilling the following condition:

$$||M_{11}||_\infty =\leq 1. \tag{4.59}$$

Nominal Performance is achieved if the performance objective is satisfied:

$$||M_{22}||_\infty =\leq 1. \tag{4.60}$$

The upper linear fractional transformation of the pair (M, Δ) can be described as:

$$z^* = \left[M_{22} + M_{21}\Delta \left(I - M_{11}\Delta\right)^{-1} M_{12}\right] w^* = \mathcal{F}_u(M, \Delta)w^*. \tag{4.61}$$

Robust Performance is achieved by fulfilling the following condition:

$$||\mathcal{F}_u(M, \Delta)||_\infty < 1. \tag{4.62}$$

Choosing of the Ideal System and the Weighting Functions In Light of Physiological Aspects

From engineering point of view, the ideal system (T_{id}) is needed to be a fast system for fast reduction of the tumor volume. Nevertheless, on the one hand it is physically impractical, on the other hand fast transients need high control signal and in medical treatments the input is always limited. Besides these, researches have shown that in the case of antiangiogenic therapy low-dose treatments can be more effective (Zhang et al. 2011 states it exactly in the context of Lewis lung carcinoma). According to the fact that tumor regression has exponential characteristics, the ideal system was found to have a relatively slow exponential decay:

$$T_{id}(s) = \frac{K}{sT + 1}, \tag{4.63}$$

where K is the initial tumor volume and T is the time constant of the ideal system ($T = 100$ days). Weighting function W_u (which penalizes large deflections of the control input) was chosen to constant value and I have run iteration to find the greatest possible value to penalize deflections. Finally I set $W_u = 0.02$.

Sensor noise, as a wide-band signal, can be modeled with a constant value. The effect of the weighting function W_n was investigated in the range of [0.0 0.2], Section 4.2.2 contains the results of this analysis.

In the case of weighting functions W_{unc} and W_{perf}, tuning of the crossover frequencies

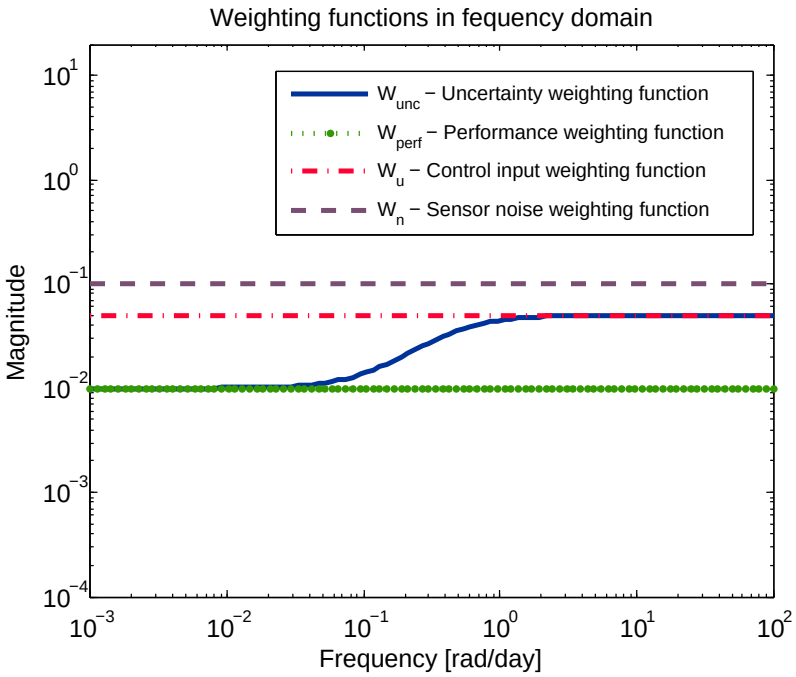

Figure 4.8: Weighting functions of the controller

was carried out to reach better performance and robustness.

$$W_{unc} = 0.05 \cdot \frac{s+0.1}{s+0.5} \tag{4.64}$$

$$W_{perf} = 0.01. \tag{4.65}$$

The chosen weighting functions can be seen in Figure 4.8.

4.2.2 Simulation Results

Frequency domain analysis (Figure 4.9) showed that the conditions of Robust Stability (4.59), Nominal Performance (4.60) and Robust Performance (4.62) are fulfilled, because all the corresponding norms are smaller than 1 for every frequency.

The reached γ value was 0.0781 and the K controller was stable, thus the designed structure provides a suboptimal H_∞ solution. According to the minimal size criteria for diagnosis in the case of Lewis lung carcinoma (tumor size has to be bigger than 3 cm (L. C. Genentech 2013) and assuming a spherical shape, simulations were run from the initial tumor volume $x_0 = 14137$ mm^3 (L. Kovács, J. Sápi, Eigner, et al. 2014).

Time domain analysis showed that control input saturation is necessary, because one-off

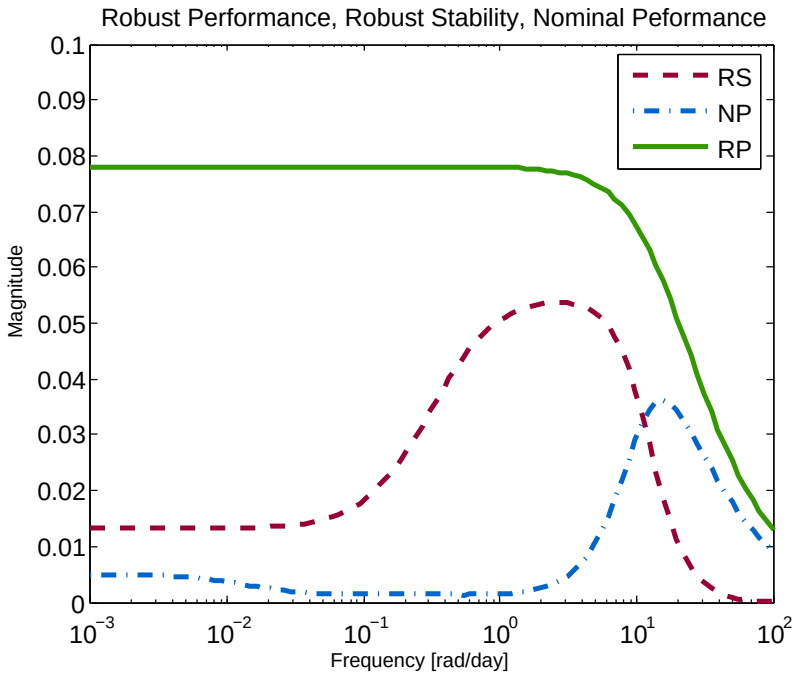

Figure 4.9: Robust Performance, Robust Stability and Nominal Performance

high dose can be tolerated by the patient; however, continuous dosage of angiogenic inhibitor is limited in concentration to around 10 mg/kg (Inoue et al. 2002). The saturation, which was resulting in the least possible control signal, but still effective H_∞ control, is 13 mg/kg; every simulation results were run with this value.

The effect of the weighting function W_n was investigated in the range of [0.0 0.2], since subcutaneous tumor volume measurement is usually carried out by calipers. Width and length of the tumor can be measured, but the third dimension is estimated; and tumor volume is approximated with a spherical shape or an ellipsoid (see Section 6.2). The results have shown that the designed H_∞ controller can handle the sensor noise in a robust way until 15%: I have found that if $W_n \leq 0.15$, tumor volume (output of the system) decreased exactly the same rate in every cases. Above this value, the control signal was not applicable. This result also shows how important the precise tumor volume measurement is, and if it is possible, Magnetic Resonance Imaging (MRI) has to be preferred as measurement method against to caliper (see Subsection 6.3.2).

Effect of the initial tumor volume at the beginning of the therapy was examined in the [100 17340] mm^3 range. The results are shown in Figure 4.10. Steady-state tumor volume is independent from the initial tumor volume; in every case tumor volume was

25.6 $mm^3 \pm 0.1\%$ (Figure 4.10 a). Steady-state inhibitor concentration (Figure 4.10 b) has showed the same result, viz. minimal deviation (8.759 mg/kg $\pm 0.07\%$). It is clear that the period of maximal inhibitor dose (Figure 4.10 c) have to increase as the simulations start from higher initial tumor volumes to ensure the appropriate steady-state tumor volume. However, a breakpoint can be determined at 2000 mm^3: below this value, initial tumor value has greater impact on the maximal inhibitor period than above this point.

Similar results can be seen in (Figure 4.10 d); total concentration of the administered inhibitor depends more on initial tumor volume below the 2000 mm^3 breakpoint than above (of course the former last two functions are not independent). Summarizing the results of these figures: at lower initial working points the dynamics of the change is larger and the controller should administer more inhibitor; however, nearly the same tumor outputs can be provided.

I have compared the H_∞ suboptimal control result with the result of LQ controller (investigating the same operating point, $x_{10} = 100$ mm^3). The outcome can be seen in Figure 4.11. The numerical results are the following.

Steady state tumor volume:

- $V_{LQ} = 7.491$ mm^3,
- $V_{H_\infty} = 25.64$ mm^3

Steady state inhibitor concentration:

- $C_{LQ} = 3.093$ mg/kg,
- $C_{H_\infty} = 8.768$ mg/kg.

Period of maximal inhibitor dose:

- $T_{LQ} = 60$ days,
- $T_{H_\infty} = 64$ days.

Total concentration of the administered inhibitor:

- $TC_{LQ} = 915$ mg/kg,
- $TC_{H_\infty} = 1173$ mg/kg.

As would be expected, the LQ optimal control provides better results, but only in the case of good model identification and minimal sensor noise. If the system contains

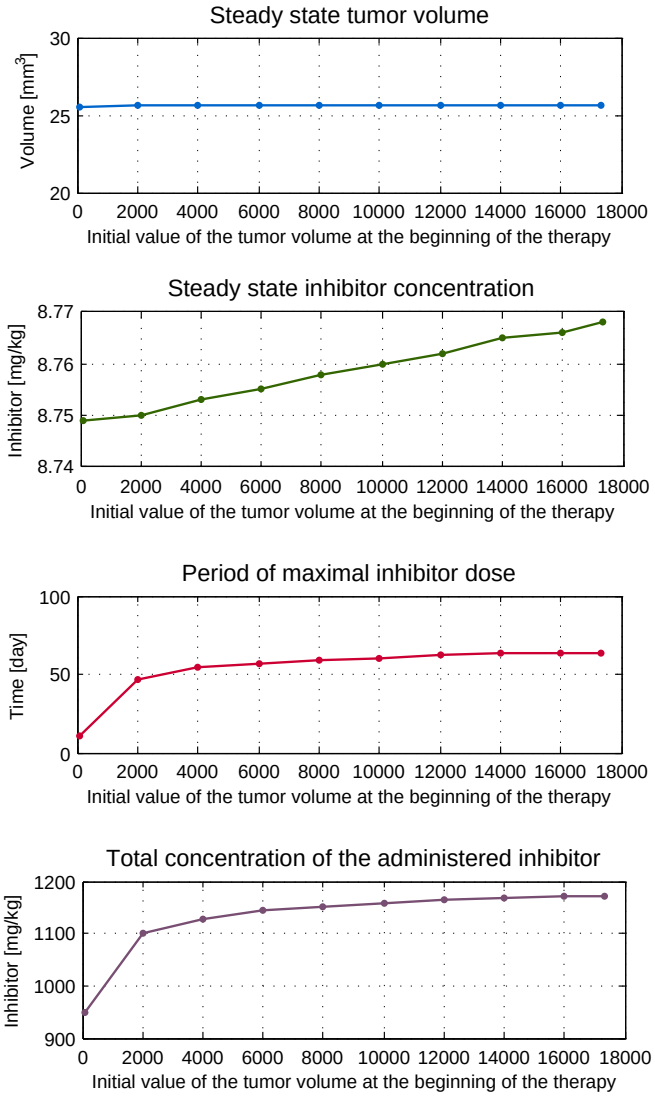

Figure 4.10: Investigating the effect of different operating points on the
a) steady state tumor volume,
b) steady state inhibitor concentration,
c) period of maximal inhibitor dose and
d) total concentration of the administered inhibitor

significant uncertainties and the measurement noise is large, the only robust control method can provide near-optimal results.

Last but not least, I have simulated and compared the changes in full-grown tumor

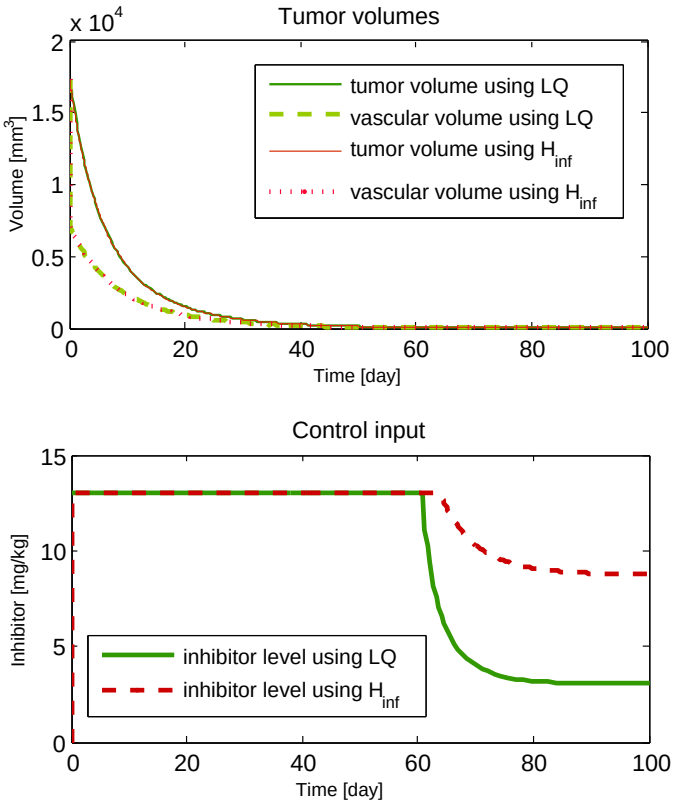

Figure 4.11: Comparison of control inputs and tumor volumes in the cases of Linear Quadratic optimal control and suboptimal Robust Control method

volume after making the diagnosis (14137 mm^3) in three different cases; Figure 4.12 shows the results (J. Sápi, D. A. Drexler, and L. Kovács 2013). The first case was a therapy when the inhibitor was administered by the H_∞ controller. In the second case the therapy was based on the Hungarian OEP (National Health Insurance Fund of Hungary) protocol for antiangiogenic monotherapy (Hungary(OEP) 2010). The third case was the simulation without therapy. From Figure 4.12 it is clear, that the intermittent dosing used by the chemotherapy protocol is not effective. The tumor volume reduced slightly as a result of one-day dose, but between the treatment phases, tumor grows back again. At the end of the whole treatment period, there is no large difference between the therapy with OEP protocol and the case without therapy.

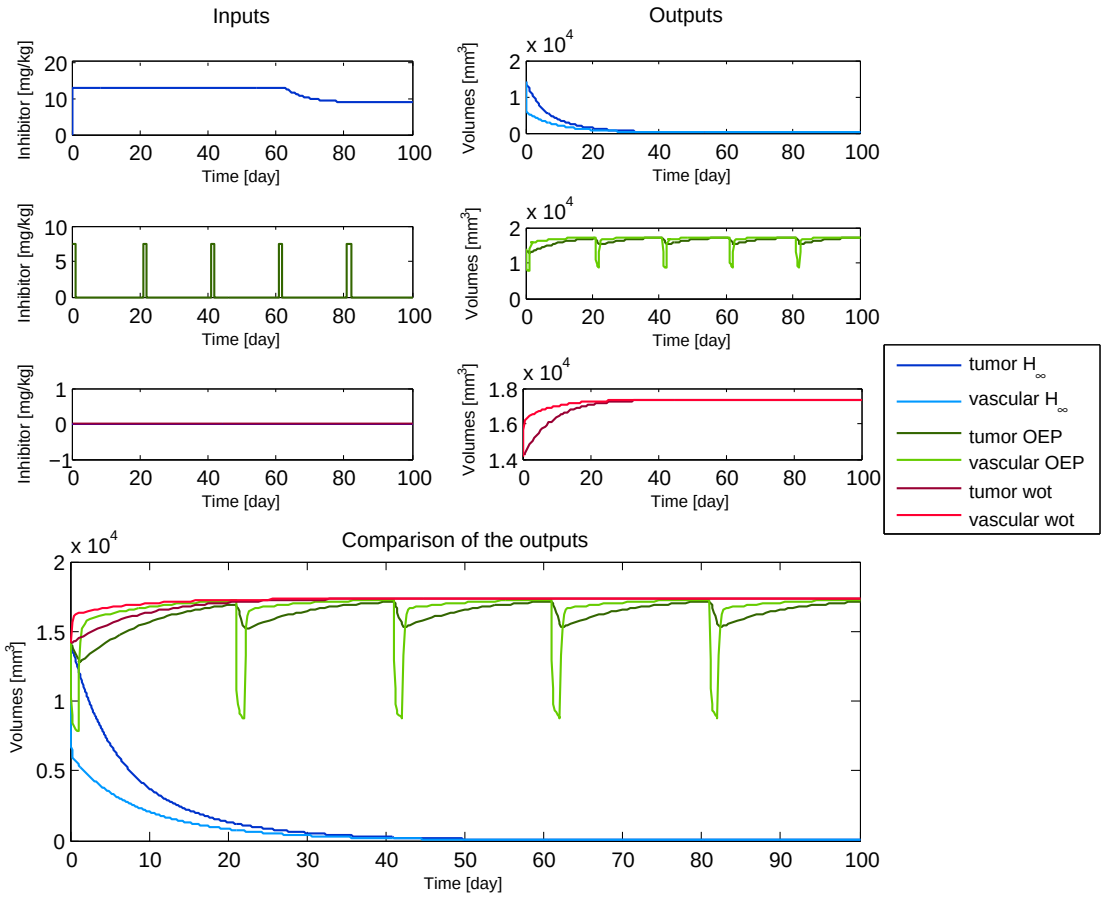

Figure 4.12: Comparison of changes in tumor volume after making the diagnosis (14137 mm^3) in three different cases:
a) therapy using the controller which was designed with Robust Control method
b) therapy based on the Hungarian OEP protocol for antiangiogenic monotherapy
c) without therapy

4.2.3 Conclusion

H_∞ controller was designed for the problem of tumor growth under angiogenic inhibition, considering the physiological aspects. Robust Stability, Nominal Performance and Robust Performance were achieved. Frequency domain analysis and time domain analysis were carried out. I have investigated the effect of the sensor noise weighting function on the robustness. I have also examined the effect of the initial tumor volume on the steady state tumor volume, on the steady state inhibitor concentration, on the period of maximal

inhibitor dose and on the total concentration of the administered inhibitor. I have compared the results of the H_∞ controller with the results of LQ optimal control and the therapy with OEP protocol.

4.2.4 Robust Control With Sensitivity Analysis

In this subsection I will present the results of robust control which was designed using sensitivity analysis. These results are not only my own results. In the current subsection I will describe only partial results which are closely connected to my *Thesis group 1*, not the whole controller design methods and full simulation results will be discussed. The aim is to investigate how the designed controller reacts to parametric changes, viz. robustness of the controller.

The current robust control was designed for the tumor growth model under angiogenic inhibition described in (3.4-3.6), and it was carried out with sensitivity analysis in order to determine the uncertainty weighting matrix, and to investigate the effect of parametric perturbation on the closed-loop system. The tumor growth model was linearized at the $x_{10} = 100$ mm^3 operation point similarly as in Subsection 4.2.1. Results were published in A. Szeles, J. Sápi, et al. 2012; A. Szeles, D. A. Drexler, et al. 2014; L Kovács, A Szeles, et al. 2014.

Sensitivity Analysis

Starting from the formal definition of the multiplicative uncertainty, parametric sensitivity analysis was performed on the nonlinear model to determine W_{unc}. The idea was partially adapted and modified from (L Kovács, Kulcsár, et al. 2011; Liu and Zeng 2012) in order to incorporate uncertain parameters into the design process. Ranges are associated to these selected parameters. By taking every single extremal combination of the parameters, linearization is performed. Finally, the frequency content of the perturbed and linearized model is compared and relative difference is computed. Instead of using the extremal values, a gridding technique is proposed. Consequently, we consider the combination of the selected parameters in a multiplicative manner.

A $\pm 5\%$ variability of the Lewis lung carcinoma parameters and a $\pm 10\%$ variability of the vascular inactivation rate was assumed (Hahnfeldt et al. 1999). For the Lewis lung carcinoma parameters, factors f_1, f_2 and f_3 were chosen from a ($+5\%$, $+2.5\%$, 0, -2.5%, -5%) grid, and for the vascular inactivation rate, factor f_4 was taken from a ($+10\%$, $+5\%$, -5%, -10%) grid. The perturbed nonlinear model is:

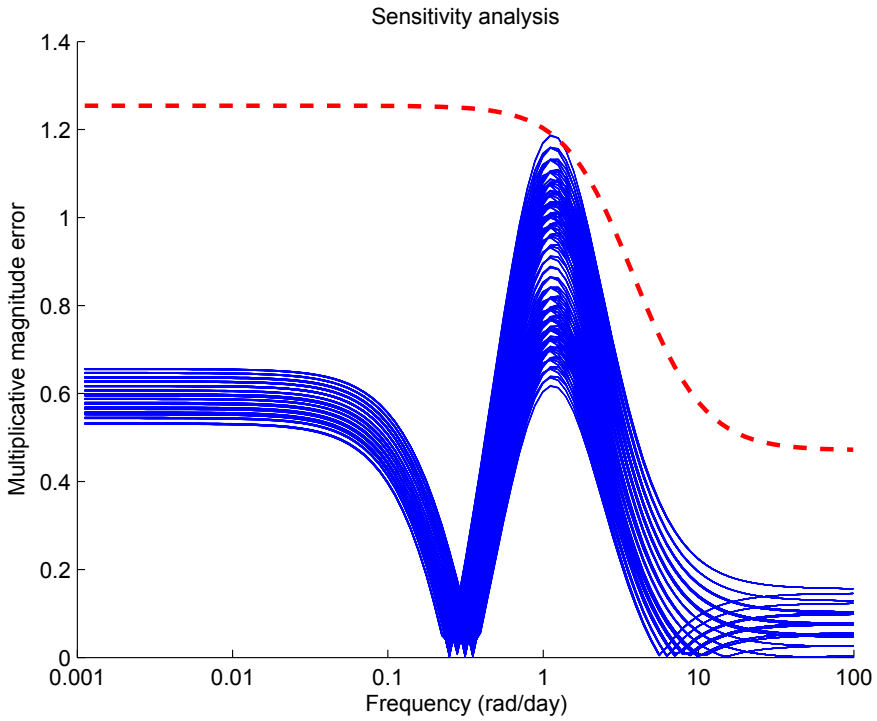

Figure 4.13: Relative modeling error functions (perturbed system compared to the nominal model) in frequency domain and uncertainty upper bound (dashed line).

$$\dot{x}_1(t) = -\overline{\lambda}_1 x_1(t) \log\left(\frac{x_1(t)}{x_2(t)}\right) \tag{4.66}$$

$$\dot{x}_2(t) = \overline{b} x_1(t) - \overline{d} x_1(t)^{2/3} x_2(t) - \overline{e} x_2(t) u(t) \tag{4.67}$$

$$y = x_1, \tag{4.68}$$

where $\overline{\lambda}_1 = (1 + f_1)\,\lambda_1$, $\overline{b} = (1 + f_2)\,b$, $\overline{d} = (1 + f_3)\,d$ and $\overline{e} = (1 + f_4)\,e$. For each possible combination, the nonlinear model was linearized at the $x_{10} = 100$ mm^3 operation point, and the obtained linear model was used to determine parametric sensitivity by determining $supW_{rel}$ of the relative uncertainty relation:

$$W_{rel}(\omega) = \left|\frac{G_p(\omega) - G_n(\omega)}{G_n(\omega)}\right|, \tag{4.69}$$

where G_p stands for the perturbed model and G_n for the nominal model. The frequency

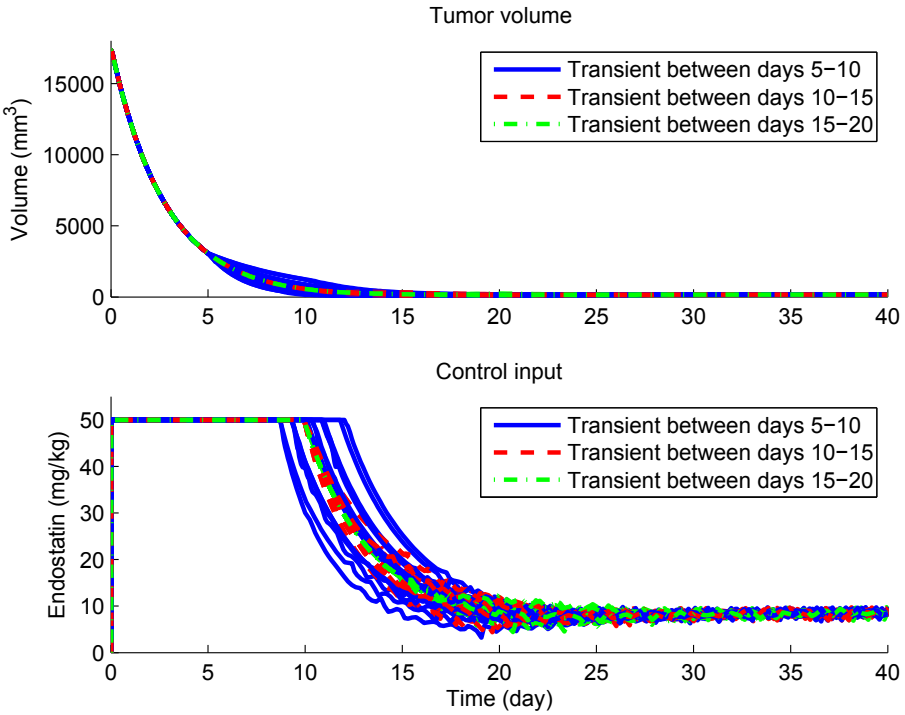

Figure 4.14: Characteristics of tumor regression and control input in case of different perturbation scenarios – parameters change between the 5th and 10th day (blue), the 10th and 15th day (red) and the 15th and 20th day (green), each model parameter is perturbed independently with a variability of ±25%.

domain of interest was $\omega \in [0.001\ 100]$ rad/day. The determined parametric sensitivity was upper bounded (Figure 4.13):

$$supW_{rel} = 0.47\frac{s+8}{s+2}. \tag{4.70}$$

The results of the sensitivity analysis show that in lower frequency domain, $\omega \in [0.001\ 0.1]$ rad/day, the model is less sensitive for parameter perturbation than in higher frequency domain, $\omega \in [0.01\ 100]$ rad/day. In the low frequency domain which is characteristic for tumor growth dynamics, the uncertainty upper bound allows 125% deviation in the gain of the transfer function relative to the nominal transfer function (Figure 4.13) instead of the 65% deviation resulted from the perturbation of the parameters. This means that significantly larger variance of the parameters is allowed in the low frequency domain, regardless of their dynamical characteristics.

The obtained uncertainty weighting function W_{unc} should work as a high pass filter to

reduce disturbance at low frequency, and to avoid strong restrictions at high frequency:

$$W_{unc} = 0.01\frac{s+2}{s+8}. \tag{4.71}$$

Sensor noise, as a wide-band signal, can be modeled with a constant value. During the design process, W_n anticipates 5% measurement noise for volume measurements. This is in accordance with the measurement noise used in (Hahnfeldt et al. 1999).

$$W_n = 0.05. \tag{4.72}$$

The control input is penalized by the weighting function W_u, wchich was chosen to

$$W_u = 0.01. \tag{4.73}$$

The zero of the weighting function was chosen based on the uncertainty weighting function to form the desired "cone" shape in frequency domain. The amplification was set to compensate the amplification of the model-matching function and to minimize oscillation in constant reference signal tracking:

$$W_{perf} = 6.5 \cdot 10^{-7}\frac{s+2}{s+8}. \tag{4.74}$$

Effect of Parametric Perturbation on the Closed-Loop System

Effect of parametric perturbation on the closed-loop system was investigated. In this case, there is no measurement noise, and the measurements are taken continuously. The parameters are perturbed independently (b, d, λ_1, e) with a variability of $\pm 25\%$ in three different time intervals:

- between the 5th and 10th day,
- between the 10th and 15th day,
- between the 15th and 20th day.

Parameter perturbation does not affect tumor regression before the 5th day because of the applied saturation. After the 20th day, steady state is achieved and the tumor volume is nearly minimal; thus, perturbations do not change significantly the performance of the controller.

If the condition of the patient changes after the 10th day of the therapy, the speed of tumor regression does not change remarkably, total inhibitor inlet varies between 815.8

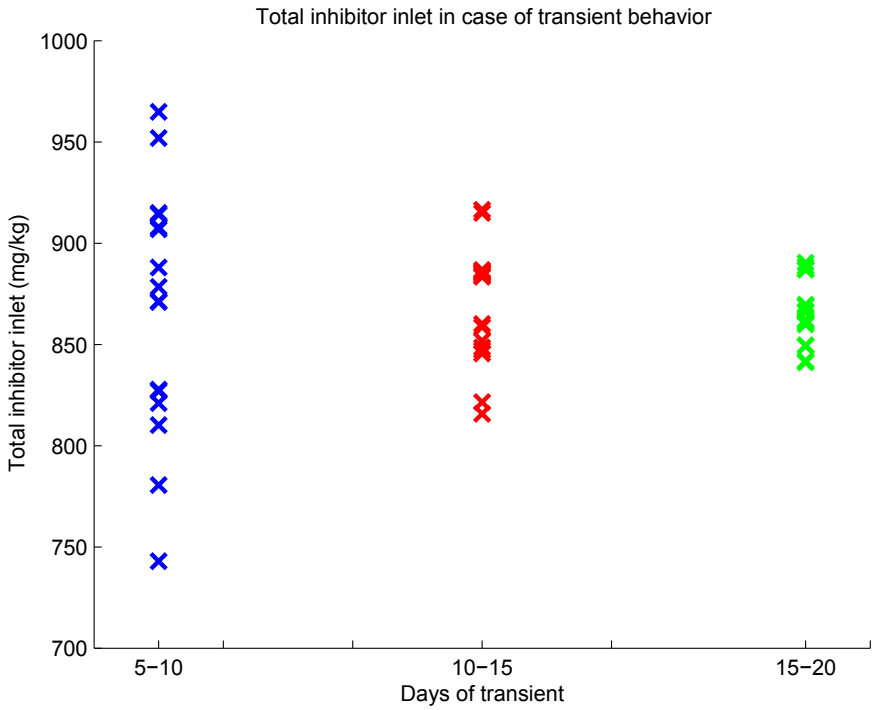

Figure 4.15: The total inhibitor inlet in case of different perturbation scenarios – parameters change between the 5th and 10th day (blue), the 10th and 15th day (red) and the 15th and 20th day (green), each model parameter is perturbed independently with a variability of ±25%.

mg/kg and 916.4 mg/kg (Figure 4.15). Parameter perturbation between the 5th and 10th day can cause both deterioration and amelioration in terms of speed of tumor regression, daily and total inhibitor inlet (Figure 4.14). The total inhibitor inlet varies between 742.9 mg/kg and 964.9 mg/kg (Figure 4.15). In the figure each cross represents a total inhibitor inlet value for a perturbed parameter, e.g. one cross means the total inhibitor inlet if the tumor growth rate (λ_1) is perturbed with +25%. One can see from the figure that the effect of the perturbation decreases as the treatment time increases.

These simulations demonstrated that the designed controller reacts to parametric changes very pliantly, as expected from robust control methodology.

4.3 Thesis Group 1

I provided a linear control synthesis for antiangiogenic therapy over the reduced tumor growth model of Hahnfeldt et al. 1999. I provided new cancer treatment opportunity

based on two different controller-managed automated angiogenic inhibitor administration. The usage of controller-based treatment can ensure effective individual treatment for the patients.

Thesis Group 1: Controller Design for the Tumor Growth Model.

Thesis 1.1

I developed the basis of a new, controller-managed automated therapy which provides optimal drug administration in the case of cancer treatments. The control method which implements this therapy is linear state-feedback control (using pole placement, LQ optimal control and linear observer). The designed controllers ensure alternatives to optimal treatments, from which the clinical doctor can choose the most appropriate, patient and tumor-specific solution. This new approach can handle the therapeutic efficacy, the cost-effectiveness and the side-effect moderation aspects as well.

Thesis 1.2

I developed the basis of a new, controller-managed automated anticancer therapy, which provides robust control and effective treatment also in the case of arising measurement noise and model uncertainties in the control loop. The stabilizing robust (H_∞) controller was designed in the light of physiological aspects, limitations and applicability. I proved using in silico simulations, that the robust controller-based treatment is more efficient than the medical protocol-based treatment.

Relevant own publications pertaining to this thesis group: [S-14; S-11; S-18; S-8; S-9; S-5; S-6; S-1; S-2; S-20; S-10; S-17; S-19; S-3; S-12].

5 Animal Experiments

The Physiological Controls Group of the Óbuda University (Budapest, Hungary) and the 1st Department of Pathology and Experimental Cancer Research of the Semmelweis University (Budapest, Hungary) began collaborating on antiangiogenic therapy research in 2012. Small MRI measurements were performed in the Preclinical Imaging Center of Gedeon Richter Ltd. (Budapest, Hungary). The aim of the experiment was to create and validate a clinically relevant tumor growth model (using B16 melanoma and C38 colon adenocarcinoma), focusing on the effect of angiogenesis. Tumor growth was investigated without therapy and with antiangiogenic therapy (using bevacizumab/ Avastin® (Mukherji 2010)). Examination of tumor growth belongs not only to basic medical research, but to the fields of biomedical engineering and applied informatics as well. Based on the experimental data, model identification can be carried out which describes the mathematical model of the investigated biological process. Using the mathematical model, different dosage algorithms can be designed for antiangiogenic cancer therapy (Chapter 4). Due to the collaboration between medical doctors and biomedical engineers, model-based treatment protocols can be created. These model-based protocols can be more effective than the current ones, since they provide individual treatment for the patients.

My main function during the experiment was to design the phases of the experiment with the supervision of *Prof. Zoltán Sápi* (Professor of Pathology, Deputy Head of the 1st Department of Pathology and Experimental Cancer Research), and to coordinate the phases and sub-processes. Besides this, I also participated in the execution of experiments. I carried out the pipetting process regarding bevacizumab administration. Drug administration, care of mice during the experiment, and sacrifice of mice at the end of the experiment was executed by *András Sztodola* (Animal Caretaker). Cuts form formalin-stored samples and Haematoxylin Eosin staining was done by *Zoltánné Polgár* (Specialist Assistant). I made the frozen cuts from frozen samples and carried out the CD31 antibody immunohistochemistry staining with the supervision of *Katalan Dezső MD. PhD* (Assistant Lecturer), and she made the fluorescent pictures with a confocal microscope. I calculated the vascularization area by using ImageJ software. Statistical

analysis was also performed by the author of the thesis. Small animal MRI measurements were supervised by *Pál Kocsis, PhD* (Researcher, Preclinical Imaging Center of Gedeon Richter Ltd.)

The chapter is organized as follows: Section 5.1 presents the ethics statement while overviews of the phases and materials are discussed in Section 5.2 and Section 5.3, respectively. Tumor types, drug and mice used in the experiment are described in Subsection 5.3.1, Subsection 5.3.2 and Subsection 5.3.3, respectively. Section 5.4 contains methods in detail: tumor implantation (Subsection 5.4.1), bevacizumab administration (Subsection 5.4.2), tumor volume measurement (Subsection 5.4.3), sacrificing mice (Subsection 5.4.4) and tumor sample processing (Subsection 5.4.5). The chapter ends with the experimental data in Section 5.5.

5.1 Ethics Statement

The study was carried out in strict accordance with the recommendations in the Guide for the Care and Use of Laboratory Animals of the National Institutes of Health. The protocol was approved by the Hungarian Animal Experimental Research Ethics Council ("Állatkísérleti Tudományos Etikai Tanács", ATET), Permit Number: 22.1/1159/3/2010. Animals were carried out in the most humane and environmentally sensitive manner possible; in addition the 3Rs principle (replacement, refinement, reduction) was adequately implemented according to the Directive 2010/63/EU of the European Parliament.

5.2 Overview of the Phases

The whole experiment consisted of three phases.

In *Phase I*, we have investigated tumor growth without therapy with two types of mouse tumor. 12 mice were transplanted subcutaneously with C38 colon adenocarcinoma, and 11 mice were injected intramuscularly with B16 melanoma. Tumor volume was measured with digital caliper (Figure 5.1).

In *Phase II*, the toxicology investigation of the applied angiogenic inhibitor (bevacizumab) was performed; there was no tumor implantation into mice in this phase. We monitored the vital parameters of 4 mice, and there was no serious toxic side-effect or lethality regarding to the usage of bevacizumab (Figure 5.2).

In *Phase III*, we have investigated C38 colon adenocarcinoma growth with bevacizumab therapy. Phase III contained three subphases, in every subphases two groups were created; control group received bevacizumab in one dose according to the protocol, while case

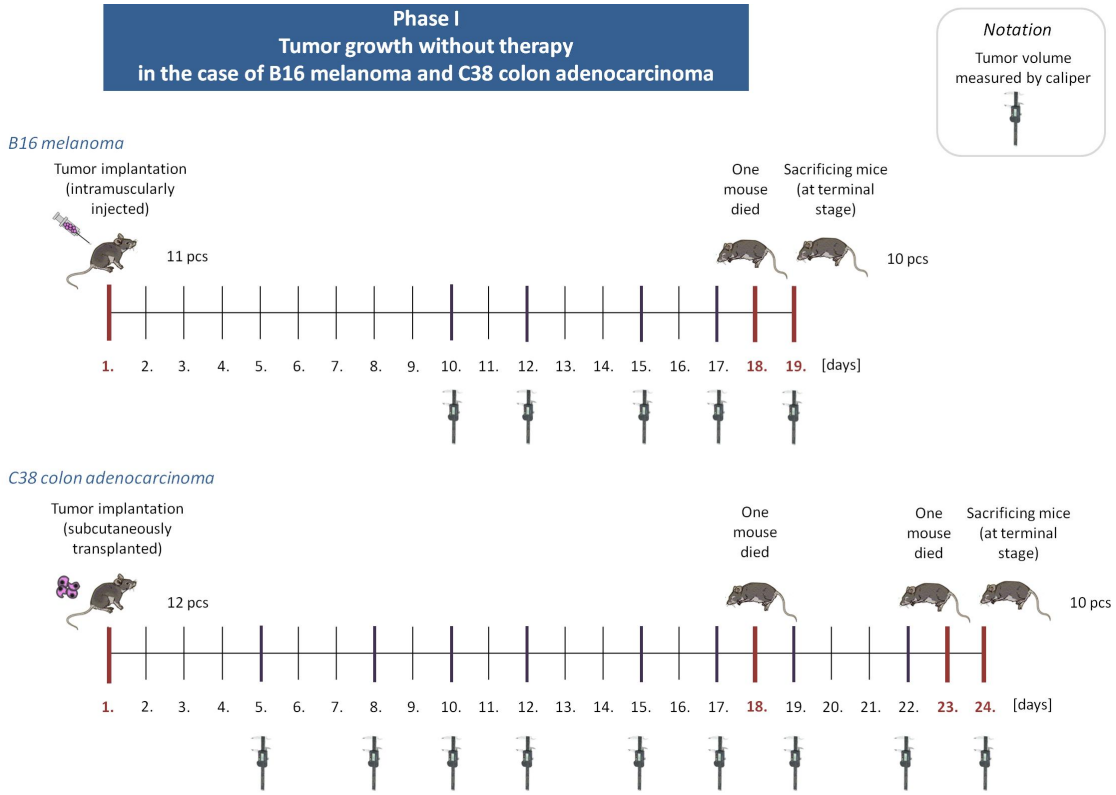

Figure 5.1: In Phase I, tumor growth was investigated without antiangiogenic therapy with two types of mouse tumor (C38 colon adenocarcinoma and B16 melanoma). Mice were sacrificed when the tumor reached a lethal size (in the case of B16 melanoma it was the 16th day of the experiment, in the case of C38 colon adenocarcinoma it was the 24th day). Tumor volume was measured with digital caliper.

group received substantially fewer doses every day.

- In the first subphase (*Phase III/1*), control group (5 mice) received 10 mg per kg body weight bevacizumab, while case group (5 mice) received one-tenth dose of control dose spread over 18 days. Bevacizumab administration was started on the 7th day in both cases. Quantity of the optimal solvent administration was also examined in this subphase. Tumor volume was measured with digital caliper (Figure 5.3).

- The second subphase (*Phase III/2*) was similar to Phase III/1, mice received the same dosage of bevacizumab as in Phase III/1, however sample size was higher (6 mice in control group, 12 mice in case group), and bevacizumab administration

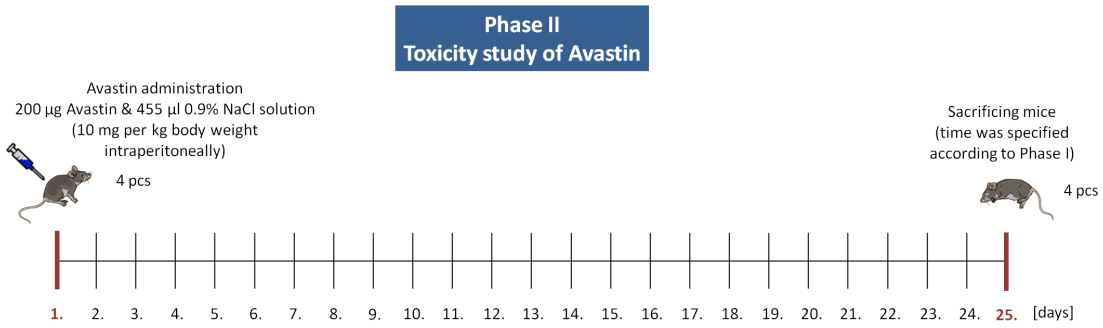

Figure 5.2: In Phase II, the toxicology investigation of the applied angiogenic inhibitor was performed. There was no serious toxic side-effect or lethality regarding to the usage of bevacizumab.

started earlier, on the 3rd day of the experiment. Tumor volume was measured with digital caliper as well (Figure 5.4).

- The third subphase (*Phase III/3*) was designed with the same bevacizumab administration as in Phase III/1 and Phase III/2; nevertheless, tumor volume was measured not only by caliper but by small animal MRI as well (Figure 5.5).

5.3 Materials

5.3.1 Tumor Types Used In the Experiment

C38 colon adenocarcinoma and B16 melanoma are widely and for a long while used mouse experimental tumors from the standard NCI (National Cancer Institute) screening (Silbermann et al. 1990, NCI 2015).

C38 colon adenocarcinoma is a mouse tumor, which is originated from columnar epithelium of colon's mucosa. Adenocarcinoma means "a malignant epithelial tumor with glandular differentiation or mucin production" (Travis et al. 2004). Properties of C38 adenocarcinoma are: (a) because this is a mouse tumor, it grows fast in mice (since 2-3 weeks it reaches a lethal size); (b) also because its specificity, there is no need to use immunosuppressed mice; (c) a piece of tumor can be implanted subcutaneously into the mice; (d) typically does not metastasize; (e) tumor cells inflict strong hypoxial reaction (Ljungkvist, Bussink, Kaanders, et al. 2005). C38 tumor also has a large relative vascular area (Laarhoven, Gambarota, Lok, et al. 2006), which is beneficial if we would like to examine the effect of angiogenic inhibition.

B16 melanoma (Abcam 2005) is a mouse tumor, it is a primer melanoma. "Melanomas

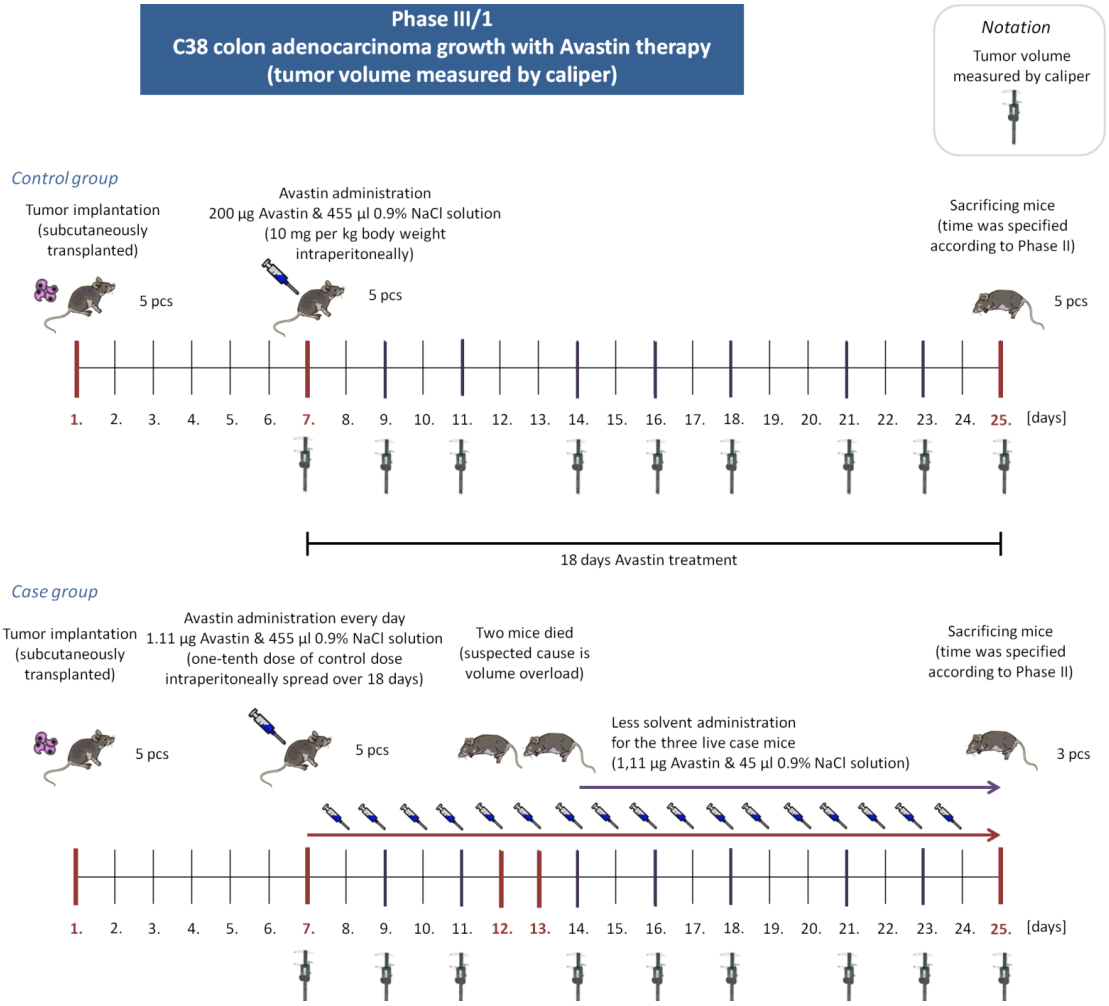

Figure 5.3: In Phase III/1, C38 colon adenocarcinoma growth was investigated with bevacizumab therapy. Control group received 10 mg per kg body weight bevacizumab, while case group received one-tenth dose of control dose spread over 18 days. Bevacizumab administration was started on the 7th day in both cases. Quantity of the optimal solvent administration was also examined in this subphase. Tumor volume was measured with digital caliper.

are malignant tumors derived from melanocytes" (Travis et al. 2004). The pattern can be variable, usually the cytoplasm contains melanin granules. Properties of B16 melanoma are: (a) because this is a mouse tumor, it grows very fast in mice (since 2 weeks it reaches a lethal size); (b) also because its specificity, there is no need to use immunosuppressed mice; (c) it can be injected intramuscularly; (d) typically does not metastasize. B16 mice melanoma can be used as a model for human melanoma (Overwijk and Restifo 2001).

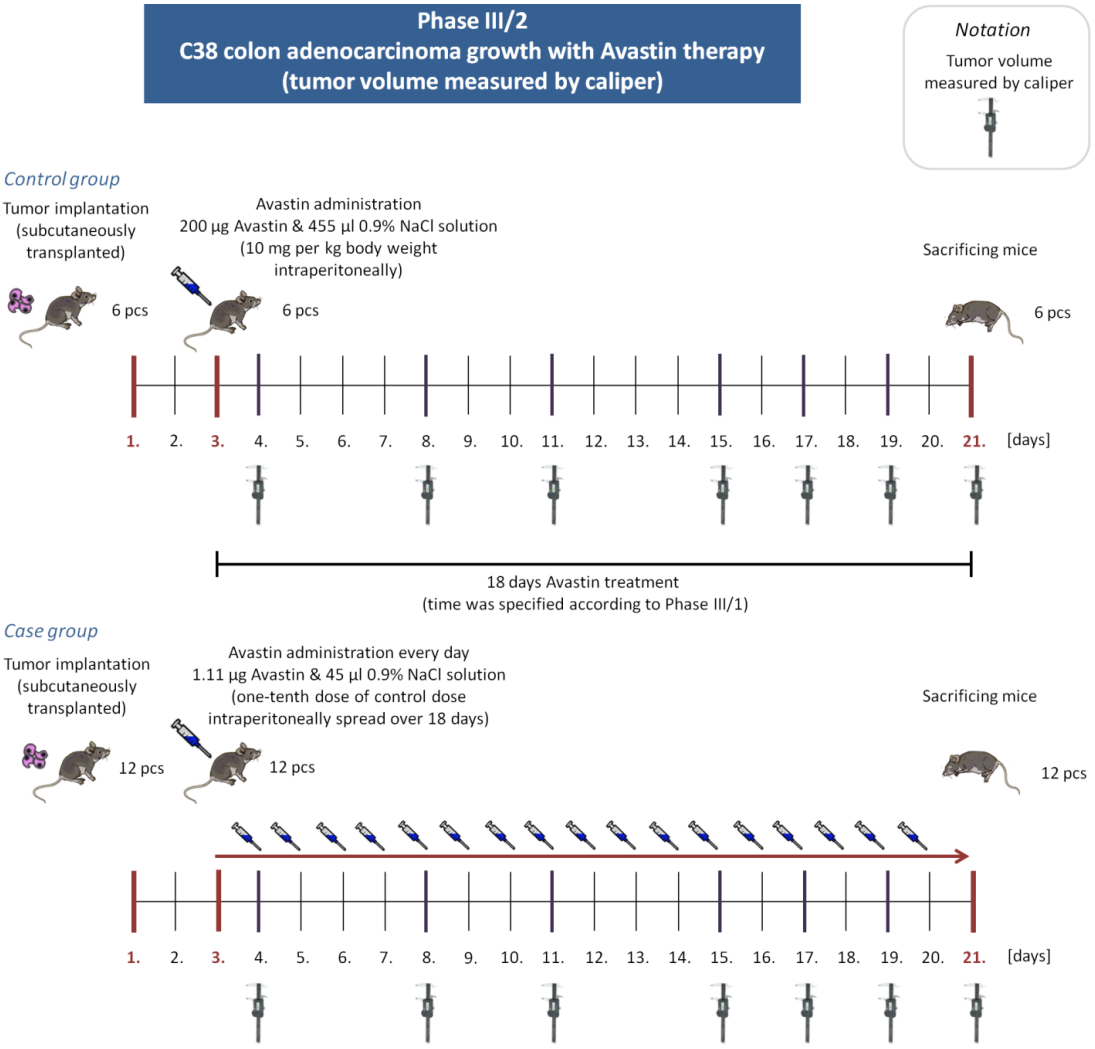

Figure 5.4: In Phase III/2, C38 colon adenocarcinoma growth was investigated with bevacizumab therapy. Control group received 10 mg per kg body weight bevacizumab, while case group received one-tenth dose of control dose spread over 18 days. Bevacizumab administration was started on the 3rd day in both cases. Tumor volume was measured with digital caliper.

5.3.2 Drug Used In the Experiment

Bevacizumab/Avastin® (Genentech 2013) is an exogenous inhibitor, which inhibits the biological activity of human VEGF (European Medicines Agency 2005). Several studies have investigated the effectiveness of bevacizumab therapy according to different types of cancer (Amit et al. 2013): lung cancer (Soria et al. 2013, Vokes, Salgia, and Karrison 2013), breast cancer (Minckwitz et al. 2012, Bear et al. 2012, Montero and Vogel 2012),

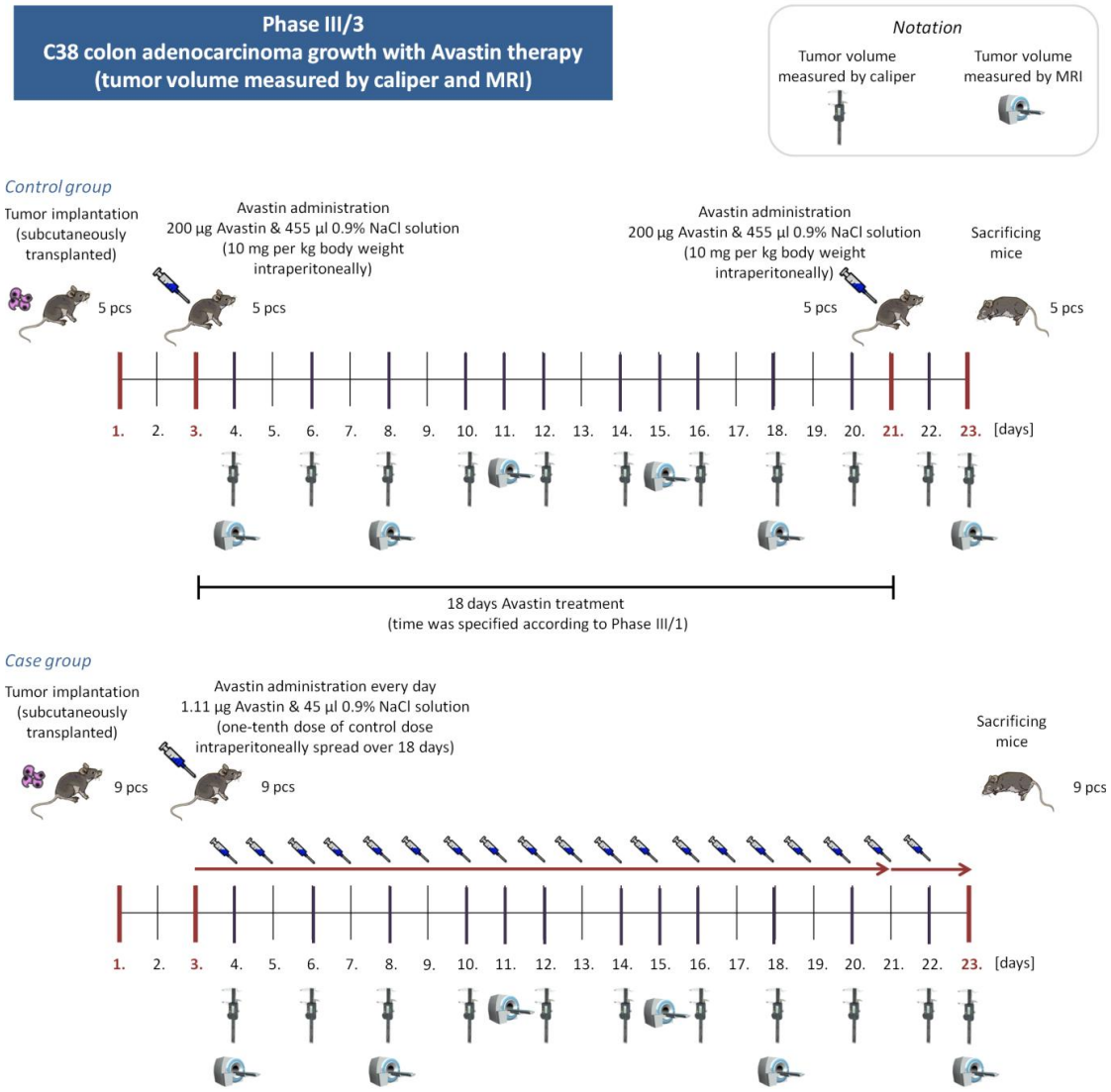

Figure 5.5: In Phase III/3, C38 colon adenocarcinoma growth was investigated with bevacizumab therapy. Control group received 10 mg per kg body weight dose for an 18-day therapy (on the 3rd and 21st days), while case group received one-tenth dose of control dose spread over 18 days (every day for 20 days). Bevacizumab administration was started on the 3rd day in both cases. Tumor volume was measured with digital caliper and by small animal MRI.

colon cancer (Tebbutt et al. 2010), renal cell carcinoma (Rini et al. 2010), gastric cancer (Ohtsu et al. 2011), pancreatic cancer (Kindler et al. 2010), prostate cancer (Kelly et al. 2012) and melanoma (Kim et al. 2012). The majority of debate over Avastin is about breast cancer because, in 2011, the US Food and Drug Administration (FDA) revoked

the approval of Avastin for breast cancer treatment in the absence of decisive therapeutic benefit; however, several clinical trials suggested that Avastin can be effective in breast cancer treatment (Minckwitz et al. 2012, Bear et al. 2012).

5.3.3 Mice Used In the Experiment

Eight weeks old male C57Bl/6 mice from the colony of the 1st Department of Pathology and Experimental Cancer Research Animal Laboratory were used for the experiments. This mice type is widely used to model human disease. The C38 colorectal carcinoma line was maintained by serial subcutaneous transplantations in C57Bl/6 mice. (Inbred C57Bl/6 mice from the institute were used throughout the studies.)

5.4 Methods

5.4.1 Tumor Implantation

In the case of C38 colon adenocarcinoma a piece of tumor was transplanted subcutaneously in the recipient animal; in the case of B16 melanoma $2 \cdot 10^6$ tumor cells were injected intramuscularly for a mouse on the 1st day of the experiment.

C38 colon adenocarcinoma was used in Phase I, Phase III/1, Phase III/2 and Phase III/3. B16 melanoma was used in Phase I. In Phase II, there was no tumor implantation into mice.

5.4.2 Bevacizumab Administration

In Phase I, there was no bevacizumab administration.

Recommended administration of bevacizumab is one $5 - 10$ mg/kg dose for 2-3 weeks (Genentech 2013). In Phase II and Phase III, we have administered 10 mg/kg body weight intraperitoneally, which means 200 μg bevacizumab per a mouse, since the mass of the mice in the experiment was approximately 20 g.

In Phase II, we have administered 200 μg bevacizumab (with 455 μl 0.9% NaCl solution) in one dose intraperitoneally for the mice on the 1st day. Effect of bevacizumab was monitored for 25 days (the time was specified according to Phase I).

In Phase III, both control and case group members received bevacizumab. The 10 mg/kg dose was used for an 18-day treatment.

- In Phase III/1, the control group members received 200 μg bevacizumab (with 455 μl 0.9% NaCl solution) in one dose intraperitoneally. The case group members

received one-tenth dose of control dose intraperitoneally spread over 18 days. It means that a mouse of the case group received 1.11 μg bevacizumab every day. This dose was administred with 450 μl 0.9% NaCl solution at the beginning of the experiment. However two mice died (one died on the 12th day, the other one died on the 13th day), and due to the fact that the suspected cause was volume overload, we reduced the volume of 0.9% NaCl solution to 45 μl from the 14th day. Bevacizumab administration started on the 7th day. The treatment period was 18 days (Figure 5.3).

- In Phase III/2, the control group members received 200 μg bevacizumab (with 455 μl 0.9% NaCl solution) in one dose intraperitoneally. The case group members received one-tenth dose of control dose intraperitoneally every day spread over 18 days (1.11 μg bevacizumab with 45 μl 0.9% NaCl solution). Bevacizumab administration started on the 3rd day. The treatment period was 18 days (Figure 5.4).

- In Phase III/3, the control group members received 200 μg bevacizumab (with 455 μl 0.9% NaCl solution) in one dose intraperitoneally on the 3rd day and on the 21st day. The case group members received one-tenth dose of control dose intraperitoneally spread over 18 days (1.11 μg bevacizumab with 45 μl 0.9% NaCl solution every day). Bevacizumab administration for the case group started on the 3rd day as well. The treatment period was 20 days (Figure 5.5).

5.4.3 Tumor Volume Measurement

Tumor volume measurement cannot happen right after tumor implantation. In the case of C38 colon adenocarcinoma first the subcutaneously transplanted piece of tumor has to disintegrate, and after that the new tumor colony (which needs to be measured) can begin to grow from the disintegrated tumor cells. The first measurement after tumor implantation occurred when the tumors have reached an average volume of $50 - 60\ mm^3$ (Online 2005). It was on the

- 5th day in Phase I in the case of C38 colon adenocarcinoma,
- 10th day in Phase I in the case of B16 melanoma,
- 7th day in Phase III/1,
- 4th day in Phase III/2,

- 4th day in Phase III/3.

Tumor volume was measured in two different ways. In the case of Phase I, Phase II, Phase III/1 and Phase III/2 tumor volume was measured by *digital caliper*; in the case of Phase III/3 tumor volume was measured by digital caliper and *small animal MRI* as well.

Tumor Volume Measurement With Digital Caliper

Using digital caliper, two tumor diameters (width, length) can be measured with caliper, but the spatial extent of tumor along the third dimension, i.e. the depth (height) can not be determined. It can be carried out in vivo during the experiment because of the subcutaneous localization of the tumor (Figure 5.6). Tumor volume (and the third diameter) has to be approximated, assuming a certain shape for the tumor. Measurements with caliper were done on the

- 5th, 8th, 10th, 12th, 15th, 17th, 19th, 22nd and 24th days in Phase I in the case of C38 colon adenocarcinoma,
- 10th, 12th, 15th, 17th and 19th days in Phase I in the case of B16 melanoma,
- 7th, 9th, 11th, 14th, 16th, 18th, 21st, 23rd days and 25th in Phase III/1,
- 4th, 8th, 11th, 15th, 17th, 19th and 21st days in Phase III/2,
- 4th, 6th, 8th, 10th, 12th, 14th, 16th, 18th, 20th, 22nd and 23rd days in Phase III/3.

Tumor Volume Measurement With Small Animal MRI

The other method what we used to measure tumor volume is small animal MRI. This non-invasive in vivo technology gives the possibility of a more precise volume measurement (Koo, Hamilton, and Williamson 2006). Particularly good contrast can be achieved using MRI when visualizing soft-tissues and lesions, which would be hidden by bone shadows in a radiograph. One of the many great advantages of this imaging technique is that it provides information about the function of the examined organ in addition to its structure. The structure of small animal MRI scanner is very similar to the typical human tunnel MRI scanners; the most significant difference is the diameter of the patient table, because in the case of small animal MRI, it is scaled down to study mice and rats. The smaller diameter results in much stronger magnetic field and more homogeneous field. The field

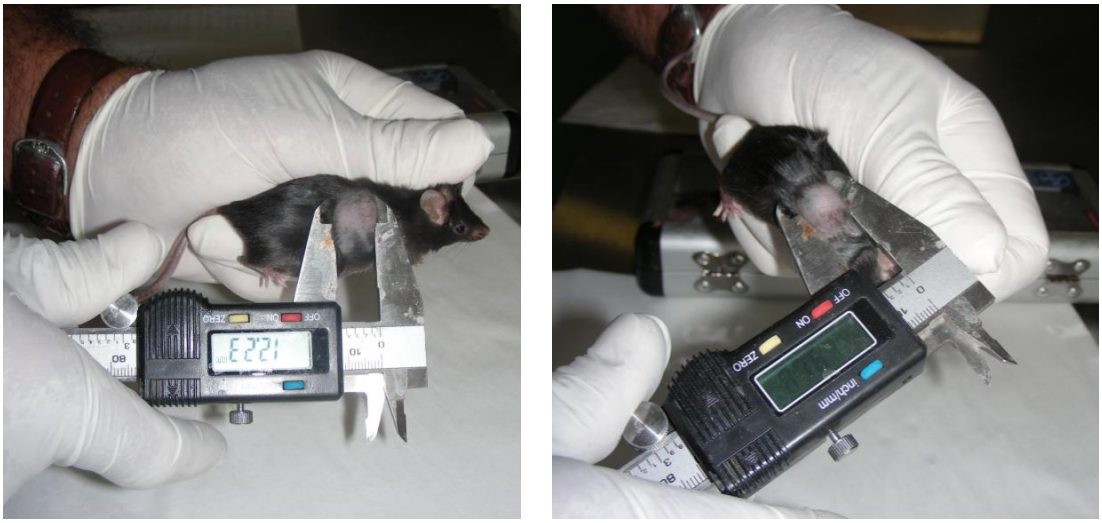

Figure 5.6: Measuring two diameters (width, length) of the tumor with digital caliper.

strength is usually in the range of [4.7, 14.1] Tesla, spatial resolution can be less than 100 micrometers, and the time of examination is shorter due to the greater signal-to-noise ration.

In the experiment 9.4 Tesla field strength Varian small animal MRI was used. Isofluorane (0.95 x 2.0%) was applied for inhalational anesthesia, and intubation was performed. Catheter was placed in the tail vein for injection – according to the mouse tail vein injection protocol (Targeson 2012) – to investigate drug effect. Position of the mouse was fixed to minimize the movement of the animal. Tumor was located in the last third of the back in every cases, thus the effect of respiratory movement was minimal. During the MRI measurements, life parameters of the mice were monitored. Breathing was monitored with piezoelectric transducer; temperature of the body was measured by rectal thermometer. The produced images were converted to NIfTI (Neuroimaging Informatics Technology Initiative) format, which is suitable for image processing. Tumor area was determined with flood fill algorithm (Pachghare 2005) from the slides; by knowing the volume of a voxel, tumor volume was calculated from these two values. Contrast agents improve the visibility, but it is an extra strain to the organism, which can be lethal to animals which are in the final stage of cancer.

We have investigated three different MRI sequences in the case of T1-weighted images in a pre-study (Kiss, J Sápi, and L Kovács 2013) to find the most suitable sequence method which provides MRI images with high resolution and good contrast, since there is no usual specification used in practice because there are different experiments with

different animals, diseases and aims.

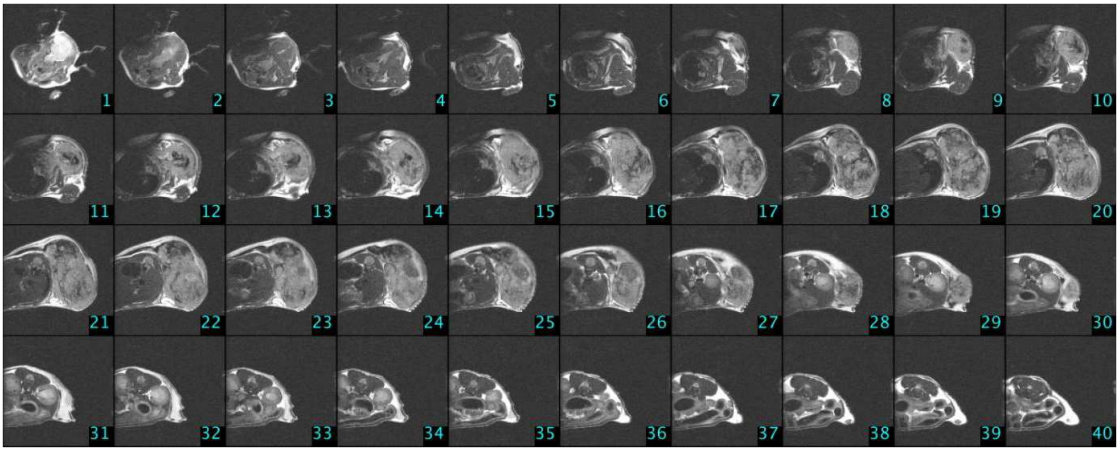

Figure 5.7: MRI slices in the case of a control group mouse (*C4*) on the 23rd day of the experiment (Phase III/3).

- *Gradient echo (T1-GE)* sequence was not appropriate to sharply separate tumor from the surrounding tissues, because both the connective tissue and the tumor can be visualized by similar bright pixels. To improve image quality and differentiate between these tissues one must increase the average number of slices, which results in longer data acquisition time. Too high TR (Repetition Time) value produces hollow images, because TR has a large effect on the contrast and also acquisition time. Too high TE (Echo Time) value causes in the image shadow artifacts over and under the mouse. It comes from the respiratory movements of the animal during scanning. Improving the resolution by halving the voxel size in the $x - y$ plane, the inner structure of the tumor can be examined. Because of the smaller voxel size, smaller volume is kindled and signals are gathered from this smaller volume, thus the volume-specific peculiarities come out.

- *Spin echo (T1-SE)* sequence raises the difference between tumor and surrounding tissues. Using weak parameter sets and very short data acquisition time, the tumor can be acceptably segmented. As we have increased acquisition time, the image became more detailed and informative. The spin echo is a commonly used sequence, because it can produce extremely good contrast, but the acquisition time strongly limits it.

- *Fast spin echo (T1-FSE)* sequence makes the data acquisition more effective, hence in addition to shorter acquisition time, high image quality and great contrast can

be achieved. The main disadvantage of FSE is the very strong gradient what is needed, however in our experiment this requirement was given.

Since FSE sequence produces detailed images in short data acquisition time, we chose this sequence for our experiment. We have found that measurements without contrast agents resulted in high quality images, where tumor can be circumscribed precisely, thus the usage of contrast is unnecessary.

In the case of Phase I, Phase II, Phase III/1 and Phase III/2 there were no MRI measurement. Measurements with small animal MRI were done on the 4th, 8th, 11th, 15th, 18th and 23rd days of the experiment in Phase III/3. In the first four measurement times 30 slices were done from each mouse; in the last two measurement times 40 slices were done from each mouse due to the larger tumor volume. One can see experimental settings in Table 5.1, while MRI image of a control group mouse ($C4$) that was measured at the end of the experiment can be found in Figure 5.7.

5.4.4 Sacrificing Mice

All surgery and sacrifice were performed under sodium pentobarbital anaesthesia (Nembutal, 70 mg/kg), and all efforts were made to minimize suffering.

In Phase I mice were sacrificed when the tumor reached a lethal size; it was on the 24th day of the experiment. In the other phases time of the experiment (and treatment time) was specified according to the previous phases. Mice were sacrificed on the

- 25th day in Phase II,
- 25th day in Phase III/1 (after 18 days treatment),
- 21st day in Phase III/2 (after 18 days treatment),
- 23rd day in Phase III/3 (after 20 days treatment).

5.4.5 Tumor Sample Processing

After sacrificing mice, tumors were removed, and their mass was measured. Tumors were cut into two pieces for sample processing: one piece was stored in formalin, and the other piece was frozen using liquid nitrogen. Tumor morphology was investigated using standard *Haematoxylin Eosin (H&E) staining* on the samples stored in formalin. Frozen samples were used to create 15 μm frozen cuts and to carry out *immunohistochemistry (IHC)*. After fixing in methanol, rat anti-mouse CD31 antibody (1:50, 550274 BD PHARMINGEN)

Table 5.1: Experimental settings for small animal MRI measurement in Phase III/3.

30 slices	**40 slices**
Pulse sequence: T1WI,	Pulse sequence: T1WI,
Sequence: FSE,	Sequence: FSE,
FOV: 25 x 25,	FOV: 30 x 30,
Spatial resolution: 128 x 128 x 30,	Spatial resolution: 128 x 128 x 40,
Voxel size: 0.1953 x 0.1953 x 1 mm,	Voxel size: 0.2343 x 0.2343 x 1 mm,
TR: 1800 ms,	TR: 2500 ms,
ESP: 7 ms,	ESP: 7 ms,
Axial orientation: axial 90°,	Axial orientation: axial 90°,
Flip angle: 90°,	Flip angle: 90°,
averages: 12, scan time: 5 min 53 s	averages: 10, scan time: 6 min 45 s

In the first four measurement times 30 slices, in the last two measurement times 40 slices were done from each mouse. Abbreviations: T1WI: T1 weighted image, FSE: Fast Spin Echo, FOV: Field of View [mm^2], TR: Repetition Time, ESP: Echo Spacing.

was applied as primer antibody, and FITC conjugated anti-rat CD31 antibody (1:100, Jackson Immunoresearch, 712-095-150) was applied on the slides as secondary antibody. After staining, fluorescence pictures were done from the slides using confocal microscope (BIO-RAD MRC-1024). These images were applied to calculate vascularization area by using ImageJ (NIH, USA) (ImageJ 1997) software (Figure 5.8).

5.5 Experimental Data

In Phase I, 12 mice were implanted with C38 colon adenocarcinoma. One of them died on the 18th day, and another one on the 23rd day, thus 10 mice were sacrificed at the 24th day of the experiment. B16 melanoma was implanted into 11 mice. One mouse died at the 18th day, therefore 10 mice were sacrificed at the 19th day of the experiment.

In Phase II, 4 mice received Avastin for toxicology investigation. No mice died during

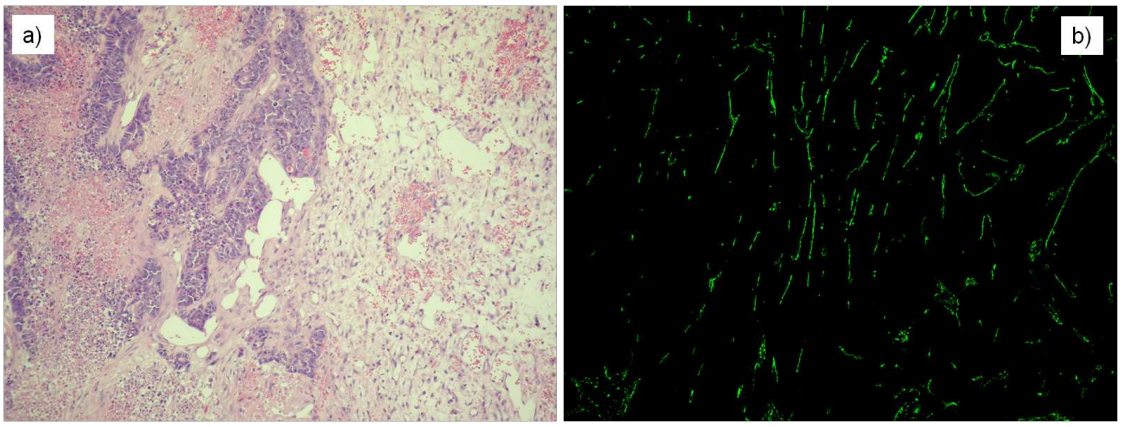

Figure 5.8: Stained slices in the case of *n1* mouse (Phase I, 24th day of the experiment). a) Haematoxylin Eosin (H&E) staining was applied to investigate tumor morphology. b) Fluorescence picture was created using CD31 antibody immunohistochemistry staining to calculate vascularization area.

the experiment.

In Phase III/1, the control group contained 5 mice, the case group contained 5 mice; all mice were implanted with C38 colon adenocarcinoma.Two mice died from the case group (one died on the 12th day, the other one died on the 13th day), therefore 5 contol and 3 case mice were sacrificed after the 18-day Avastin treatment, on the 25th day of the experiment.

In Phase III/2, the control group contained 6 mice, the case group contained 12 mice; all mice were implanted with C38 colon adenocarcinoma. No mice died during the experiment, therefore 6 contol and 12 case mice were sacrificed after the 18-day Avastin treatment, on the 21*st* day of the experiment.

In Phase III/3, the control group contained 5 mice, the case group contained 9 mice; all mice were implanted with C38 colon adenocarcinoma. No mice died during the experiment, therefore 5 mice from the control group, and 9 mice from the case group were sacrificed after the 20-day Avastin treatment, on the 23rd day.

6 Tumor Growth Model Identification

Since the Hahnfeldt model – for which controllers were designed – has some limitations according to the newest medical research in the field of angiogenic tumor growth (viz. VEGF inhibition leads to apoptosis only in newly-built vessels in tumors, but does not have an effect on vessels which have already existed), new tumor growth model identification is needed.

Three main classes of mathematical models have been created in the field of antiangiogenic therapy (Mriouah et al. 2012; Peirce 2012): a) temporal models (Hahnfeldt et al. 1999; A D'Onofrio and A Gandolfi 2009), b) spatiotemporal models (Chaplain 2000; Finley et al. 2011) and c) multiscale models (Gevertz 2011; Stephanou et al. 2005). The main disadvantage of these models is that they are mechanistic or semi-mechanistic (Ribba et al. 2011) models built up from physical equations, and they have not been validated with in vivo data in most of the cases. Exceptions (validated models) exist; however they have other problems. The Hahnfeldt model (Hahnfeldt et al. 1999) is not valid any more in light of new medical results. A newly created and validated model posed by Gevertz 2011 takes into account numerous effects and, as a result, it is overly difficult (it contains 13 variables and 21 parameters).

Consequently, there is a strong need to create a mathematical model which describes the tumor growth dynamics under angiogenic inhibition. This model has to take into account the previously mentioned models and their results, but it also has to be sufficiently simple to be manageable for both real-life applicability and controller design.

The chapter is organized as follows: Section 6.1 discusses statistical analysis methods which were used to evaluate the experimental results.

Section 6.2 contains the model identification of tumor growth without therapy for C38 colon adenocarcinoma (Subsection 6.2.1) and B16 melanoma (Subsection 6.2.2). Both subsections contain sub-subsections according to parametric identification (Sub-subsection 6.2.1 for C38 colon adenocarcinoma and Sub-subsection 6.2.2 for B16 melanoma); and the relationship investigation between tumor volume, mass and vascularization (Subsubsection 6.2.1 for C38 colon adenocarcinoma and Subsubsection 6.2.2 for B16 melanoma). The section ends with the conclusions in Subsection 6.2.3.

Section 6.3 contains the model identification of tumor growth with antiangiogenic therapy. Subsection 6.3.1 presents the results of Phase III/2, while Subsection 6.3.2 presents the results of Phase III/3. Phase III/2 results contain parametric identification (Sub-subsection 6.3.1) and relationship investigation between tumor volume, mass and vascularization (Sub-subsection 6.3.1). Phase III/3 results contain tumor volume estimation (Sub-subsection 6.3.2). Both Phase III/2 and Phase III/3 evaluation contain sub-subsections according to effective dosage investigation for optimal therapy (Sub-subsection 6.3.1 for Phase III/2 and Sub-subsection 6.3.2 for Phase III/3); and conclusions (Su-bsubsection 6.3.1 for Phase III/2 and Sub-subsection 6.3.2 for for Phase III/3).

The chapter ends with Thesis Group 2 in Section 6.4.

6.1 Statistical Analysis Methods to Evaluate the Experimental Results

6.1.1 Parametric Identification

In tumor growth there are two main processes which take place. The first process, actually the engine of tumor growth is the vascular growth; new blood vessels are indispensable for the tumor to pick up enough nutrients and oxygen. With the support of vasculature, tumor mass growth can occur as the second process. Taking into account these two dynamics behind tumor growth, we are seeking for a second order system for identification. The simplest dynamic model is a linear one; in this case the response of the system consists of exponential functions. The second order system has two exponential functions in its response, thus parametric identification was carried out by fitting a curve with two exponential functions. The curve was fitted to the average tumor volume of each mouse at the measurement points (days) using Least Squares (LS) method.

6.1.2 Finding the Relationship Between Tumor Volume, Mass and Vascularization

Three attributes of the lethal sized tumor were measured: tumor volume, tumor mass and vascularization. Relationship between these tumor attributes was investigated with linear regression analysis (Montgomery, Peck, and Vining 2012). To decide whether the relationship is significant or not between two variables, I used the following statistics. Pearson correlation coefficient (R) describes strength of the correlation (linear dependence) between the variables. Coefficient of determination (R^2) tells how many percent of the variability in a data can be explained by the given statistical model (which is a linear

model in every investigated cases). Using Analysis of Variance (ANOVA) test (Larson 2008) we can decide that the regression analysis is valid or not (level of significance was chosen to $p = 0.05$).

6.1.3 Investigating the Effective Dosage for Optimal Therapy

To compare the results of the investigated cases (results from the different phases), statistical analysis was used. PASW Statistics 18 (SPSS Statistics, IBM, USA) and Matlab R2009b (MathWorks, USA) were used for statistical analysis. Before the usage of any statistical tests, one has to examine the normality and homogeneity of variance (homoscedasticity) of the distributions. Normality was investigated with one-sample Kolmogorov-Smirnov test, and homogeneity of variance (homoscedasticity) was examined with Levene's test. After confirming normality and homoscedasticity, parametric statistical analysis can be used. Analysis of Variance (ANOVA) test was used to compare more than two samples. To find those samples, which have significantly different means, pairwise comparison was done. Tukey's honest significant difference (HSD) test was used as post hoc test.

6.2 Model Identification of Tumor Growth Without Therapy

6.2.1 C38 Colon Adenocarcinoma Growth Identification Without Therapy

Experiment results from Phase I were evaluated in two different ways in the case of C38 colon adenocarcinoma, since tumor volume was estimated using two different calculation. Tumor diameters (width (w) and length (l)) were measured with a digital caliper, the third dimension of the tumor (height (h)) was approximated.

- **Estimation 1 (rectangular prism)** Tumor volume was estimated with the volume of the rectangular prism which can be drawn around the tumor (J Sápi, D A Drexler, I Harmati, A Szeles, et al. 2013; L. Kovács, J. Sápi, Ferenci, et al. 2013). It is an upper bound for the tumor volume ($O(V)$ estimation). Tumor height was approximated with the arithmetic mean of width and length, multiplied by 2/3. Thus, the tumor volume in mm^3 was calculated by the formula:

$$V = w \cdot l \cdot \frac{w + l}{3}. \tag{6.1}$$

- **Estimation 2 (ellipsoid)** Tumor volume was estimated assuming ellipsoid shape. Tumor height was approximated with the length multiplied by 2/3. Therefore

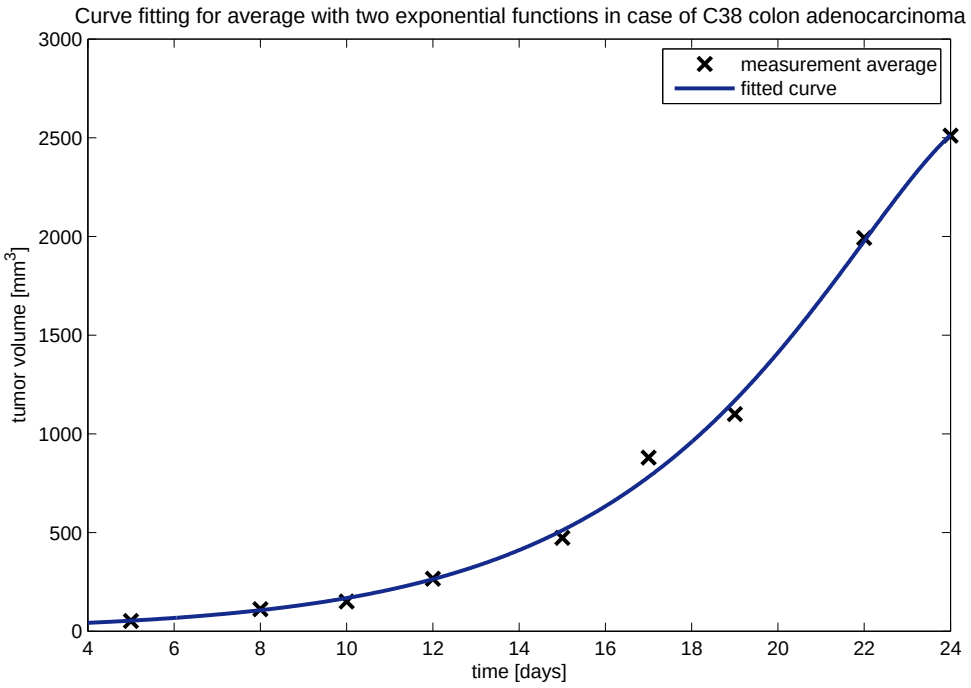

Figure 6.1: Exponential curve fitting for average in the case of C38 colon adenocarcinoma $(y(t) = -0.076 \cdot \exp(0.4239t) + 16.87 \cdot \exp(0.2329t)$

tumor volume in mm^3 was calculated by the formula:

$$V = \frac{4}{3} \cdot \pi \cdot \frac{l}{2} \cdot \frac{w}{2} \cdot \frac{l}{3}. \tag{6.2}$$

In this subsection I will evaluate the results of Estimation 1. Results of Estimation 2 will be discussed and compared to the results of Phase III/2 in Subsection 6.3.1.

Parametric Identification

The result of curve fitting on the average of the measurements can be found in Figure 6.1. The response of the system is described by:

$$y(t) = -0.076 \cdot \exp(0.4239t) + 16.87 \cdot \exp(0.2329t) \tag{6.3}$$

The time constants of the identified model are $T_1 = 2.3589$ days, and $T_2 = 4.2938$ days. The coefficients of the exponentials are positive, thus the system is unstable, as it is required from a tumor growth.

This fitting were done with Matlab and results were verified with SPSS. Using SPSS, I have examined other fitting curve types and four curves had equal or better coefficient of determination than 0.99 (exponential $R^2 = 0.990$, growth $R^2 = 0.990$, compound $R^2 = 0.990$, cubic $R^2 = 0.991$). Cubic curve fits better for the sample points than the other, but outside of the sample range, the extrapolation is worse. Exponential, growth and compound models fitted the same curves.

Another model used to describe tumor growth is Gompertzian curve (Yorke et al. 1993), which describes a dynamic process that has a plateau. In this model tumor cell number also depends on the initial tumor size, the elapsed time and a constant, but at the end of the growth period growth narrows and cell number has a plateau:

$$N(t) = N_0 \cdot exp\left[ln\left(\frac{N_\infty}{N_0}\left[1 - exp\left(-bt\right)\right]\right)\right], \tag{6.4}$$

where N_∞ is the plateau and parameter b is related to the initial tumor growth rate. This model describes that tumor growth is nutrient-, and oxygen-limited. However, in the plateau phase tumor size and toxicity is lethal for the host organism without therapy. In our experiments the last measured tumor volume is approximately equal to the plateau cell number. Nevertheless Gompertzian curve is more difficult than the exponential one, and may even vary considerably for patients with the same type of cancer.

Finding the Relationship Between Tumor Volume, Mass and Vascularization

As discussed previously, we have measured three data of the lethal sized tumor: tumor volume, tumor mass and vascularization. I have investigated the relationship between these tumor attributes with linear regression analysis. In Figure 6.2 the relationship between *tumor mass and volume* can be seen. The coefficient of determination is $R^2 = 0.871$, this means that 87.1% variability in a data can be explained by the given statistical model. Pearson correlation coefficient is $R = 0.933$, thus there is a strong correlation (linear dependence) between these variables. Using ANOVA test, a strong significant regression relationship was detected ($p < 0.0001$). C38 colon adenocarcinoma is a solid tumor – this type of tumor usually does not contain cysts or liquid area, thus tumor mass has high density.

The association between *tumor mass and vascularization* is shown in Figure 6.3. The coefficient of determination is $R^2 = 0.039$, Pearson correlation coefficient is $R = 0.198$, and ANOVA p-value is $p = 0.584$. From each parameter we can see that there is a weak, not significant relationship between tumor mass and vascularization. Similar results can

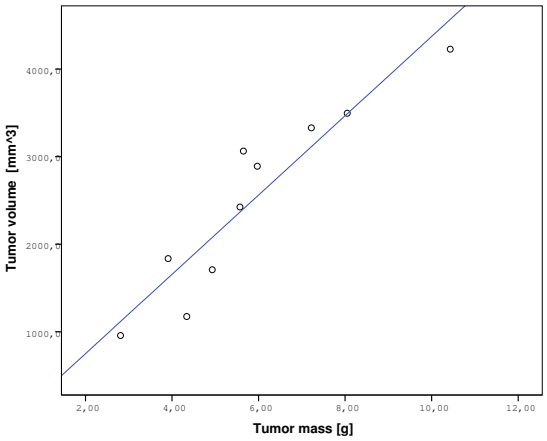

Figure 6.2: Linear regression between tumor mass and volume in the case of C38 colon adenocarcinoma ($R^2 = 0.871, R = 0.933, p < 0.0001$)

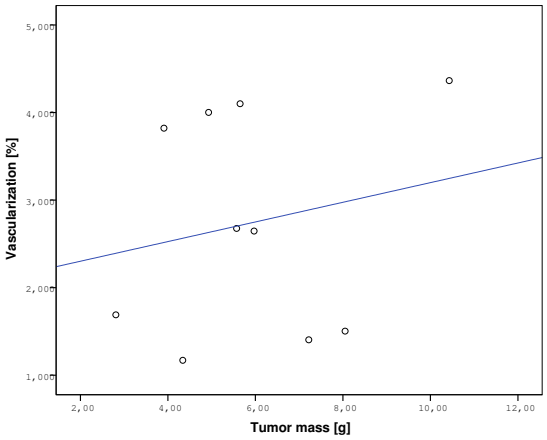

Figure 6.3: Linear regression between tumor mass and vascularization in the case of C38 colon adenocarcinoma ($R^2 = 0.039, R = 0.198, p = 0.584$)

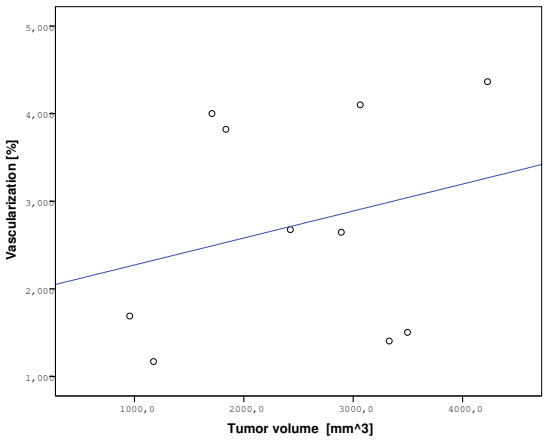

Figure 6.4: Linear regression between tumor volume and vascularization in the case of C38 colon adenocarcinoma ($R^2 = 0.069, R = 0.263, p = 0.462$)

be observed in the case of *tumor volume and vascularization* (Figure 6.4). The coefficient of determination is $R^2 = 0.069$, Pearson correlation coefficient is $R = 0.263$, and ANOVA p-value is $p = 0.462$. This can be explained by the following. Rapidly dividing tumor cells need lots of oxygen. When proliferation begins, small sized tumor can pick up oxygen from near capillaries. After a certain size ($1 - 2$ mm diameter) tumor development stops, because a part of the tumor gets too far from capillaries and can't pick up enough oxygen. Tumor needs own blood vessels to grow, however, due to this hurried vessel forming, a part of tumor still can't get enough oxygen, whereupon these cells first inflict hypoxial reaction, then die. In C38 colon adenocarcinoma there are several necrotic regions, thus the whole mass contains relatively few viable cells and vessels (Kamm et al. 1996).

6.2.2 B16 Melanoma Growth Identification Without Therapy

In the case of B16 melanoma experiment, tumor volume was calculated according to (6.1).

Parametric Identification

The average values of the measurements and the fitted multiexponential curve can be seen in Figure 6.5. The result of the parametric identification is the following function:

$$y(t) = -511.6 \cdot \exp(0.54781t) + 512.3 \cdot \exp(0.54775t) \tag{6.5}$$

The time constants of the system are $T_1 = 1.8256$ days and $T_2 = 1.8254$ days. The parametric identification results in almost identical time constants, however the multiexponential characteristic is important. This simple model even results in a plateau like characteristics at high tumor volume values, without the nonlinear model of the Gompertzian growth. The coefficients of the exponential functions are positive in this case as well, resulting in an unstable system.

Finding the Relationship Between Tumor Volume, Mass and Vascularization

As at analysis of C38 colon adenocarcinoma, this fitting was also done with Matlab and results were verified with SPSS. Examined best fitting curve types and coefficient of determination values are: exponential $R^2 = 0.955$, growth $R^2 = 0.955$, compound $R^2 = 0.955$, cubic $R^2 = 0.981$. Also in this case cubic fits better, but has the same problem (wrong extrapolation and prediction). Exponential, growth and compound models fitted the same curves.

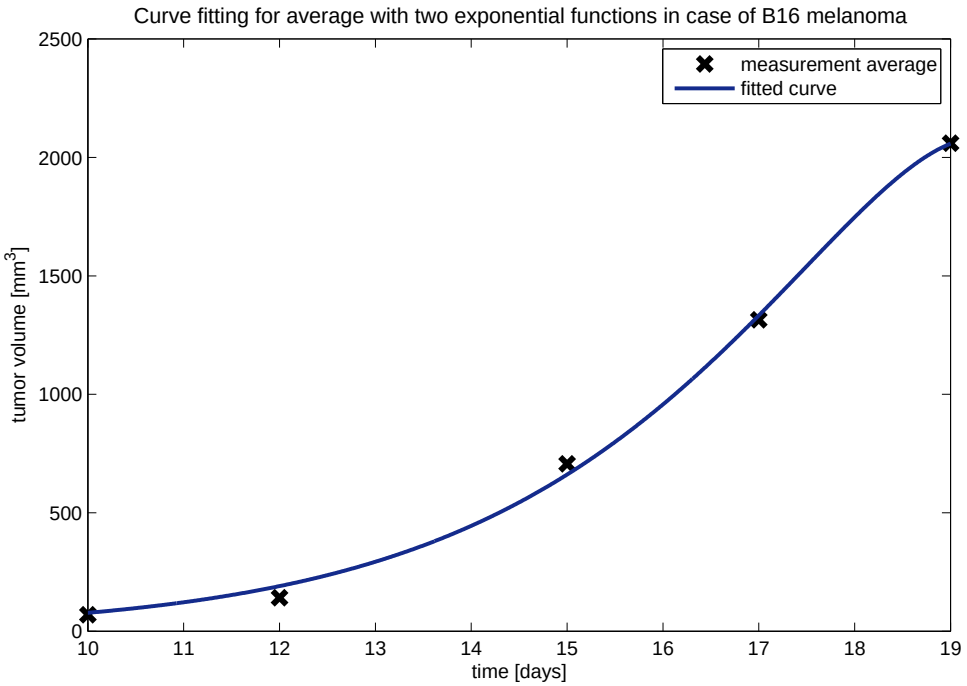

Figure 6.5: Exponential curve fitting for average in the case of B16 melanoma ($y(t) = -511.6 \cdot \exp(0.54781t) + 512.3 \cdot \exp(0.54775t)$)

In Figure 6.6 the relationship between *tumor mass and volume* can be seen. The coefficient of determination is $R^2 = 0.421$, Pearson correlation coefficient is $R = 0.649$. These parameters show correlation, but not as strong as in case of C38 colon adenocarcinoma. Using ANOVA test, also a weaker, but significant regression relationship can be detected ($p = 0.042$). B16 melanoma is a solid tumor as well, but cell growth leads to necrosis and liquefaction of muscle tissues. Because of that the removed mass contains liquefied areas, which have lower density.

The association between *tumor mass and vascularization* is shown in Figure 6.7. The coefficient of determination is $R^2 = 0.215$, Pearson correlation coefficient is $R = 0.463$, and ANOVA p-value is $p = 0.177$. One can see the relationship between *tumor volume and vascularization* in Figure 6.8. The coefficient of determination is $R^2 = 0.029$, Pearson correlation coefficient is $R = 0.170$, and ANOVA p-value is $p = 0.638$. Vascularization does not have significant relationship with tumor mass, neither with tumor volume.

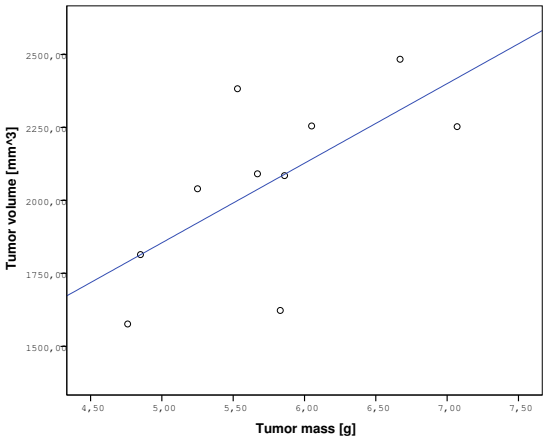

Figure 6.6: Linear regression between tumor mass and volume in the case of B16 melanoma ($R^2 = 0.421, R = 0.649, p = 0.042$)

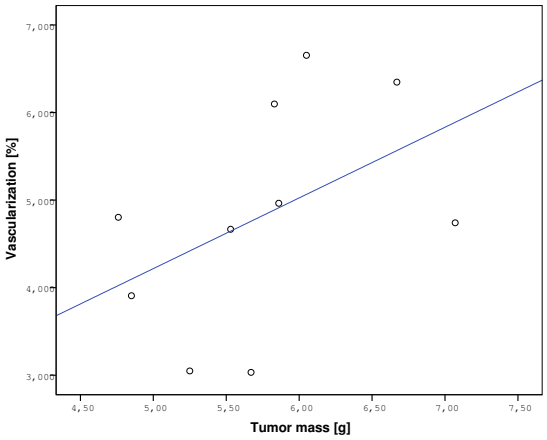

Figure 6.7: Linear regression between tumor mass and vascularization in the case of B16 melanoma ($R^2 = 0.215, R = 0.463, p = 0.177$)

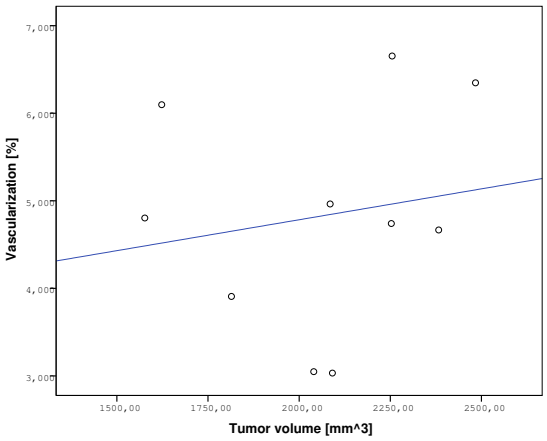

Figure 6.8: Linear regression between tumor volume and vascularization in the case of B16 melanoma ($R^2 = 0.029, R = 0.170, p = 0.638$)

6.2.3 Conclusion

From the results the general assumption that tumor cells grow exponentially (Shackney 1993) is verifiable. My results show that tumor growth dynamics can be described with a second order linear system. Examining the tumor attributes, we can say that not each attributes correlates, thus not only tumor mass and tumor volume is important to be measured. The relevant tumor attribute that have to be measured is based on the therapy applied. In the case of antiangiogenic therapy, vascularization can be more important than tumor mass or tumor volume.

6.3 Model Identification of Tumor Growth With Antiangiogenic Therapy

6.3.1 C38 Colon Adenocarcinoma Growth Identification With Bevacizumab Therapy – Results of Phase III/2

Evaluating the results of Phase III/2, tumor volume was calculated according to (6.2). These results are compared with the results of Phase I, using the same calculation method (6.2) in this subsection (J Sápi, D A Drexler, Z. Sápi, et al. 2014).

Parametric Identification

Result of the parametric identification in the case of C38 colon adenocarcinoma growth without antiangiogenic therapy (Phase I) was:

$$y_{pI}(t) = 29020 \cdot \exp(0.29788t) - 29010 \cdot \exp(0.29789t) \tag{6.6}$$

Time constants of the system are $T_1 = 3.3570$ days, $T_2 = 3.3568$ days.

Result of the parametric identification in the case of C38 colon adenocarcinoma growth with bevacizumab therapy (Phase III/2), control group was:

$$\begin{aligned} y_{pIII/2control}(t) = \\ 2.28171 \cdot 10^6 \cdot \exp(0.114578t) \\ +2.28170 \cdot 10^6 \cdot \exp(0.114579t) \end{aligned} \tag{6.7}$$

Time constants of the system are $T_1 = 8.7277$ days, $T_2 = 8.7276$ days.

Result of the parametric identification in the case of C38 colon adenocarcinoma growth

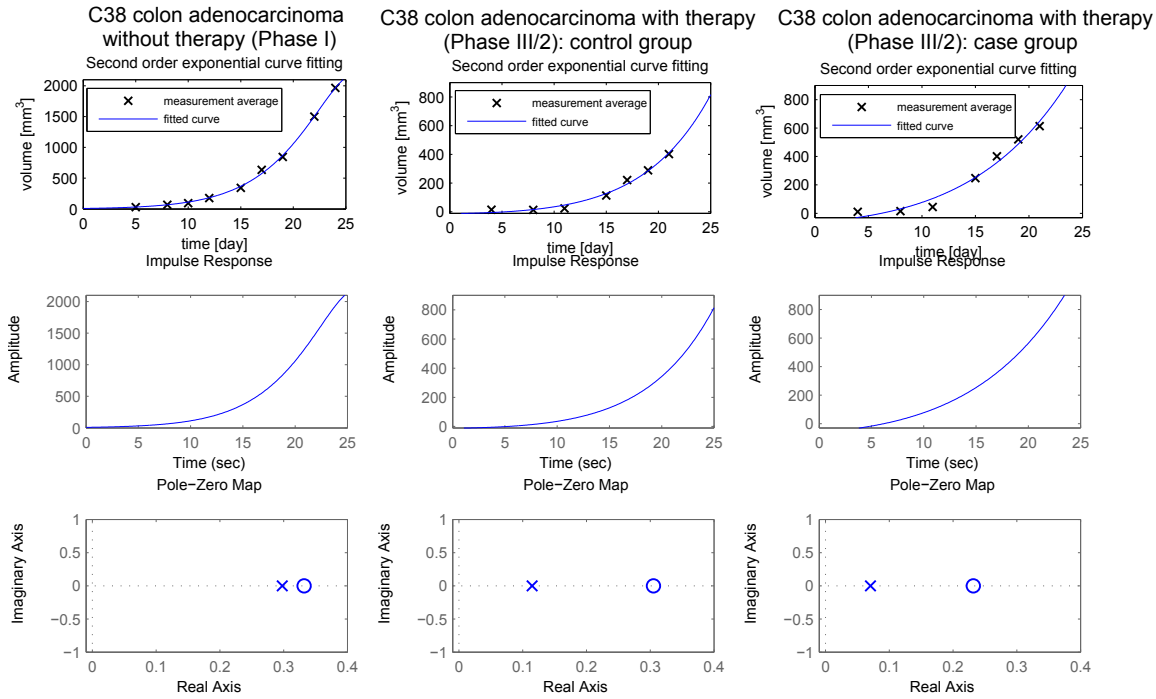

Figure 6.9: Comparison of C38 colon adenocarcinoma growth in three different cases. In Phase I, tumor growth was investigated without antiangiogenic therapy; in Phase III/2, control group members received one 200 μg bevacizumab dose for a 18-day therapy; in Phase III/2, case group members received 1.11 μg bevacizumab every day for 18 days. The first row shows the second order exponential curve fitting for the average of measurement points; in the second row one can see the impulse response of the identified systems; while the third row shows the poles and zeros of the identified systems.

with bevacizumab therapy (Phase III/2), case group was:

$$y_{pIII/2case}(t) = \\ 1.37190 \cdot 10^6 \cdot \exp(0.07045t) \\ -1.37196 \cdot 10^6 \cdot \exp(0.07044t) \tag{6.8}$$

Time constants of the system are $T_1 = 14.1935$ days, $T_2 = 14.1950$ days.

Comparison of the results in the three different cases can be found in Figure 6.9. The coefficients of the exponential functions are positive in every case, reflecting the unstability of the system (as it is required from a tumor growth model). As one can see, in every cases parametric identification resulted in almost identical time constants

(similarly to the results of identification without therapy (Section 6.2); however, the usage of two exponential function is not pointless. From the physiological point of view there are two concrete dynamics which have to be modeled. The engineering interpretation of this result is an integrator series, which means that the change of the first state variable (which is also the output of the system that is the tumor volume) depends on the second state variable (vascularization). In addition, the change of the second state variable depends on the input. Both interpretations are physiologically correct.

From the fitted curves, transfer function of the models can be calculated.

Transfer function of C38 colon adenocarcinoma growth without antiangiogenic therapy (Phase I) resulted in:

$$W_{pI}(s) = \frac{8.715s - 2.895}{s^2 - 0.5958s + 0.08874} \tag{6.9}$$

Poles of the system are $p_{pI,1} = 0.29788$, $p_{pI,1} = 0.29789$.

Transfer function of C38 colon adenocarcinoma growth with bevacizumab therapy (Phase III/2), control group resulted in:

$$W_{pIII/2control}(s) = \frac{-12.34s + 3.764}{s^2 - 0.2292s + 0.01313} \tag{6.10}$$

Poles of the system are $p_{pIII/2control,1} = 0.11457$, $p_{pIII/2control,2} = 0.11458$.

Transfer function of C38 colon adenocarcinoma growth with bevacizumab therapy (Phase III/2), case group resulted in:

$$W_{pIII/2case}(s) = \frac{-61.79s + 14.33}{s^2 - 0.1409s + 0.004963} \tag{6.11}$$

Poles of the system are $p_{pIII/2case,1} = 0.07044$, $p_{pIII/2case,2} = 0.07045$.

From the poles of the systems (third row of Figure 6.9) we can conclude that each system is unstable. To verify the goodness of the created transfer functions, impulse response of each transfer function was plotted (second row of Figure 6.9), which shows quite similar result to the curve fitting (first row of Figure 6.9).

Finding the Relationship Between Tumor Volume, Mass and Vascularization

Results are summarized in Figure 6.10. As one can see, the relationship between tumor volume and mass is significant and positive in all cases, which means that the larger the volume, the higher the mass is. The third attribute, tumor vascularization shows interesting results.

On the one hand, vascularization does not have significant relationship with volume or

	C38 colon adenocarcinoma without therapy (Phase I)	C38 colon adenocarcinoma with therapy (Phase III/2): control group	C38 colon adenocarcinoma with therapy (Phase III/2): case group
tumor volume and mass	R = 0.941 R^2 = 0.885 p < 0.0001 positive correlation	R = 0.955 R^2 = 0.911 p = 0.003 positive correlation	R = 0.913 R^2 = 0.834 p < 0.0001 positive correlation
tumor volume and vascularization	R = 0.269 R^2 = 0.072 p = 0.453 positive correlation	R = - 0.619 R^2 = 0.383 p = 0.190 negative correlation	R = 0.078 R^2 = 0.006 p = 0.811 positive correlation
tumor mass and vascularization	R = 0.198 R^2 = 0.039 p = 0.584 positive correlation	R = - 0.780 R^2 = 0.608 p = 0.067 negative correlation	R = 0.150 R^2 = 0.023 p = 0.641 positive correlation

Notation: significant relationship | near-significant relationship | nonsignificant relationship

Figure 6.10: Linear regression analysis for tumor volume – tumor mass, tumor volume – vascularization, and tumor mass – vascularization pairs. In Phase I, tumor growth was investigated without antiangiogenic therapy; in Phase III/2, control group members received one 200 μg bevacizumab dose for a 18-day therapy; in Phase III/2, case group members received 1.11 μg bevacizumab every day for 18 days. R is the Pearson correlation coefficient, R^2 is the coefficient of determination, p is the ANOVA significance value (level of significance is $p = 0.05$).

mass in neither case. It is the same result what was obtained in the case of identification without therapy (Subsection 6.2.1).

On the other hand in the case of Phase III/2 control group, tumor volume and tumor mass both have negative correlation with vascularization, however these relationships are not significant (tumor mass – vascularization have near-significant relationship). The possible explanation is the following (Reinacher-Schick, Pohl, and Schmiegel 2008). In the case when angiogenesis occurs according to normal trigger, pro- and antiangiogenic factors have balance; consequently the newly formed vessels are normal with effective blood supply. However, in the case of tumor-induced angiogenesis, there is an extra proangiogenic factor produce due to hurried vessel forming, which result in abnormal vessels (high vascular permeability, poor perfusion) with inefficient blood supply. High interstitial fluid pressure can compress the vessels; thereafter abnormal tumor growth may continue, however delivery of therapeutic agents to the tumor is obstructed. Therefore, first abnormal vessels have to be normalized with the balance of pro- and antiangiogenic

factors, thus vascular network can be restored. This creates the possibility of efficient therapeutic agent use. In the case of Phase III/2 control group, mice received a big dose of bevacizumab according to the protocol. This resulted in a sudden preponderance of anti-factors; however, due to abnormal vessel network, the utilization of the antiangiogenic molecules was not effective. Despite the high dose, only a small fraction could be used. That is why larger tumors had fewer viable vessels in control group. In contrast in the case of Phase III/2 case group, mice received a small dose of bevacizumab, which – with the continuous, slow increase of antiangiogenic factors – enabled the normalization of blood vessels (Willett 2004); hence bevacizumab could be used more efficiently.

Investigating the Effective Dosage for Optimal Therapy

Investigating normality and homogenity of variance, I found that each sample has normal distribution ($p_{pI} = 0.966$, $p_{pIII/2control} = 0.999$, $p_{pIII/2case} = 0.608$), and the sample variances are equal ($p = 0.266$). ANOVA test was resulted in $p = 0.038$ value, which means that we have to reject the null hypothesis according to which there are no differences between the means of the samples (using a $p = 0.05$ level of significance). Using a post hoc test, I found that Phase I and Phase III/2 control group are significantly different ($p = 0.034$), which means that bevacizumab – administered according to the protocol – is an effective drug to reduce tumor volume. Phase III/2 control group and Phase III/2 case group are not significantly different ($p = 0.416$), however Phase I and Phase III/2 case group are not significantly different ($p = 0.227$) either. This means that the effectiveness of the quasi-continuous (daily) $^1/_{180}$ dosage (1.11 μg relative to 200 μg) is comparable with the effectiveness of one large dose.

Conclusion

I have found that the effectiveness of the quasi-continuous (daily) $^1/_{180}$ dosage (1.11 μg relative to 200 μg) is comparable with the effectiveness of one large dose. In addition, this is a short-term result (18-day treatment); predicted long-term results are more better, since the identified model for case group has slower dynamics (time constants of the system are approx. 14 days) than the identified model for control group (time constants of the system are approx. 8 days). Taking into account the physiological aspects as well, on the one hand, small daily dosage is better than one large dose, because it enables the normalization of blood vessels (Willett 2004); hence bevacizumab could be used more efficiently. On the other hand, if antiangiogenesis is persistent, it can completely destroy the vascular network which leads to tumor necrosis (death of tumor) (Reinacher-Schick,

Pohl, and Schmiegel 2008). Furthermore, should not be ignored that a considerably lower dose has considerably lower side-effects (or virtually nothing).

6.3.2 C38 Colon Adenocarcinoma Growth Identification With Bevacizumab Therapy – Results of Phase III/3

In Phase III/3, tumor volume was measured not only by caliper, but by small animal MRI as well. It created the possibility to examine the tumor volume estimation more precisely, and to investigate the effectiveness of bevacizumab administration more reliably.

Tumor Volume Estimation

My goal was to find an appropriate mathematical model for tumor volume evaluation from caliper-measured data. According to the Xenograft tumor model protocol (Protocol Online 2005), tumor volume has to be calculated using the following formula:

$$V = w^2 \cdot \frac{l}{2}. \tag{6.12}$$

The advantage of this model is that there is no need to approximate tumor height (which could result in error).

In several recent studies (Tomayko and Reynolds 1989; Jensen et al. 2008), tumor volume is calculated assuming ellipsoid shape:

$$V = \frac{4}{3} \cdot \pi \cdot \frac{l}{2} \cdot \frac{w}{2} \cdot \frac{h}{2}. \tag{6.13}$$

Whilst studies have shown that tumors can be better estimated with ellipsoid shape than using (6.12), calculating the volume of an ellipsoid requires the knowledge of the third parameter. A possible solution for height approximation is (as it was done in Subsection 6.3.1):

$$h = \frac{2}{3} \cdot l. \tag{6.14}$$

Another relatively new but not widely used approach to estimate tumor volume is to assume hemi-ellipsoid shape (Heitjan, Manni, and Santen 1993). In this case, tumor volume has to be calculated in the following way:

$$V = \pi \cdot \frac{l}{2} \cdot \frac{w}{2} \cdot \frac{h}{2}. \tag{6.15}$$

This estimation has the same disadvantage as ellipsoid estimation, i.e. tumor height

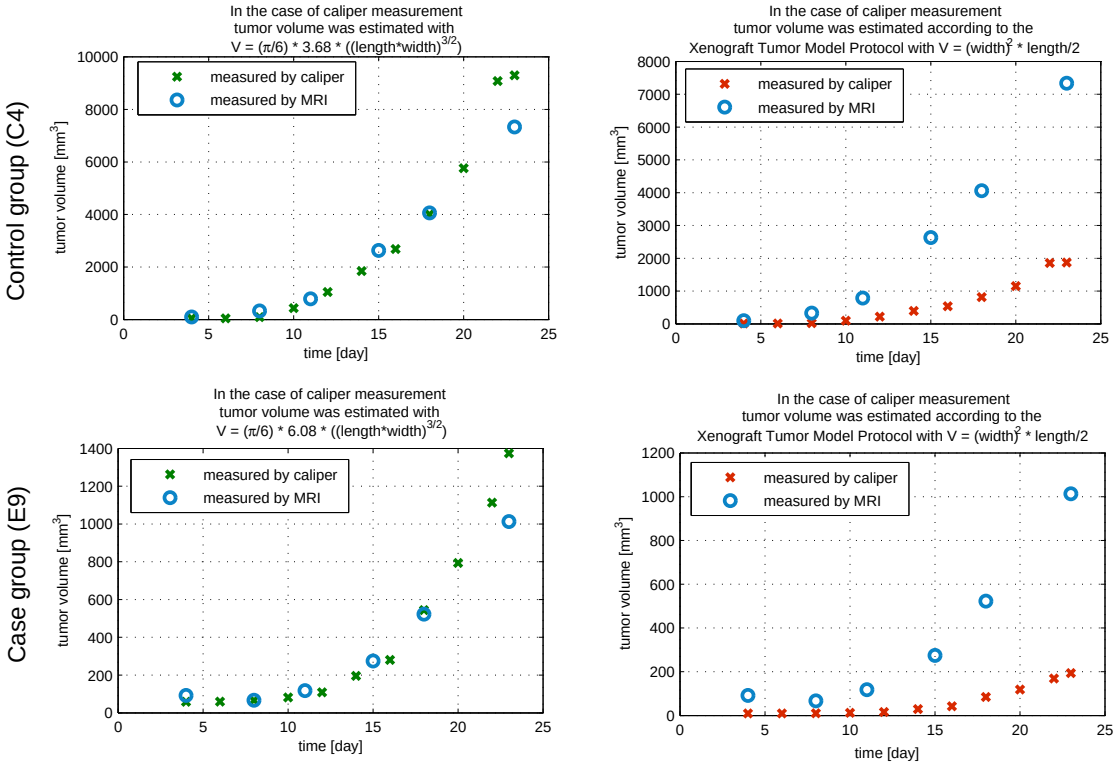

Figure 6.11: Validation of caliper-measured data. The figure shows the results of a mouse (*C4*) from control group (first row), and a mouse (*E9*) from case group (second row). The first column shows the tumor values which were calculated using the two-dimensional mathematical model; the second column represents the protocol-based tumor volumes. In each case the reference value is the MRI-measured tumor volume. One can see that the two-dimensional mathematical model fits to the MRI-measured values, while the protocol-based values present totally different curve.

has to be approximated.

From the abovementioned methods, the consequence is that the promising new direction in tumor volume evaluation is the dimension reduction, namely to find a statistical constant which can replace the need of measuring the tumor height. A two-dimensional mathematical model was created from the experimental results of BALB/c mice with KHJJ tumor line (Feldman et al. 2009):

$$V = \frac{\pi}{6} \cdot f \cdot (l \cdot w)^{3/2}, \tag{6.16}$$

where f is a constant which belongs to a certain tumor type. This formula was the

starting point of my examination to find an appropriate mathematical model.

In Phase III/3, MRI-measured tumor volume values are available which can be used as reference values for caliper-measured data. Applying the two-dimensional mathematical model (described in Equation 6.16) the goal is to find the f constant which belongs to the C38 colon adenocarcinoma and the treatment type. Starting with $f = 1$, I have investigated the goodness of the fitting, using an iterative method. Results for the case group (daily, quasi-continuous small amount administration) and the control group (one big dose according to the protocol) are

$$V_{pIII/3\_case} = \frac{\pi}{6} \cdot 6.08 \cdot (l \cdot w)^{3/2} \rightarrow f_{pIII/3\_case} = 6.08, \tag{6.17}$$

$$V_{pIII/3\_control} = \frac{\pi}{6} \cdot 3.68 \cdot (l \cdot w)^{3/2} \rightarrow f_{pIII/3\_control} = 3.68. \tag{6.18}$$

Usage of this formula to calculate tumor volume from length and width values resulted in much more precise approximation of the MRI-measured tumor volume than protocol-based calculation. Numerical result can be found in Table 6.1, and Figure 6.11 presents graphical results.

To find the f constant for tumor growth without therapy (Phase I), first reliable tumor volume values had to be found, since there was no MRI measurement in Phase I. Beside tumor diameters, tumor mass was measured and vascularization area was calculated in the case of the removed tumors. I have investigated the relationship between MRI-measured tumor volume and vascularization area (Phase III/3 case and control groups, 23rd (final) day of the experiment) but no significant correlation was found (same results were found in the case of Phase I (Subsection 6.2.1) and Phase III/2 (Subsection 6.3.1)). Examining the relationship between MRI-measured tumor volume and tumor mass values, I have found a very strong linear correlation ($R = 0.998$, $R^2 = 0.996$, $p < 0.0001$). It means that knowing the tumor mass, tumor volume can be estimated with suitable accuracy; hence the lack of MRI measurement can be replaced in the case of Phase I. In the light of the above mentioned, linear curve fitting was carried out to find the mathematical relationship between MRI-measured tumor volume and tumor mass (Phase III/3 case and control groups). The resulted linear curve is

$$v = 1047.7m + 67.1, \tag{6.19}$$

where v is tumor volume [mm^3] and m is tumor mass [g]. Substituting tumor mass values which were measured in Phase I into (6.19), the corresponding tumor volume values can be evaluated (one can find numerical results in Table 6.1 *Tumor volume "MRI"*

Table 6.1: Experimental data (tumor length, tumor width, tumor mass and tumor volume).

Phase III/3 control group (23rd day)						
Code of the mouse	Tumor length[a] $[mm]$	Tumor width[a] $[mm]$	Tumor mass[a] $[g]$	Tumor volume caliper, protocol[b] $[mm^3]$	Tumor volume caliper, 2-D model[b] $[mm^3]$	Tumor volume MRI[c] $[mm^3]$
C1	15.3	11.4	3.38	994	4439	3666
C2	26.5	18.4	8.67	4486	20746	9239
C3	13.0	9.4	2.11	574	2603	2081
C4	21.8	13.1	7.05	1871	9299	7335
C5	10.8	11.6	2.58	727	2702	2726
Phase III/3 case group (23rd day)						
Code of the mouse	Tumor length[a] $[mm]$	Tumor width[a] $[mm]$	Tumor mass[a] $[g]$	Tumor volume caliper, protocol[b] $[mm^3]$	Tumor volume caliper, 2-D model[b] $[mm^3]$	Tumor volume MRI[c] $[mm^3]$
E1	7.6	6.4	1.08	284	1080	1129
E2	9.1	6.6	0.98	390	1482	924
E3	10.7	10.0	2.34	927	3524	2707
E4	11.5	8.4	2.10	795	3023	2480
E5	10.3	8.4	1.95	674	2562	2226
E6	14.3	9.0	2.03	1223	4648	1929
E7	11.6	7.0	1.57	613	2329	1930
E8	19.7	14.3	5.00	3961	15052	5243
E9	8.4	6.8	0.86	362	1374	1013
Phase I (24th day)						
Code of the mouse	Tumor length[a] $[mm]$	Tumor width[a] $[mm]$	Tumor mass[a] $[g]$	Tumor volume caliper, protocol[b] $[mm^3]$	Tumor volume caliper, 2-D model[b] $[mm^3]$	Tumor volume "MRI"[d] $[mm^3]$
n1	21.9	15.1	7.22	2497	8029	7631
n2	13.8	10.2	2.81	718	2230	3011
n3	15.1	10.8	4.34	881	2781	4614
n4	23.0	15.1	8.05	2622	8642	8501
n5	25.4	15.8	10.43	3170	10734	10995
n6	19.1	13.8	5.57	1819	5714	5903
n7	exit: 18th day					
n8	exit: 23rd day					
n9	20.7	14.9	5.65	2298	7232	5987
n10	17.5	12.1	4.93	1281	4114	5232
n11	18.2	12.3	3.91	1377	4472	4164
n12	23.1	13.7	5.97	2168	7517	6322

Data was measured at the final day of Phase I (24th day) and Phase III/3 (23rd day).
[a] Directly measured data (tumor length, tumor width, tumor mass)
[b] Estimated data (tumor volume measured by caliper, calculated according to Xenograft tumor model protocol or two-dimensional mathematical model)
[c] MRI-measured data (tumor volume calculated with flood fill algorithm)
[d] Evaluated data ("MRI" tumor volume calculated from linear curve fit (see Equation 6.19))

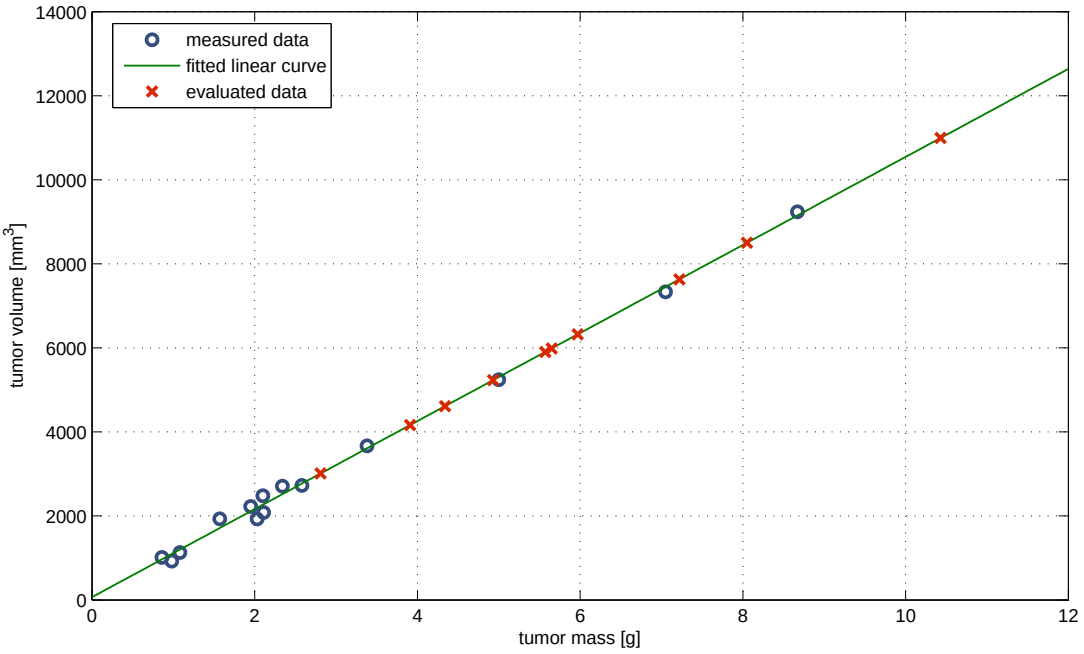

Figure 6.12: Evaluation of Phase I tumor volume values. ”Measured data” is the MRI-measured tumor volume – tumor mass pairs on the 23rd day of Phase III/3 (case and control group). For this dataset, linear curve fitting was carried out (”fitted linear curve”) to find the mathematical relationship between MRI-measured tumor volume and tumor mass. Substituting tumor mass values – which were measured on the 24th day of Phase I – to the equation of the resulted curve, the corresponding tumor volume values can be evaluated (”evaluated data”).

column; and graphical results in Figure 6.12). The last step is to find the f constant of the two-dimensional mathematical model for tumor growth without therapy (Phase I). Using the above mentioned iterative method, the resulted equation is

$$V_{pI} = \frac{\pi}{6} \cdot 2.55 \cdot (l \cdot w)^{3/2} \rightarrow f_{pI} = 2.55. \tag{6.20}$$

One can see from Table 6.1 that the goodness of the fit is different in the case of Phase I (tumor growth without therapy) and in the case of Phase III/3 (tumor growth with antiangiogenic therapy). Investigating the results of Phase III/3 one can observe that the two-dimensional mathematical model has good estimation property when the tumor width and length values are small; however, for large tumor diameter values the estimation could result in significant error, the estimated value is greater than the

measured one (outliers are *E8*, *C2*). In the case of Phase I, no similar problem occurs; the two-dimensional mathematical model can handle great values as well (e.g. *n5*). This problem can be explained by our observation, namely tumors which were grown without therapy have more symmetric and solid closed shape, in contrast to tumors which were grown under antiangiogenic therapy. We have found that mice which have received therapy had tumor with irregular, and in several cases berry-shaped structure, especially when reaching large volume. In that case – even though all the three diameters can be measured – the estimation of the volume has quite a large error. A 3-D illustration can be found in Figure 6.13.

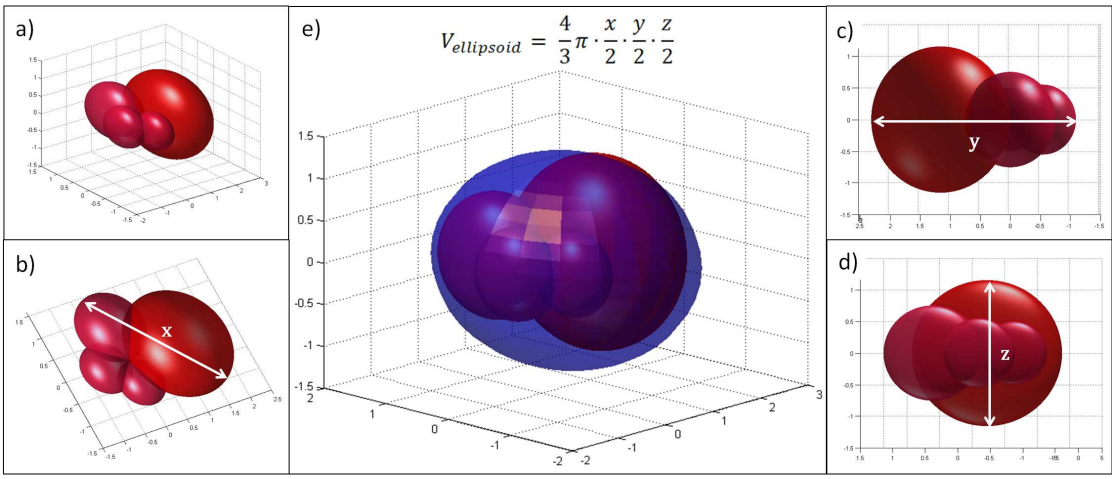

Figure 6.13: Illustration for tumor with irregular structure (berry-shaped). a) berry-shaped tumor; b) x-diameter of the tumor; c) y-diameter of the tumor; d) z-diameter of the tumor; e) berry-shaped tumor with ellipsoidal estimation. Even though all the three diameters can be measured, the estimation of the volume has quite a large error.

Investigating the Effective Dosage for Optimal Therapy

This subsection provides the comparison of the effectiveness of bevacizumab administration in the case of protocol-based and quasi-continuous therapies (J Sápi, L Kovács, et al. 2015). The effectiveness strongly depends on the administration, and a drug which is effective on a molecular level can be applied in a less effective way because of the incorrectly chosen administration. My hypothesis was (based on the results of Subsection 6.3.1) that the effectiveness of a lower dosage with a quasi-continuous therapy can be comparable with the protocol therapy.

The results of the three investigated cases (Phase I, Phase III/3 control group, Phase

III/3 case group) were compared using tumor volume values from MRI measurements (Phase III/3 control and case group, 23rd day) and evaluated data (Phase I "MRI" tumor volume calculated from linear curve fit, 24th day). One can find datasets in the last column of Table 6.1. Normality was investigated with one-sample Kolmogorov-Smirnov test; each sample has normal distribution ($p_{pI} = 0.883$, $p_{pIII/3\_case} = 0.716$, $p_{pIII/3\_control} = 0.869$). Homogeneity of variance was examined with Levene's test; the sample variances are equal ($p = 0.052$).

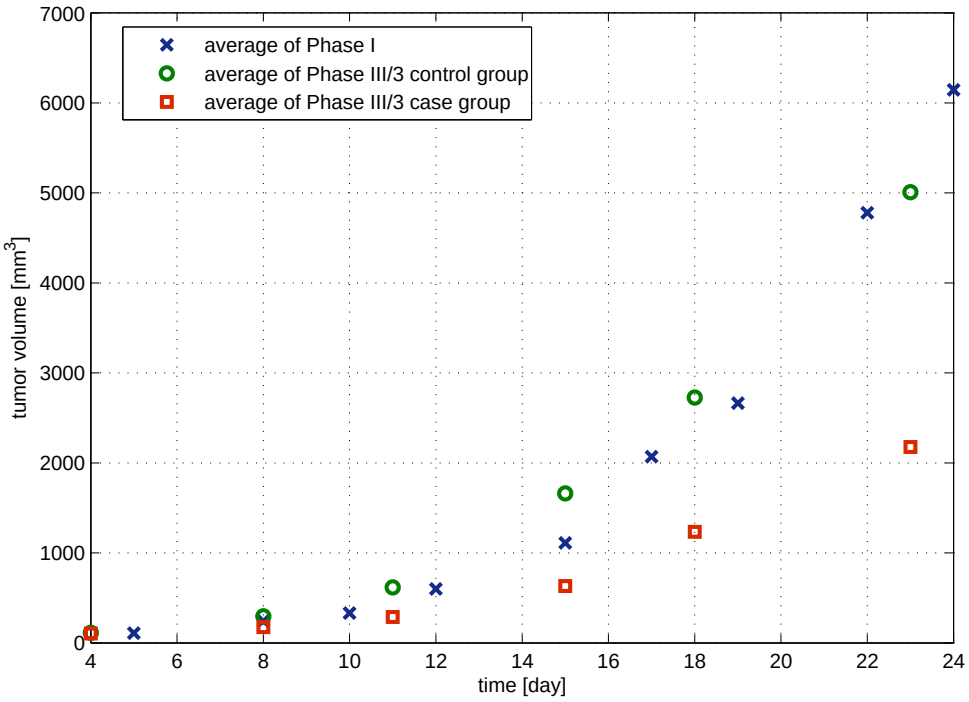

Figure 6.14: Average of tumor volumes for every measurement days of the experiment in the case of Phase I, Phase III/3 control and Phase III/3 case group. The significant difference between quasi-continuous therapy (Phase III/3 case group) and tumor growth without treatment (Phase I) was proved with statistical analysis as well.

To compare more than two samples, ANOVA test was applied. I have found that there is significant difference between the means of the samples ($p = 0.002$, using 0.05 level of significance). Pairwise comparison was done by Tukey's honest significant difference test to find those samples, which have significantly different means. The post hoc test resulted in the following. Phase I and Phase III/3 control group are not significantly

different ($p = 0.572$), while Phase I and Phase III/3 control group are significantly different ($p = 0.002$). This means that mice which were treated with the recommended bevacizumab protocol (one 200 μg bevacizumab dose for an 18-day therapy) did not have significantly smaller tumor volume than mice which did not receive therapy at all. However mice which were treated with a quasi-continuous therapy (one-tenth dose of control dose spread over 18 days, i.e. 1.11 μg bevacizumab every day) had significantly smaller tumor volume than mice that did not receive therapy. Average of tumor volumes for every measurement days of the experiment can be seen in Figure 6.14.

Conclusion

Since 2004, the target therapy of bevacizumab (Avastin) is widely used to treat colorectal (Tebbutt et al. 2010), kidney (Rini et al. 2010), cervical (Monk et al. 2009), ovarian (Kumaran, Jayson, and Clamp 2009), non-small cell lung cancers (Vokes, Salgia, and Karrison 2013), melanoma (Kim et al. 2012) and certain brain tumors (e.g. recurrent glioblastoma (rGBM) (Friedman et al. 2009)) as a first or second line treatment, usually in combination with chemo- or immunotherapy. The usual administration is via intravenous infusion; once every 2 or 3 weeks. The dose depends mainly on weight. However, most serious questions are: for how long and continuous or not? The most recent ESMO (European Society for Medical Oncology) consensus guidelines suggest that treatment discontinuation or maintenance are feasible options after 4-6 months of full-dose first-line therapy to treat colon and rectal adenocarcinoma (Schmoll et al. 2012). However, if the treatment is lengthy, the problem of side-effects also has to be considered. To overcome all of these difficulties (continuity of the administration and side-effects), model identification should be determined and then a control algorithm (controller) can be designed for the created mathematical model. Of course, for the closed-loop design frequent and precise tumor volume measurements are required, thus the problem of tumor volume measurement has to be solved as well. Finding the mathematical relationship between MRI-measured tumor volume and tumor mass creates the possibility to estimate tumor volume from caliper-measured data. However, it has to be taken into consideration that in several cases using antiangiogenic therapy, tumor shape is irregular (berry-shaped). Consequently, when tumor mass data is unavailable (during the experiment), tumor volume value can be validated with MRI; in that way outlier data points (which were calculated using the two-dimensional mathematical model) can be filtered out. In clinical practice, the determination of the tumor size (volume) is done by MRI and/or CT, but this is for the purpose of validating the effectiveness of the treatment, and therefore it is not a continuous monitoring. In the concept of model-based treatment, a continuous

and precise tumor volume monitoring is needed concerning which, may be possible in the near future by nanotechnology (McCarroll et al. 2014).

According to angiogenic inhibitor administration, my hypothesis was that the effectiveness of a lower dosage with a quasi-continuous therapy can be comparable with the protocol therapy. Nevertheless the result of this experiment shows that the effectiveness is even better. Consequences are manifold. First of all, my hypothesis according to the importance of administration is proved. The effectiveness of the quasi-continuous (daily) 1/180 dosage (1.11 μg relative to 200 μg) was more effective than one large dose. Similarly, Zhang et al. 2011 have found that the combination of low-dose cyclophosphamide and ginsenoside Rg3 therapy can be more effective than the normal administration. Although the low dose bevacizumab therapy is well known in the literature, I found no article (in the English literature) regarding very low dose and quasi-continuous bevacizumab therapy, as used in this experiment. Secondly, the aspect of side-effects is not inconsiderable. For example, one of the main reasons why the US FDA revoked the approval of Avastin for treating advanced breast cancer is the high rate of side-effects when bevacizumab was applied (Carey 2012). Typical side-effects and adverse events are arterial and venous thromboembolic events, bleeding, hypertension, febrile neutropenia, infections, proteinuria, mucositis, and hand-foot syndrome. Using an extremely low dosage (as in our experiments), there is a high probability that these adverse effects can be minimized.

I have applied a two-dimensional mathematical model and determined the corresponding tumor- and therapy-specific constants in the three investigated cases (C38 colon adenocarcinoma growth without therapy, C38 colon adenocarcinoma growth with protocol-based bevacizumab therapy and C38 colon adenocarcinoma growth with quasi-continuous bevacizumab therapy). This helps to calculate accurate tumor volume from caliper measured data which will be useful for further animal experiments and as a consequence no small MRI measurements will be needed. In addition, I have found that the quasi-continuous administration of bevacizumab is effective against tumor growth of C38 colon adenocarcinoma, in contrast to protocol-based treatment. Considering the possibility of precise tumor volume determination and the effective quasi-continuous drug administration, it opens a new treatment choice based on closed-loop control. In other fields, such as treatment of diabetes mellitus this closed-loop control is already solved; known as artificial pancreas (continuous glucose sensor for measurements, insulin pump for infusion and control algorithm) (Cobelli, Eric Renard, and Kovatchev 2014; L Kovács, Benyó, et al. 2011). Similarly, we may have the possibility to a) measure the tumor volume using nanotechnology, b) create a pump for drug administration and c) design control algorithms for specific tumor types. Controller-based therapy has

the obvious advantage against e.g. constant low-dose therapy because in the case of controller-based administration, the control signal (administration dose) can vary from zero to the maximum tolerable dose according to the perceived tumor volume. In this way, the targeted therapy can be used in a much more individualized form.

6.4 Thesis Group 2

I provided mathematical models which describe the tumor growth dynamics without therapy and under angiogenic inhibition. I investigated the relationship between the measured tumor attributes and applied the results to create a new model for precise tumor volume evaluation. I examined the effective dosage of angiogenic inhibitor for optimal cancer therapy.

Thesis Group 2: Tumor Growth Model Identification.

Thesis 2.1
I provided linear model identification of tumor growth dynamics without therapy using parametric identification for two tumor types (C38 colon adenocarcinoma and B16 melanoma). The resulted models are clinically valid.

Thesis 2.2
I provided linear model identification of C38 colon adenocarcinoma growth dynamics under bevacizumab inhibition using parametric identification. The resulted models are clinically valid and sufficiently simple to be manageable for both real-life applicability and controller design.

Thesis 2.3

I provided a new model for tumor volume evaluation from caliper measured data, based on the results of linear regression analysis of three measured tumor attributes (tumor mass, tumor volume and vascularization). The model uses two tumor diameters (width and length) of the tumor to evaluate precisely the tumor volume without requiring the approximation of the third diameter (height) and assumption of the tumor shape. I have demonstrated that this model results in a more precise tumor volume evaluation than the currently recommended Xenograft Tumor Model Protocol.

Thesis 2.4

I compared the effectiveness of bevacizumab administration in the case of protocol-based therapy and quasi-continuous therapy. I have demonstrated that the effectiveness of the quasi-continuous (daily) very low dose administration was more effective than one large dose. I provided a methodology for effective dosage of angiogenic inhibitor for optimal cancer therapy, which opens a new treatment opportunity based on closed-loop control.

Relevant own publications pertaining to this thesis group: [S-13; S-15; S-4; S-7; S-16].

7 Conclusion

Thesis group 1 discusses controller synthesis and design for the simplified version of tumor growth model under angiogenic inhibition (Hahnfeldt et al. 1999). Linear state-feedback control was designed using pole placement and LQ optimal control and, in addition, linear observer was also designed for both state-feedback methods (since not every state-variables of the system can be measured). Simulation results demonstrated that the nonlinear model has to be linearized at a low operating point in order to achieve successful control; in increasing the operating point, the control signals become too low to sufficiently reduce the tumor volume (because of the nonlinearity). According to various aspects, the most effective control was the LQ control method: (a) for two criteria (total concentration of the administered inhibitor during the treatment and steady state inhibitor concentration at the end of the treatment), this controller had the best results; (b) the minimal value of the third criterion (steady state tumor volume at the end of the treatment) can be well approximated with the LQ control method; (c) this was the only controller which ensures successful control for high operating points. I provided a set of controllers which can handle the therapeutic efficacy, cost-effectiveness and side-effect moderation aspects as well.

To deal with model uncertainties and measurement noises, a stabilizing robust (H_∞) controller was designed where ideal system and weighting functions were chosen in light of physiological aspects. The results of robust control were compared to the results based on LQ optimal control and THE Hungarian OEP (National Health Insurance Fund of Hungary) protocol. As would be expected, the LQ optimal control provides better results, but only in the case of good model identification and minimal sensor noise. If the system contains significant uncertainties and the measurement noise is large, only the robust control method can provide near-optimal results. Simulations show that the intermittent dosing used by the OEP chemotherapy protocol is not effective; the tumor volume reduced slightly as a result of a one-day dose, but between the treatment phases, the tumor grows back again. At the end of the whole treatment period, there is no large difference between the therapy with OEP protocol and the case without therapy.

Thesis group 2 discusses newly created mathematical models which describe the tumor

growth dynamics without therapy and under angiogenic inhibition. Besides this, a two-dimensional mathematical model for tumor volume evaluation from caliper-measured data was also provided. This model results in more precise tumor volume evaluation than the Xenograft Tumor Model Protocol. The results of parametric identification show that tumor growth dynamics can be described with a second order linear system. Examining the tumor attributes, I found that not each attribute correlates, thus not only tumor mass and tumor volume is important to be measured. The relevant tumor attribute that has to be measured is based on the therapy applied.

Tumor growth was investigated under antiangiogenic therapy using protocol-based and quasi-continuous (daily) administration. The effectiveness of the antiangiogenic therapy strongly depends on the administration, and a drug which is effective on a molecular level can be applied in a less effective way because of the incorrectly chosen administration. Phase III/2 (where tumor volume was measured by digital caliper) results showed that a daily $^{1}/_{180}$ dosage is comparable with the effectiveness of one large dose (protocol). Furthermore Phase III/3 (where tumo volumer was measured by digital caliper and also small animal MRI) results showed that the effectiveness of small daily doses is even better than one large dose. Taking into account the physiological aspects as well, on the one hand, a small daily dosage is better than one large dose, because it enables the normalization of blood vessels; hence bevacizumab could be used more efficiently. On the other hand, if antiangiogenesis is persistent, it can completely destroy the vascular network which leads to tumor necrosis (death of tumor). Furthermore, it should not be ignored that a considerably lower dose has considerably lower side-effects (or virtually nothing).

Further work is to apply the previously designed controller structures for the newly identified tumor growth models.

Bibliography

References

Abcam (2005). *B16 (Mouse melanoma cell line) Nuclear Lysate*. http://www.abcam.com/B16-Mouse-melanoma-cell-line-Nuclear-Lysate-ab14638.html. 01.03.2015.

ACS, American Cancer Society (2011). *The History of Cancer*. http://www.cancer.org/acs/groups/cid/documents/webcontent/002048-pdf.pdf. 01.03.2015.

Amit, L, I Ben-Aharon, L Vidal, L Leibovici, and S Stemmer (2013). "The Impact of Bevacizumab (Avastin) on Survival in Metastatic Solid Tumors - A Meta-Analysis and Systematic Review". In: *PLoS One.* 8(1), e51780.

Bear, H D, G Tang, P Rastogi, C E Jr Geyer, and A Robidoux (2012). "Bevacizumab Added to Neoadjuvant Chemotherapy for Breast Cancer". In: *N Engl J Med.* 366(4), pp. 310–320.

Becker, MD (2011). *FDA Approved Monoclonal Antibodies (mAbs) for Cancer Therapy*. http://lifesciencedigest.com/2011/03/05/fda-approved-mabs-for-cancer-therapy. 01.03.2015.

Bergers, G. and L. E. Benjamin (2003). "Tumorigenesis and the angiogenic switch". In: *Nat Rev Cancer.* 3(6), pp. 401–410.

Boehm, T., J. Folkman, T. Browder, and M. S. O'Reilly (1997). "Antiangiogenic therapy of experimental cancer does not induce acquired drug resistance". In: *Nature* 390, pp. 404–407.

Bokor, J, P Gáspár, and Z Szabó (2012). *Robust Control Theory with automotive applications*. TYPOTEX Kiadó.

Carey, K (2012). "Avastin loses breast cancer indication". In: *Nature Biotechnology* 30, p. 6.

Chang, J H, N K Garg, E Lunde, K Y Han, S Jain, and D T Azar (2012). "Corneal Neovascularization: An Anti-VEGF Therapy". In: *Review. Surv Ophthalmol* 57(5), pp. 415–429.

Chaplain, M A (2000). "Mathematical modelling of angiogenesis". In: *J. Neurooncol* 50, pp. 37–51.

Cobelli, C, E Eric Renard, and B Kovatchev (2014). "The artificial pancreas: a digital-age treatment for diabetes". In: *Lancet Diabetes Endocrinol.* 2(9), pp. 679–681.

Connell, P. P. and S. Hellman (2009). "Advances in radiotherapy and implications for the next century: a historical perspective". In: *Cancer Res.* 69(2), pp. 383–392.

Dinda, S. (2012). "Anti-hormones: mechanism and use in treatment of breast cancer". In: *Clin Lab Sci.* 25(1), pp. 45–49.

Döme, B, M J Hendrix, S Paku, J Tóvári, and J Tímár (2007). "Alternative vascularization mechanisms in cancer: Pathology and therapeutic implications". In: *Am J Pathol* 170(1), pp. 1–15.

d'Onofrio, A. and P. Cerrai (2009). "A bi-parametric model for the tumour angiogenesis and antiangiogenesis therapy". In: *Mathematical and Computer Modelling* 49, pp. 1156–1163.

D'Onofrio, A. and A. Gandolfi (2004). "Tumour eradication by antiangiogenic therapy: analysis and extensions of the model by Hahnfeldt et al." In: *Mathematical Biosciences* 191, pp. 159–184.

D'Onofrio, A and A Gandolfi (2009). "A family of models of angiogenesis and anti-angiogenesis anti-cancer therapy". In: *Math Med Biol* 26, pp. 63–95.

d'Onofrio, A., A. Gandolfi, and A. Rocca (2009). "The dynamics of tumour-vasculature interaction suggests low-dose, time-dense antiangiogenic scheduling". In: *Cell Proliferation* 42, pp. 317–329.

D'Onofrio, A., U. Ledzewicz, H. Maurer, and H. Schättler (2009). "On optimal delivery of combination therapy for tumors". In: *Mathematical Biosciences* 222(4), pp. 13–26.

Dredge, K., A. G. Dalgleish, and J. B. Marriott (2003). "Angiogenesis inhibitors in cancer therapy". In: *Curr Opin Investig Drugs.* 4(6), pp. 667–674.

Ellis, L. M. and D. G. Haller (2008). "Bevacizumab Beyond Progression: Does This Make Sense?" In: *J Clin Oncol.* 26(33), pp. 5313–5315.

Ergun, A., K. Camphausen, and L. M. Wein (2003). "Optimal scheduling of radiotherapy and angiogenic inhibitors". In: *Bulletin of Mathematical Biology* 65, pp. 407–424.

European Medicines Agency (2005). *Scientific discussion of Avastin.* Available: http://www.ema.europa.eu/docs/en_GB/document_library/EPAR_-_Scientific_Discussion/human/000582/WC500029262.pdf. 01.03.2015.

Feig, Barry W., David H. Berger, and George M. Fuhrman (2006). *The M.D. Anderson Surgical Oncology Handbook.* fourth ed., Lippincott Williams and Wilkins.

Feldman, J P, R Goldwasser, S Mark, J Schwartz, and I Orion (2009). "A mathematical model for tumor volume evaluation using two-dimensions". In: *J. Appl. Quant. Methods* 4, pp. 455–462.

Femke, H and A W Griffioen (2007). "Tumour vascularization: sprouting angiogenesis and beyond". In: *Cancer Metastasis Rev* 26(3-4), pp. 489–502.

Finley, S D, M O Engel-Stefanini, P I Imoukhuede, and A S Popel (2011). "Pharmacokinetics and pharmacodynamics of VEGF-neutralizing antibodies". In: *BMC Syst Biol* 21, pp. 193–213.

Frank, D. A. (2012). *Signaling Pathways in Cancer Pathogenesis and Therapy*. first ed., Springer.

Friedman, H S, M D Prados, P Y Wen, T Mikkelsen, D Schiff, L E Abrey, W K Yung, N Paleologos, M K Nicholas, R Jensen, J Vredenburgh, J Huang, M Zheng, and T Cloughesy (2009). "Bevacizumab alone and in combination with irinotecan in recurrent glioblastoma". In: *J Clin Oncol.* 27(28), pp. 4733–4740.

Gazda, M. J. and R. C. Lawrence (2001). *Principles of radiation therapy, Cancer management: a multidisciplinary approach*. http://www.thymic.org/uploads/reference_sub/02radtherapy.pdf/. 01.03.2015.

Genentech (2013). *Prescribing information of Avastin (Bevacizumab)*. Available: http://www.gene.com/download/pdf/avastin_prescribing.pdf. 01.03.2015.

Genentech, Lung Cancer (2013). *Prognostic factors of Non-Small Cell Lung Cancer (general information for health professionals)*. http://www.cancer.gov/cancertopics/pdq/treatment/non-small-cell-lung/healthprofessional. 01.03.2015.

Gerber, D. E. (2008). "Targeted therapies: a new generation of cancer treatments". In: *Am Fam Physician.* 77(3), pp. 311–319.

Gevertz, J L (2011). "Computational modeling of tumor response to vascular-targeting therapies – part I: validation". In: *Comput Math Methods Med.* http://lifesciencedigest.com/2011/03/05/fda-approved-mabs-for-cancer-therapy.

Goffman, T. E. and E. Glatstein (2002). "Intensity-modulated radiation therapy". In: *Radiat Res.* 158(1), pp. 115–117.

Goitein, M. and M. Jermann (2003). "The relative costs of proton and X-ray radiation therapy". In: *Clin Oncol (R Coll Radiol).* 15(1), S37–50.

Hahnfeldt, P., D. Panigrahy, J. Folkman, and L. Hlatky (1999). "Tumor development under angiogenic signaling: A dynamical theory of tumor growth, treatment response, and postvascular dormancy". In: *Cancer research* 59, pp. 4770–4775.

Heitjan, D F, A Manni, and R J Santen (1993). "Statistical analysis of in vivo tumor growth experiments". In: *Cancer Res.* 53(24), pp. 6042–6050.

Hoeben, A., B. Landuyt, M.S. Highley, H. Wildiers, A. T. Van Oosterom, and E. A. De Bruijn (2004). "Vascular Endothelial Growth Factor and Angiogenesis". In: *Pharmacol Rev.* 56, pp. 549–580.

Holland, J. F. and E. Frei (2003). *Cancer Medicine*. ISBN-10: 1-55009-213-8. sixth ed., BC Decker, Hamilton, Ontario.

Holzheimer, R. G. and J. A. Mannick (2001). *Surgical Treatment: Evidence-Based and Problem-Oriented*. ISBN-10: 3-88603-714-2. Munich: Zuckschwerdt.

Hungary(OEP), National Health Insurance Fund of (2010). *Hungarian chemotherapy protocol*. http://www.gyogyinfok.hu/magyar/fekvo/kemo/Kemo_protokoll_valtozasok.pdf. 01.03.2015.

ImageJ (1997). *Image Processing and Analysis in Java*. Available: http://rsbweb.nih.gov/ij/index.html. 01.03.2015.

Inoue, K, M Chikazawa, S Fukata, C Yoshikawa, and T Shuin (2002). "Frequent administration of angiogenesis inhibitor TNP-470 (AGM-1470) at an optimal biological dose inhibits tumor growth and metastasis of metastatic human transitional cell carcinoma in the urinary bladder". In: *Clin Cancer Res* 8(7), pp. 2389–2398.

Isidori, A. (1995). *Nonlinear Control Systems*. Springer-Verlag London.

Jensen, M M, J T Jørgensen, T Binderup, and A Kjaer (2008). "Tumor volume in subcutaneous mouse xenografts measured by microCT is more accurate and reproducible than determined by 18F-FDG-microPET or external caliper". In: *BMC Med Imaging*. Pp. 8–16.

Kalva, S. P., S. Namasivayam, and D. V. Sahani (2008). "Imaging Angiogenesis". In: *Antiangiogenic Agents in Cancer Therapy*. Ed. by B. A. Teicher and L. M. Ellis. second ed., Humana Press, Springer.

Kamm, Y. J., A. Heerschap, G. Rosenbusch, I. M. Rietjens, J. Vervoort, and D. J. Wagener (1996). "5-Fluorouracil metabolite patterns in viable and necrotic tumor areas of murine colon carcinoma determined by 19F NMR spectroscopy". In: *Magn Reson Med.* 53(13), pp. 2987–2993.

Karayiannakis, A. J., K. N. Syrigos, A. Polychronidis, A. Zbar, G. Kouraklis, C. Simopoulos, and G. Karatzas (2002). "Circulating VEGF levels in the serum of gastric cancer patients: correlation with pathological variables, patient survival, and tumor surgery". In: *Ann Surg.* 236(1), pp. 37–42.

Kasibhatla, S. and B. Tseng (2003). "Why target apoptosis in cancer treatment?" In: *Mol Cancer Ther.* 2(6), pp. 573–580.

Kassara, K. and A. Moustafid (2011). "Angiogenesis inhibition and tumor-immune interactions with chemotherapy by a control set-valued method". In: *Mathematical Biosciences* 231(2), pp. 135–143.

Kastan, M. B. and J. Bartek (2004). "Cell-cycle checkpoints and cancer". In: *Nature* 432(7015), pp. 316–323.

Kaur, G., C. R. Long, and J. M. Dufour (2012). "Genetically engineered immune privileged Sertoli cells: A new road to cell based gene therapy". In: *Spermatogenesis* 2(1), pp. 23–31.

Kelloff, G. J., C.W. Boone, V.E. Steele, J.R. Fay, R.A. Lubet, J.A. Crowell, and C.C. Sigman (1994). "Mechanistic considerations in chemopreventive drug development". In: *J Cell Biochem Suppl.* 20, pp. 1–24.

Kelly, W K, S Halabi, M Carducci, D George, J F Mahoney, W M Stadler, M Morris, P Kantoff, J P Monk, E Kaplan, N J Vogelzang, and E J Small (2012). "Randomized, double-blind, placebo-controlled phase III trial comparing docetaxel and prednisone with or without bevacizumab in men with metastatic castration-resistant prostate cancer: CALGB 90401". In: *J Clin Oncol.* 30(13), pp. 1534–1540.

Kerbel, R. (1997). "A cancer therapy resistant to resistance". In: *Nature* 390, pp. 335–336.

Kerbel, R. and J. Folkman (2002). "Clinical translation of angiogenesis inhibitors". In: *Nat Rev Cancer.* 2(10), pp. 727–739.

Kim, K B, J A Sosman, J P Fruehauf, G P Linette, S N Markovic, D F McDermott, J S Weber, H Nguyen, P Cheverton, D Chen, and O'Day S J Peterson A C Carson WE 3rd (2012). "BEAM: a randomized phase II study evaluating the activity of bevacizumab in combination with carboplatin plus paclitaxel in patients with previously untreated advanced melanoma". In: *J Clin Oncol.* 30(1), pp. 34–41.

Kindler, H L, D Niedzwiecki, D Hollis, S Sutherland, D Schrag, H Hurwitz, F Innocenti, M F Mulcahy, E O'Reilly, T F Wozniak, J Picus, P Bhargava, R J Mayer, R L Schilsky, and R M Goldberg (2010). "Gemcitabine plus bevacizumab compared with gemcitabine plus placebo in patients with advanced pancreatic cancer: phase III trial of the Cancer and Leukemia Group B (CALGB 80303)". In: *J Clin Oncol.* 28(22), pp. 3617–3622.

Koo, V, P W Hamilton, and K Williamson (2006). "Non-invasive in vivo imaging in small animal research". In: *Cell Oncol* 28(4), pp. 127–139.

Kovács, L, B Benyó, J Bokor, and Z Benyó (2011). "Induced L2-norm Minimization of Glucose-Insulin System for Type I Diabetic Patients". In: *Comput Methods Programs Biomed.* 102(2), pp. 105–118.

Kovács, L, B Kulcsár, A György, and Z Benyó (2011). "Robust servo control of a novel type 1 diabetic model". In: *Optimal Control Applications and Methods* 32, pp. 215–238.

Kreipe, H. H. and R. Wasielewski (2007). "Beyond Typing and Granding: Target Analysis in Individualized Therapy as a New Challenge for Tumour Pathology". In: *Recent*

Results In Cancer Research, Targeted Therapies in Cancer. Ed. by M. Dietel. Springer - Verlag Berlin Heidelberg.

Kumaran, G C, G C Jayson, and A R Clamp (2009). "Antiangiogenic drugs in ovarian cancer". In: *Br J Cancer* 100(1), pp. 1–7.

Laarhoven, H. W. van, G Gambarota, J. Lok, et al. (2006). "Carbogen breathing differentially enhances blood plasma volume and 5-fluorouracil uptake in two murine colon tumor models with a distinct vascular structure". In: *Neoplasia.* 8(6), pp. 477–487.

Lai-Cheong, J.E., J.A. McGrath, and J. Uitto (2011). "Revertant mosaicism in skin: natural gene therapy". In: *Trends Mol Med.* 17(3), pp. 140–148.

Larson, M. G. (2008). "Statistical Primer for Cardiovascular Research. Analysis of Variance". In: *Circulation* 117, pp. 115–121.

Ledzewicz, U., J. Marriott, H. Maurer, and H. Schättler (2010). "Realizable protocols for optimal administration of drugs in mathematical models for anti-angiogenic treatment". In: *Mathematical Medicine and Biology* 27(2), pp. 157–179.

Ledzewicz, U. and H. Schättler (2005). "A synthesis of optimal controls for a model of tumor growth under angiogenic inhibitors". In: *Proc. of the 44th IEEE Conference on Decision and Control, and the European Control Conference, Seville, Spain*, pp. 934–939.

— (2007). "Anti-angiogenic therapy in cancer treatment as an optimal control problem". In: *SIAM Journal on Control and Optimization* 46, pp. 1052–1079.

— (2008). *Optimal and suboptimal protocols for a class of mathematical models of tumor antiangiogenesis.*

— (2009). *On an extension of a mathematical model for tumor anti-angiogenesis.*

Liu, Y. and G. Zeng (2012). "Cancer and innate immune system interactions: translational potentials for cancer immunotherapy". In: *J Immunother.* 35(4), pp. 299–308.

Ljungkvist, A. S., J. Bussink, J. H. Kaanders, et al. (2005). "Hypoxic cell turnover in different solid tumor lines". In: *Int J Radiat Oncol Biol Phys.* 62(4), pp. 1157–1168.

Lowe, S. W. and A. W. Lin (2000). "Apoptosis in cancer". In: *Carcinogenesis* 21(3), pp. 485–195.

Malvezzi, M, P Bertuccio, F Levi, C La Vecchia, and E Negri (2014). "European cancer mortality predictions for the year 2014". In: *Ann Oncol* 00, pp. 1–7.

McCarroll, J, J Teo, C Boyer, D Goldstein, M Kavallaris, and P A Phillips (2014). "Potential applications of nanotechnology for the diagnosis and treatment of pancreatic cancer". In: *Front Physiol.* 5, 2(1–10).

McDonald, D. M. (2008). "Angiogenesis and Vascular Remodeling in Inflammation and Cancer: Biology and Architecture of the Vasculature". In: *Angiogenesis: An*

Integrative Approach from Science to Medicine. Ed. by W. D. Figg and J. Folkman. Springer Science+Business Media, LLC.

Minckwitz, G von, H Eidtmann, M Rezai, P A Fasching, and H et al. Tesch (2012). "Neoadjuvant chemotherapy and bevacizumab for HER2-negative breast cancer". In: *N Engl J Med* 366(4), pp. 299–309.

Monk, B J, M W Sill, R A Burger, H J Gray, T E Buekers, and L D Roman (2009). "Phase II trial of bevacizumab in the treatment of persistent or recurrent squamous cell carcinoma of the cervix: a gynecologic oncology group study". In: *J Clin Oncol* 27(7), pp. 1069–1074.

Montero, A J and C Vogel (2012). "Fighting fire with fire: rekindling the bevacizumab debate". In: *N Engl J Med.* 366(4), pp. 374–375.

Montgomery, D. C, E. A. Peck, and G. G Vining (2012). *Introduction to Linear Regression Analysis, fifth edition*. John Wiley & Sons, Inc., Hoboken, New Jersey.

Mriouah, J, C Boura, M Thomassin, T Bastogne, D Dumas, B Faivre, and M Barberi-Heyob (2012). "Tumor vascular responses to antivascular and antiangiogenic strategies: looking for suitable models". In: *Trends Biotechnol* 30(12), pp. 649–958.

Mukherji, S K (2010). "Bevacizumab (Avastin)". In: *AJNR Am J Neuroradiol.* 31(2), pp. 235–236.

NCI, National Cancer Institute (2015). *eMICE: electronic Models Information, Communication, and Education*. http://emice.nci.nih.gov/. 01.03.2015.

Nishimoto, N., N. Miyasaka, K. Yamamoto, S. Kawai, T. Takeuchi, J. Azuma, and T. Kishimoto (2009). "Study of active controlled tocilizumab monotherapy for rheumatoid arthritis patients with an inadequate response to methotrexate (SATORI): significant reduction in disease activity and serum vascular endothelial growth factor by IL-6 receptor inhibition therapy". In: *Mod Rheumatol.* 19(1), pp. 12–19.

Ohlmann, C. H., J. Kamradt, and Stöckle M. (2012). "Third generation anti-androgen therapy of advanced prostate cancer". In: *Urologe A.* 51(4), pp. 522–526.

Ohtsu, A, M A Shah, E Van Cutsem, S Y Rha, A Sawaki, S R Park, H Y Lim, Y Yamada, J W u, B Langer, M Starnawski, and Y K Kang (2011). "Bevacizumab in combination with chemotherapy as first-line therapy in advanced gastric cancer: a randomized, double-blind, placebo-controlled phase III study". In: *J Clin Oncol.* 29(30), pp. 3968–3976.

O'Mahony, D. and M. R. Bishop (2006). "Monoclonal antibody therapy". In: *Front Biosci.* 11, pp. 1620–1635.

Online, Protocol (2005). *Xenograft Tumor Model Protocol*. http://www.protocol-online.org/prot/Protocols/Xenograft-Tumor-Model-Protocol-3810.html. 01.03.2015.

O'Reilly, M. S., T. Boehm, Y. Shing, N. Fukai, G. Vasios, W. S. Lane, E. Flynn, J. R. Birkhead, B. R. Olsen, and J. Folkman (1997). "Endostatin: An endogenous inhibitor of angiogenesis and tumor growth". In: *Cell* 88, pp. 277–285.

Overwijk, W. W. and N. P. Restifo (2001). "B16 as a mouse model for human melanoma". In: *Curr Protoc Immunol.* Chapter 20. Unit 20.

Pachghare, V K (2005). *Comprehensive Computer Graphics: Including C++*. Laxmi Publications, pp. 22–23.

Page, R. and C. Takimoto (2001). *Principles of chemotherapy, Cancer management: a multidisciplinary approach*. http://www.thymic.org/uploads/reference_sub/03chemoprinc.pdf/. 01.03.2015.

Peirce, SM (2012). "Tumor vascular responses to antivascular and antiangiogenic strategies: looking for suitable models". In: *Trends Biotechnol* 30(12), pp. 649–958.

Perry, M. C. (2008). *The Chemotherapy Source Book*. fourth ed., Lippincott Williams and Wilkins.

Petersen, I (2007). "Antiangiogenesis, anti-VEGF(R) and outlook". In: *Recent Results In Cancer Research, Targeted Therapies in Cancer*. Ed. by M Dietel. Springer – Verlag.

Pluda, J.M. (1997). "Tumor-associated angiogenesis: mechanisms, clinical implications, and therapeutic strategies". In: *Semin Oncol.* 24(2), pp. 203–218.

Pollock, Raphael E. (2008). *Advanced Therapy in Surgical Oncology*. BC Decker, Hamilton, Ontario, Canada.

Protocol Online (2005). *Xenograft tumor model protocol*. Available: http://www.protocol-online.org/prot/Protocols/Xenograft-Tumor-Model-Protocol-3810.html. 01.03.2015.

Reinacher-Schick, A., M. Pohl, and W. Schmiegel (2008). "Drug insight: antiangiogenic therapies for gastrointestinal cancers–focus on monoclonal antibodies". In: *Nat Clin Pract Gastroenterol Hepatol.* 5(5), pp. 250–267.

Ribba, B, E Watkin, M Tod, P Girard, E Grenier, B You, E Giraudo, and G Freyer (2011). "A model of vascular tumour growth in mice combining longitudinal tumour size data with histological biomarkers". In: *Eur J Cancer* 47, pp. 479–490.

Rini, B I, S Halabi, J E Rosenberg, W M Stadler, D A Vaena, L Archer, J N Atkins, J Picus, P Czaykowski, J Dutcher, and E J Small (2010). "Phase III trial of bevacizumab plus interferon alfa versus interferon alfa monotherapy in patients with metastatic renal

cell carcinoma: final results of CALGB 90206". In: *J Clin Oncol.* 28(13), pp. 2137–2143.

Samson, D. J., T. A. Ratko, B. M. Rothenberg, and et al. (2010). *Comparative Effectiveness and Safety of Radiotherapy Treatments for Head and Neck Cancer, Rockville (MD): Agency for Healthcare Research and Quality (US), Comparative Effectiveness Reviews, No. 20.* http://www.ncbi.nlm.nih.gov/books/NBK45242/. 01.03.2015.

Schmoll, H J, E Van Cutsem, A Stein, V Valentini, B Glimelius, and et al. (2012). "ESMO Consensus Guidelines for management of patients with colon and rectal cancer: A personalized approach to clinical decision making". In: *Ann Oncol.* 23(10), pp. 2479–2516.

Shackney, S. E. (1993). "Tumor Growth, Cell Cycle Kinetics, and Cancer Treatment". In: *Medical Oncology: Basic Principles and Clinical Management of Cancer.* Ed. by P. Calabresi and P. S. Schein. McGraw Hill, New York.

Silbermann, M. H., B. Vecht, G Stoter, K Nooter, and J. Verweij (1990). "Combination therapy of ACNU and ifosfamide in tumor bearing mice with M2661 breast cancer, B16 malignant melanoma or C38 colon cancer". In: *Eur J Cancer.* 26(3), pp. 321–325.

Soria, J C, A Mauguen, M Reck, A B Sandler, N Saijo, D H Johnson, D Burcoveanu, M Fukuoka, B Besse, and J P Pignon (2013). "Systematic review and meta-analysis of randomised, phase II/III trials adding bevacizumab to platinum-based chemotherapy as first-line treatment in patients with advanced non-small-cell lung cancer". In: *Ann Oncol.* 24(1), pp. 20–30.

Srinivas, C. (2010). "Anti-Angiogenic Drugs: A Chemotherapy?" In: *Journal of Young Investigators* 17. http://www.jyi.org/features/ft.php?id=1117, 17.04.2012.

Stephanou, A, l S R McDougal, A R A Anderson, and M A J Chaplain (2005). "Mathematical modelling of flow in 2D and 3D vascular networks: Applications to anti-angiogenic and chemotherapeutic drug strategies". In: *Math Comput Model* 41, pp. 1137–1156.

Tachibana, K. E., M. A. Gonzalez, and N. Coleman (2005). "Cell-cycle-dependent regulation of DNA replication and its relevance to cancer pathology". In: *J Pathol.* 205(2), pp. 123–129.

Tang, M., M. Gonen, A. Quintas-Cardama, J. Cortes, H. Kantarjian, C. Field, T.P. Hughes, S. Branford, and F. Michor (2011). "Dynamics of chronic myeloid leukemia response to long-term targeted therapy reveal treatment effects on leukemic stem cells". In: *Blood.* 118(6), pp. 1622–1631.

Tao, M., Y. Teng, H. Shao, P. Wu, and E. J. Mills (2011). "Knowledge, perceptions and information about hormone therapy (HT) among menopausal women: a systematic review and meta-synthesis". In: *PLoS One.* 6(9), e24661.

Targeson (2012). *Mouse Tail Vein Injection Protocol*. Available: http://www.targeson.com/sites/default/files/content/pages/pdfs/tail_vein_protocol_2012_0.pdf. 01.03.2015.

Tebbutt, N C, K Wilson, V J Gebski, M M Cummins, D Zannino, G A van Hazel, B Robinson, A Broad, V Ganju, S P Ackland, G Forgeson, D Cunningham, M P Saunders, M R Stockler, Y Chua, J R Zalcberg, R J Simes, and T J Price (2010). "Capecitabine, bevacizumab, and mitomycin in first-line treatment of metastatic colorectal cancer: results of the Australasian Gastrointestinal Trials Group Randomized Phase III MAX Study". In: *J Clin Oncol.* 28(19), pp. 3191–3198.

Tomayko, M M and C P Reynolds (1989). "Determination of subcutaneous tumor size in athymic (nude) mice". In: *Cancer Chemother Pharmacol.* 24(3), pp. 148–154.

Travis, W. D. et al. (2004). *Pathology and Genetics: Tumours of the Lung, Pleura, Thymus and Heart (World Health Organization Classification of Tumours)*. International Agency for Research on Cancer, p. 35.

Verma, S., Y. Madarnas, S. Sehdev, G. Martin, and J. Bajcar (2011). "Patient adherence to aromatase inhibitor treatment in the adjuvant setting". In: *Curr Oncol.* 18 (Suppl 1), S3–S9.

Vokes, E E, R Salgia, and T G Karrison (2013). "Evidence-based role of bevacizumab in non-small cell lung cancer". In: *Ann Oncol.* 24(1), pp. 6–9.

Waldmann, T. A. (2003). "Immunotherapy: past, present and future". In: *Nat Med.* 9(3), pp. 269–277.

Willett, C.G. et al. (2004). "Direct evidence that the VEGF-specific antibody bevacizumab has antivascular effects in human rectal cancer". In: *Nat Med.* 10(2), pp. 145–147.

Yorke, E. D., Z. Fuks, L. Norton, W. Whitmore, and C. C. Ling (1993). "Modeling the development of metastases from primary and locally recurrent tumors: comparison with a clinical data base for prostatic cancer". In: *Cancer Res.* 53(13), pp. 2987–2993.

Zhang, D., E. M. Hedlund, S. Lim, F. Chen, Y. Zhang, B. Sun, and Y. Cao (2011). "Antiangiogenic agents significantly improve survival in tumor-bearing mice by increasing tolerance to chemotherapy-induced toxicity". In: *Proc Natl Acad Sci USA* 108(10), pp. 4117–4122.

Zhou, K (1996). *Robust and Optimal Control*. Prentice-Hall.

Own Publications Pertaining to Theses

S-1 Drexler, D. A., L. Kovács, J. Sápi, I. Harmati, and Z. Benyó (2011). "Model-based analysis and synthesis of tumor growth under angiogenic inhibition: a case study."

In: *IFAC WC 2011 – 18th World Congress of the International Federation of Automatic Control*. Milano, Italy, pp. 3753–3758.

S-2 Drexler, D. A., J. Sápi, A. Szeles, I. Harmati, A. Kovács, and L. Kovács (2012). "Flat control of tumor growth with angiogenic inhibition". In: *SACI 2012 – 6th International Symposium on Applied Computational Intelligence and Informatics (IEEE)*. Timisoara, Romania, pp. 179–183.

S-3 Drexler, D A, J Sápi, A Szeles, I Harmati, and L Kovács (2012). "Comparison of Path Tracking Flat Control and Working Point Linearization Based Set Point Control of Tumor Growth with Angiogenic Inhibition". In: *Scientific Bulletin of the "Politehnica" University of Timisoara, Transactions on Automatic Control and Computer Science* 57 (71):(2), pp. 113–120.

S-4 Kiss, B, J Sápi, and L Kovács (2013). "Imaging method for model-based control of tumor diseases". In: *SISY 2013 – 11th IEEE International Symposium on Intelligent Systems and Informatics*. Subotica, Serbia, pp. 271–275.

S-5 Kovács, L., T. Ferenci, Sápi, and P. Szalay (2012). "Népegészségügyi problémák számítógépes modellezése (in Hungarian)". In: *Informatika és menedzsment az egészségügyben: az egészségügyi vezetők szaklapja* XI:(8), pp. 49–55.

S-6 Kovács, L., J. Sápi, Gy Eigner, T. Ferenci, P. Szalay, J Klespitz, B Kurtán, M Kozlovszky, D. A. Drexler, P Pausits, I. Harmati, Z. Sápi, and I. Rudas (2014). "Model-based healthcare applications at Obuda University". In: *SACI 2014 – 9th IEEE International Symposium on Applied Computational Intelligence and Informatics*. Timisoara, Romania, pp. 183–187.

S-7 Kovács, L., J. Sápi, T. Ferenci, P. Szalay, D. A. Drexler, Gy. Eigner, P. I. Sas, I. Harmati, M Kozlovszky, and Z. Sápi (2013). "Model-based optimal therapy for high-impact diseases". In: *INES 2013 – 17th International Conference on Intelligent Engineering Systems (IEEE)*. San Jose, Costa Rica, pp. 209–214.

S-8 Kovács, L., P. Szalay, T. Ferenci, D. A. Drexler, J. Sápi, I. Harmati, and Z. Benyó (2011). "Modeling and Optimal Control Strategies of Diseases with High Public Health Impact". In: *INES 2011 – 15th International Conference on Intelligent Engineering System (IEEE)*. Poprad, Slovakia, pp. 23–28.

S-9 Kovács, L., P. Szalay, T. Ferenci, J. Sápi, P. I. Sas, D. A. Drexler, I. Harmati, B. Benyó, and A. Kovács (2012). "Model-based control algorithms for optimal therapy of high-impact public health diseases". In: *INES 2012 – 16th International Conference on Intelligent Engineering Systems (IEEE)*. Lisbon, Portugal, pp. 531–536.

S-10 Kovács, L, A Szeles, J Sápi, D A Drexler, I Rudas, I Harmati, and Z Sápi (2014). "Model-based angiogenic inhibition of tumor growth using modern robust control method". In: *Comput Methods Programs Biomed.* 114(3), e98–110.

S-11 Sápi, J., D. A. Drexler, I. Harmati, Z. Sápi, and L. Kovács (2012). "Linear state-feedback control synthesis of tumor growth control in antiangiogenic therapy". In: *SAMI 2012 – 10th International Symposium on Applied Machine Intelligence and Informatics (IEEE)*. Herlany, Slovakia, pp. 143–148.

S-12 Sápi, J, D A Drexler, I Harmati, Z Sápi, and L Kovács (2015). "Qualitative analysis of tumor growth model under antiangiogenic therapy – choosing the effective operating point and design parameters for controller design". In: *Submitted to Optimal Control Applications and Methods*.

S-13 Sápi, J, D A Drexler, I Harmati, A Szeles, B Kiss, Z Sápi, and L Kovács (2013). "Tumor growth model identification and analysis in case of C38 colon adenocarcinoma and B16 melanoma". In: *SACI 2013 – 8th IEEE International Symposium on Applied Computational Intelligence and Informatics*. Timisoara, Romania, pp. 303–308.

S-14 Sápi, J., D. A. Drexler, and L. Kovács (2013). "Parameter optimization of H_∞ controller designed for tumor growth in the light of physiological aspects". In: *CINTI 2013 – 14th IEEE International Symposium on Computational Intelligence and Informatics*. Budapest, Hungary, pp. 19–24.

S-15 Sápi, J, D A Drexler, Z Sápi, and L Kovács (2014). "Identification of C38 colon adenocarcinoma growth under bevacizumab therapy and without therapy". In: *CINTI 2014 – 15th IEEE International Symposium on Computational Intelligence and Informatics*. Budapest, Hungary, pp. 443–448.

S-16 Sápi, J, L Kovács, D A Drexler, P Kocsis, D. Gajári, and Z Sápi (2015). "Tumor Volume Estimation and Quasi-Continuous Administration for Most Effective Bevacizumab Therapy". In: *Submitted to Plos One*.

S-17 Szeles, A, D A Drexler, J Sápi, I Harmati, and L Kovács (2014). "Model-based Angiogenic Inhibition of Tumor Growth using Adaptive Fuzzy Techniques". In: *Periodica Polytechnica Electrical Engineering and Computer Science* 58:(1), pp. 29–36.

S-18 Szeles, A., D. A. Drexler, J. Sápi, I. Harmati, and L. Kovács (2014). "Study of Modern Control Methodologies Applied to Tumor Growth under Angiogenic Inhibition". In: *IFAC WC 2014 – 19th World Congress of the International Federation of Automatic Control*. Cape Town, South Africa, pp. 9271–9276.

S-19 Szeles, A, D A Drexler, J Sápi, Z Sápi, I Harmati, and L Kovács (2013). "Model-based Angiogenic Inhibition of Tumor Growth using Feedback Linearization". In: *CDC 2013 – 52nd IEEE Conference on Decision and Control*. Florence, Italy, pp. 2054–2059.

S-20 Szeles, A., J. Sápi, D. A. Drexler, I. Harmati, Z. Sápi, and L. Kovács (2012). "Model-based Angiogenic Inhibition of Tumor Growth using Modern Robust Control Method". In: *IFAC BMS 2012 – 8th IFAC Symposium on Biological and Medical Systems*. Budapest: IFAC by Pergamon Press, pp. 113–118.

Own Publications Not Pertaining to Theses

Sx-1 Changchien, Y C, P Tátrai, G Papp, J Sápi, L Fónyad, M Szendrői, Z Pápai, and Z Sápi (2012). "Poorly differentiated synovial sarcoma is associated with high expression of enhancer of zeste homologue 2 (EZH2)". In: *J Transl Med.* 10:216. DOI: 10.1186/1479-5876-10-216.